EINDHOVEN UNIVERSITY OF TECHNOLOGY

Tracking Control for Mechanical Systems Experiencing Simultaneous Impacts and Spatial Friction

M. Bouma (0784690)
Department of Mechanical Engineering
Dynamics and Control group
Eindhoven University of Technology
DC 2019.XXX

Project Supervisor
PROF. DR. IR. N. VAN DE WOUW

Daily Supervisors
DR.IR A. SACCON
IR. M.W.L.M. RIJNEN

Committee
PROF. DR. IR. N. VAN DE WOUW ∗
DR. IR. A. SACCON ∗
IR. M.W.L.M. RIJNEN ∗
T.B.D. †

∗ Eindhoven University of Technology (Dynamics and Control)
† Eindhoven University of Technology (Control Systems Technology)

November 1, 2018

Abstract

Acknowledgments

Contents

Nomenclature

Acronyms

$(.)_{\text{cl}}$	The closed-contact mode sub/superscript
$(.)_{\text{op}}$	The open-contact mode sub/superscript
$(.)_{\text{sl}}$	The slip-contact mode sub/superscript
$(.)_{\text{st}}$	The stick-contact mode sub/superscript
$o(.)$	Higher order terms
LTTHS	Linear Time Triggered Hybrid System
NCP	Nonlinear Complementarity Problem
NSITHS	Nonlinear State-Input Triggered Hybrid System
PHTTHS	Positively Homogeneous Time Triggered Hybrid System
RS	Reference-Spreading

Counters

ι	The contact point counter
i	The macro-event counter
j	The classic hybrid-time event counter
k	The micro-event counter

Parameters

$\mathcal{I}$	A set of contact points
κ_ι	Magnitude of the tangential velocity of contact point ι
μ_ι	The friction coefficient of contact point ι
c	The number of contact points
c_i	The event-character of macro-event i
$e_{n,\iota}$	
$e_{t,\iota}$	
I	Domain of a segment
l_i	The amount of simultaneous activations of macro-event i
N	The number of events

Variables

$(.)_\epsilon$	A variable dependent on the initial perturbation
$\boldsymbol{A}$	Linear state matrix
$\boldsymbol{\alpha}$	The nominal reference trajectory
$\boldsymbol{B}$	Linear input matrix
$\boldsymbol{C}$	The column containing centripedal, Coriolis and gravitational effects
χ	The set of guard function identifiers of guards that can be activated
$\boldsymbol{D}$	Delassus matrix
Δ	The linearization of the perturbed event time around zero perturbation
ϵ	Initial state and input perturbation
η	A guard function identifier
$\boldsymbol{f}$	A nonlinear continuous function
Γ	An impulsive guard function
γ	A flow guard function
$\boldsymbol{g}$	A jump map
$\boldsymbol{G}_{\boldsymbol{v},i}$	Positive homogeneous jump gain for the perturbed input direction
$\boldsymbol{G}_{\boldsymbol{z},i}$	Positive homogeneous jump gain for the perturbed state direction
$\boldsymbol{H}$	The positive homogeneous jump gain
$\Lambda_{n,\iota}$	The normal impulsive reaction force of contact point ι
$\lambda_{n,\iota}$	The normal reaction force of contact point ι
$\boldsymbol{\Lambda}_{t,\iota}$	The tangential impulsive reaction force of contact point ι
$\boldsymbol{\lambda}_{t,\iota}$	The tangential reaction force of contact point ι
$\mathcal{D}_i$	The discrete event set of event i
$\boldsymbol{M}$	The mass matrix
$\boldsymbol{\mu}$	The nominal reference input
$\boldsymbol{q}$	The generalized coordinates
$\boldsymbol{S}$	The matrix containing generalized directions of the actuator forces
σ_i	The system-mode descriptor of event i
τ	The nominal event time
$\boldsymbol{u}$	The input
$\boldsymbol{v}$	The perturbed input direction
$\boldsymbol{w}_{n,\iota}$	The normal jacobian of contact point ι
$\boldsymbol{W}_{t,\iota}$	The tangential jacobian of contact point ι
$\boldsymbol{x}$	The state coordinates
$\boldsymbol{\xi}$	The generalized coordinates defined on the continuous segments of a trajectory
$\boldsymbol{z}$	The perturbed state direction

$\zeta_{n,\iota}$	Normal velocity of contact point ι
$\boldsymbol{\zeta}_{t,\iota}$	Tangential velocity of contact point ι
D	A discrete event set
$D_i(.)$	The derivative with respect to the ith term
$h_{n,\iota}$	Contact distance of contact point ι
S_i^k	The historical notation of macro-event i from micro-event 0 up to k
s_i^k	The event-mode descriptor of macro-event i and micro-event k
t	Regular time
t_i^k	The perturbed event time of macro-event i and micro-event k

Chapter 1

Introduction

1.1 High performance physical interaction in robotics

In many applications of mechanical systems physical interaction with the environment is necessary to function, particularly in robotics. Humanoid robots, quadrupeds, and industrial robots are some examples of robots that repeatedly interact with their environment. Common control strategies that are available for these applications are limiting in performance. To avoid complexity of the controller, they often assume contact with their environment to happen at zero relative speed. This makes the robots less suitable for situations where speed is of significance, e.g., an industrial robot aiming to reach a certain throughput or a quadruped performing a trotting motion. Examples of such robots the SimLab quadruped [1] and the ABB IRB 360 flexpicker [2], which are depicted in Figure 1.1. High performance is desirable in such cases, and zero velocity contact limits this performance. Therefore it is clear that the field of robotics can benefit from control strategies that are capable of handling non-zero relative velocity. Such controllers, however, are more complex than the controllers that require zero velocity contact situations.

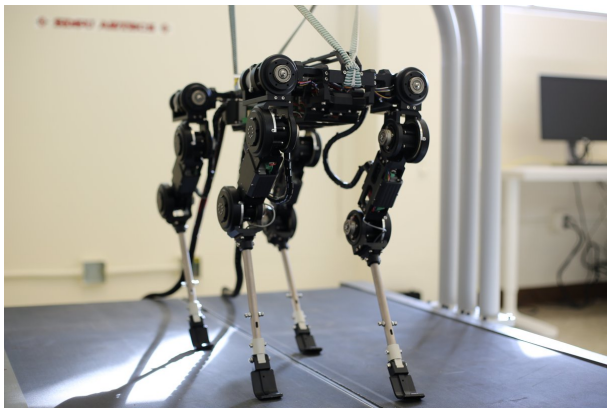

(a) *SimLab quadruped used at Virginia Tech [1].*

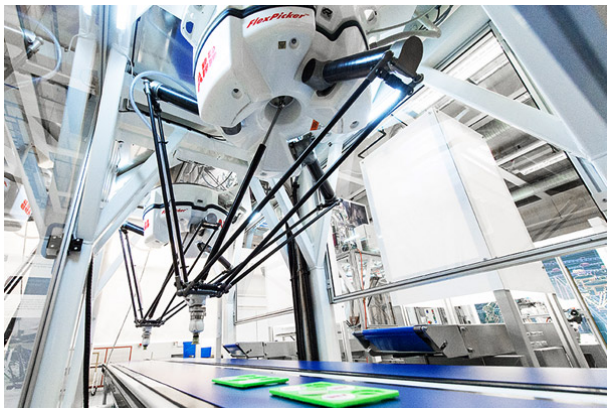

(b) *The ABB IRB 360 FlexPicker [2].*

Figure 1.1: *Two examples of robots with physical interaction that can benefit from high performance control strategies.*

When two bodies make physical contact at non-zero velocity, impact occurs. Impact is a complex physical event, that is characterized by short timescales, high force levels, high energy dissipation rates, and large accelerations and decelerations. Due to the small time scale at which impacts happen, their effect is often modeled as instantaneous. In such a modeling setting, the contact

forces are impulsive and the velocity illustrates jumps during an impact. Such modeling is called *nonsmooth*. Nonsmooth mechanical systems with impact are systems that have discontinuities in their state-evolution. Mechanical systems with unilateral constraints are an example of systems that can exhibit nonsmooth behavior, as they experience velocity jumps when their unilateral constraints are closed at non-zero velocities. Control strategies for such systems are necessary to achieve higher performance.

1.2 Nonsmooth modeling frameworks

Nonsmooth systems can be described by several mathematical frameworks, e.g., singularly perturbed systems, hybrid systems, complementarity systems, and (measure-)differential inclusions [3]. The singular perturbation framework approximates the nonsmooth behaviour using a singularly perturbed smooth system. In this way, the singularly perturbed system can be evaluated numerically using a single smooth differential equation. However, due to the smooth approximation, extremely small time-steps are necessary which makes the system very stiff. More suitable for numerical evaluation are differential inclusions, which are applicable to systems with a discontinuous right-hand side but a time-continuous state-evolution (also called Filippov-systems [4]). A common example of Filippov-systems are systems experiencing dry friction. The differential inclusion gives a description of the nonsmooth dynamics in a single inclusion. However, mechanical systems with unilateral constraints and impact do not satisfy the requirement of having a time-continuous state-evolution. A measure-differential inclusion describes the continuous as well as the impulsive dynamics of a nonsmooth system [5]. In this way, measure-differential inclusions are suitable for systems with time-discontinuities in their state-evolution [6, 7]. Using this approach, the dynamics can be accurately integrated using the timestepping method [8]. From a control point-of-view the complementarity framework is often considered. This framework describes nonsmoothness through a combination of differential equations and inequalities [9,10]. In [11], the complementarity problem is used to describe mechanical systems with unilateral constraints. It plays a key role in mathematical programming, and several solutions for trajectory tracking using complementarity systems exist [12, 13]. In recent years, the hybrid systems framework has drawn more interest for solving the trajectory tracking problem of nonsmooth systems [14,15]. A hybrid system is a dynamical system that exhibits both continuous and discrete dynamics behaviour, where it reinitializes the state and switches (discrete behaviour) between several differential equations (continuous behaviour) [16]. According to [17], the hybrid systems framework is suitable for the modeling of mechanical systems with unilateral constraints as well as robotics. In a hybrid dynamical model guard sets are defined, which when entered by the system's state, will cause the dynamics to switch from one differential equation to another and possibly reinitialize the state. This makes it a very intuitive approach to the modeling of nonsmoothness. A known difficulty with this description however, is a phenomenon called Zeno-behaviour. One speaks of Zeno-behaviour when an infinite amount of guard activations happen in a finite time. A classic example is the bouncing ball. Measure-differential inclusions with a timestepping scheme would be more suitable in such a situation, since the combined effect of several state resets is captured in a single time step. An advantage of using the hybrid systems framework, is that it is a more intuitive description of the dynamics whereas measure-differential inclusions are more abstract. The stability analyses for these frameworks are well-developed, i.e., [16, 18, 19] for hybrid systems, [20–22] for measure differential inclusions, and [7, 23, 24] for linear complementarity problems.

1.3 Tracking control for nonsmooth systems

Legged robotic systems account for a substantial part of the research done into the trajectory tracking control of mechanical systems with unilateral constraints. Many results in this area deal with the stability of periodic orbits of systems with impacts. In [25], a first big step has been made into modeling and controlling a one-legged hopping robot. In this research, the energy-loss during impact is modeled through damping and coupling effects are modeled as perturbations. Other pioneering works can be found in [26–28]. In [15, 29], the hybrid framework is adopted to find stable walking gaits for biped robots. Using Poincaré maps, the stability of periodic orbits with discontinuities of under-actuated systems are analyzed. Phases can be distinguished where the system is fully actuated and where the system is under-actuated. The fully actuated phase can then be used to stabilize the periodic trajectory despite the under-actuated phase. The work is continued in [30], generating control laws using data of walking humans and in [31] the energy-efficiency of generated walking gaits has been the focus. An example of a humanoid robot on which such controllers have been implemented is Agility Robotics' Cassie [32], which is depicted in Figure 1.2. An extensive survey in the field of bipedal robotic walking can be found in [33]. The analysis of stable walking gaits is applied to the MIT Cheetah in [14], where a stability analysis and controller design is presented for the trot-running of a quadrupedal robot.

Figure 1.2: *The bipedal robot Cassie developed by Agility Robotics [32].*

Considerable progress has been made in the field of walking robots and billiards, but it is easy to think of an example where nonperiodic trajectories are of interest. Under the assumption that the state trajectory jumps at the exact same time as the reference trajectory, the trajectory tracking problem for nonsmooth systems has been solved for several types of systems. The tracking problem for Lur'e type systems has been analyzed in [34, 35], using MDI's to describe nonsmooth and impulsive dynamics. The work uses the convergence property to provide a solution to the tracking problem, where the solution may be time-varying and exhibit state-jumps. In [12], a passivity-based approach is used to solve the tracking control problem of complementarity Lagrangian systems. Asymptotic stability is achieved for Lagrangian systems with unilateral constraints. The same approach has been applied to the hybrid system framework in [36], which results in a control law that can guarantee stability of a trajectory with multiple impacts. By embedding the reference trajectory with discontinuities into a set, Lyapunov tools can be used to analyze stability as in [37,38]. In [39] a stability analysis of systems with impacts and friction has been presented. The results are obtained

using the measure-differential inclusion framework, resulting in a smooth control law. The planning and control of non-periodic bipedal locomotion with impacts and friction is discussed in [40].

In the prior discussed work, the tracking problem has been solved under the assumption that the jump of the state trajectory occurs at the same time-instant as the jump of the reference trajectory, i.e., in [36, 38, 39]. In reality, especially in high velocity conditions, the time instant of the state jump and that of the reference trajectory jump are noncoincident more often than not. In this case a phenomenon called *peaking* occurs [41]. Spikes in the tracking error will arise around the jump times, which generate large actuation forces and contradict stability. Solutions exist for periodic orbits in [42,43], where the results are compatible with a mismatch in reference jump-time and state jump-time for infinite time periodic trajectories with infinitely many state-jumps. Such trajectories are often found in so called *Birkhoff Billiards* where the coefficient of restitution is 1. [44] also presents results for billiards, applicable to a large class of trajectories than [42, 43]. In [41, 45], a novel definition of the tracking error is introduced, using a distance function which is not sensitive to jumps of the state and the reference trajectory. Lyapunov-based conditions for the global asymptotic stability of non-smooth trajectories have been derived. Another solution for the problem of a jump-time mismatch is proposed in [46] in the form of a distance function similar to [41, 45] based on a quotient metric. When a state jump happens at a different time than the reference jump, this approach applies the jump map to the reference to be able to compare the state to the reference. In [47], a novel controller design using gluing functions is introduced to connect the start and end point of a jump in the state space. After gluing, the system can be considered a continuous or piecewise continuous function without state jumps. In [48], a tracking error is defined by taking the smallest of two values: the ante-impact tracking error and post-impact tracking error.

1.4 Reference spreading control

In [49, 50] a novel notion of error is introduced for systems with state jumps, by extending the reference trajectory segments, and considering the error between the reference trajectory and state trajectory that have encountered the same number of jumps. This way, an ante-event state trajectory can always be compared to an ante-event reference trajectory and a post-event state trajectory can always be compared to a post-event reference trajectory, even when the event times do not coincide. The authors of [49,50] then use that notion of error as the basis for extending the sensitivity analysis introduced in [51] to the hybrid system framework. These results are then used to obtain a local approximation of the perturbed state dynamics. This analysis gives insight in how the system behaves under the presence of perturbations, which is useful during controller design. Experimental results for this control law are presented in [52], where a 1-DOF robot arm performs an impacting trajectory using the control law proposed in [49]. In [53], a control strategy for hybrid systems with state triggered jumps is used on a hopping robotic leg model from [54]. The control strategy is named *reference spreading control* in [55], due to the extensions made on the reference trajectories in the notion of error. In [56], the reference spreading control law is used in simulations with an iCub robot. The iCub robot balances on one foot and keeps himself standing upright by making and breaking contact with a wall using one of its arms. Some snapshots of the motion are depicted in Figure 1.3. As mentioned earlier, many works in literature assume that the exact impact time is known. This is extremely limiting during implementation of the control law. Using the reference spreading approach, the impact time of the state is allowed to deviate from that of the reference, making implementation of the control law in practical applications more viable while still allowing for state-jumps.

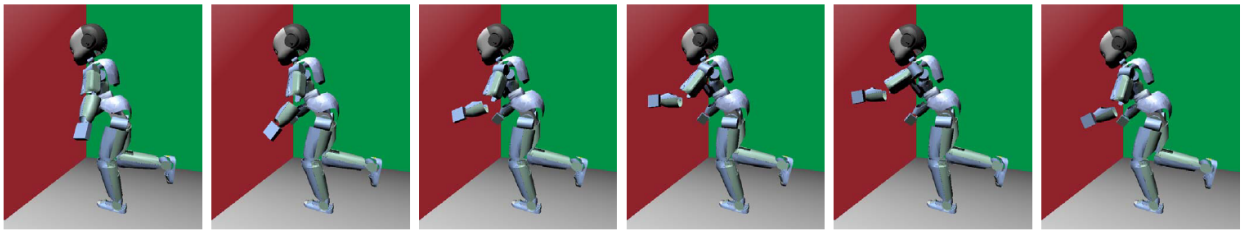

Figure 1.3: *Snapshots of the motion the iCub robot makes in the simulation done in [56] using reference spreading control.*

As is the case in the simulations with the iCub in Figure 1.3, impacts are often modeled using a one-point contact between two bodies. However, in practice, more complex geometries can make contact with each other. The feet of Cassie in Figure 1.2 for example, have a clear resemblance to human feet, which often results in distinct heel and toe strikes during walking motions. A more realistic contact geometry is used in [57], in which the foot strike of a humanoid bipedal robot is modeled using multiple impacts. One strike is modeled by a heel impact, a toe impact, a heel release, and finally a toe release, resulting in a more realistic model of the walking gait of the bipedal robot. In such a movement, the order of impacts is known.

When considering a trajectory with multiple contacts closing at one time-instant, the problem becomes more complex. Imagine for example the iCub in [56] having a physically realistic geometry at the end of its arm. Consider Figure 1.4. The arm can first make a point contact, then a line contact, and finally a surface contact to make full contact with the wall. It can also track a trajectory where the surface of the arm makes a surface contact with the wall at one time-instant. Such events can be considered as multiple impacts happening at the same time-instant and are called *simultaneous impacts*. One can imagine that a small perturbation can significantly change the behavior of a simultaneous impact. Instead of the expected single jump in the state, a perturbation can cause the state to have multiple jumps. Also the order of impacts of the several parts of the arm is not known beforehand. In Figure 1.4 a 2-dimensional representation of the wrist of the iCub robot is illustrated. This image clearly visualizes the effect a perturbation has on a trajectory with simultaneous impacts. The approach used in [57] is not suitable for these situations.

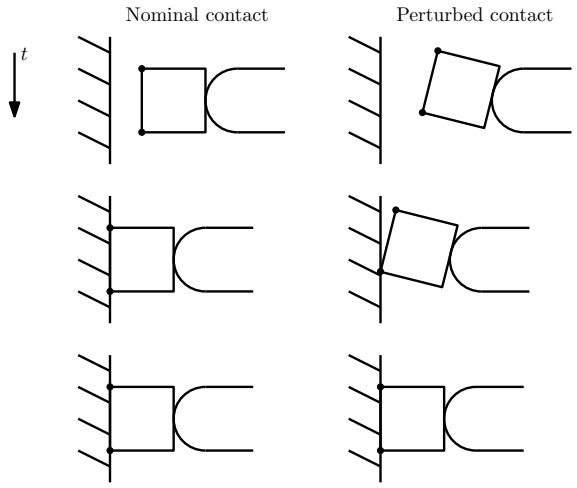

Figure 1.4: *A 2-dimensional illustration of the end effector of the wrist of the iCub robot. On the left a nominal trajectory is illustrated (from top to bottom), where a simultaneous impact happens. The wrist immediately makes a line-contact with the surface. On the right the trajectory is perturbed, which results in two impacts instead of one.*

The phenomenon of simultaneous impacts is first introduced in [58], where the first step is taken into solving the trajectory tracking problem for such impacts. A hybrid system framework is used to model the impacts, where multiple guards can be activated at once. The reference spreading control in [53,55] and the sensitivity analysis to approximate a system's behavior around trajectories with single guard activation, introduced in [49], are extended to be suitable for simultaneous guard activation. The results of the sensitivity analyses are used to find a first order approximation of the perturbed trajectory, which can be used to find suitable feedback gains. In addition to an impulse perpendicular to the impact-surface, taking friction into account will result in a tangential impulse. Also the release phase is not considered in [58]. During the release phase, no discontinuity in the state-evolution is seen, only a change in the number of active constraints on the system occurs. The aim of this research is to apply the reference spreading control strategy and sensitivity analysis to systems experiencing both impacts including friction and releasing motions.

1.5 Contribution

Simultaneous impacts with friction

Friction elements are often disregarded when analyzing impacts. However, to set up a unifying theory, friction elements should not be ignored. Tangential impulses can have a considerable effect on a system's dynamics. The impact laws used in the work of [58] can be extended using one of the several available friction laws [22]. When impact laws are supplemented with a tangential element, this is often done using a Coulomb friction law [59]. Besides the tangential impulse, also a Filippov-like discontinuity will be present due to Coulomb friction. Also in this work a Coulomb friction law will be used, which can lead to more accurate models and controllers for mechanical systems with unilateral constraints.

Research Objective:
Find a model suitable to describe mechanical systems with unilateral constraints and spatial friction. The sensitivity analysis and mathematical notation presented in [58] shall be adjusted to be

compatible with such models.

Simultaneous impacts with release

In [53] and [60], the release phase of a system with a reference spreading controller has been extensively researched. However, these results only include single guard activation. The release phase for multiple guard activation is not yet investigated. In [58], only the establishment of contact is simulated and detachment is not included. Extending the sensitivity analysis in [58] to be suitable for simultaneous releases would make it possible to simulate and control one trajectory with several simultaneous contacts and releases.

Research Objective:
Adjusting the sensitivity analysis presented in [58] such that it is suitable for input-dependent guard functions.

1.6 Report outline

The modeling of mechanical systems with unilateral constraints and spatial friction is discussed in Chapter 2. The generic dynamics of a mechanical system including contact and friction laws are derived, eventually resulting in a hybrid system with impulsive effects. Then, in Chapter 3, a tracking control strategy for hybrid systems with ordered state-input-triggered events is presented. In Chapter 4, this tracking control strategy is extended to trajectories involving simultaneous impacts. An example of a mechanical system with unilateral constraints and spatial friction is given in Chapter 5, which is used for a numerical validation of the presented control strategy. Finally, in Chapter 6, conclusions are drawn and recommendations for future research are provided.

Chapter 2

Mechanical Systems with Unilateral Constraints and Spatial Friction

In this chapter, several modeling approaches of mechanical systems with unilateral constraints and spatial friction are presented. In mechanics, a unilateral constraint is a constraint that prevents two bodies from penetrating. When such a unilateral constraint is activated, the differential equation that describes the dynamics of the system can change. The state even goes through a reinitialization when the constraint is activated with non-zero velocity. Two bodies already in contact can also experience changes in their dynamics, as a result from the friction between these bodies. This behavior can be described by dynamics consisting of a continuous part and a discrete part; the continuous part describes the flow of the state, and the discrete part describes the reinitialization of the state. The occurrence of a change in differential equation and a possible state reinitialization are referred to as *events*. To be able to detect when the system goes through a such an event, contact points are defined on the bodies. These contact point can open and close contact, and when in contact can transition between stick and slip. Whether the contact point is in open-contact, closed-contact stick, or in closed-contact slip, is referred to as the *mode* of the contact point. Using these contact points, a method is presented to model mechanical systems with unilateral constraints and spatial friction. First, a general representation of mechanical systems is given, which is followed by sections introducing several formulations of the contact and friction laws in these systems. A complementarity problem formulation is presented, which is a complete and often used formulation for mechanical systems with unilateral constraints. From the complementarity formulation a hybrid system formulation is derived, which is a more intuitive formulation from a control point-of-view. The hybrid system formulation is the model that will be used in this work to define a control strategy for the tracking of trajectories of mechanical systems with unilateral constraints and spatial friction.

2.1 General system definition

For mechanical systems, a set of contact points $\iota \in \{\iota_1, \iota_2, ..., \iota_c\}$ is defined, with c being the number of considered contact points. A set $\mathcal{I}_{\text{cl}}$ is defined as the set of c_{cl} closed contact points, such that a contact $\iota \in \mathcal{I}_{\text{cl}}$ has closed a unilateral constraint. The set of contact points in open contact is defined as $\mathcal{I}_{\text{op}} := \{\iota \mid \iota \notin \mathcal{I}_{\text{cl}}\}$. Note that in a physics-based engine the set $\mathcal{I}_{\text{op}}$ is often undefined, because not all contact points are tracked. Only the contact points generating reaction forces are tracked. The set $\mathcal{I}_{\text{op}}$ is only defined for convenience when the mode of the system is discussed. When a unilateral constraint is activated at a nonzero velocity impact happens, meaning a jump in the velocity will appear. The result is that the generalized velocity $\dot{\boldsymbol{q}}$ is not continuously defined

over the entire domain of a trajectory with impacts. Therefore $\boldsymbol{\xi} := \dot{\boldsymbol{q}}$ is defined, except at impact-times τ^j. Here j is a counter for unilateral constraint activations where $j \in \{1, 2, ..., N\}$, with N the number of jumps in a trajectory. $h_{n,\iota}$ is the normal contact distance and $\zeta_{n,\iota}$ and $\boldsymbol{\zeta}_{t,\iota}$ represent the relative velocities in normal and tangential direction, respectively.

In Figure 2.1 a body and a fixed world surface are illustrated. A contact point ι is defined on the body, on which a plane tangent to the surface of the body is spanned. On the normal direction of this plane, the contact distance $h_{n,\iota}(\boldsymbol{q})$ is defined. This is the distance between the contact point and the surface that it can make contact with. By taking the time derivative of $h_{n,\iota}(\boldsymbol{q})$, the relative normal velocity of contact point ι is found to be

$$\zeta_{n,\iota} = \frac{\partial h_{n,\iota}}{\partial \boldsymbol{q}} \frac{\mathrm{d}\boldsymbol{q}}{\mathrm{d}t} = \boldsymbol{w}_{n,\iota}^T \dot{\boldsymbol{q}}, \tag{2.1}$$

with $\boldsymbol{w}_{n,\iota}$ representing the Jacobian of the normal velocity $\zeta_{n,\iota}$. The relative tangential velocity $\boldsymbol{\zeta}_{t,\iota}$ is defined in the tangent plane of ι, and thus lies perpendicular to $\zeta_{n,\iota}$. Using the tangential velocity Jacobian $\boldsymbol{W}_{t,\iota}$, the relative tangential velocity is defined as

$$\boldsymbol{\zeta}_{t,\iota} = \boldsymbol{W}_{t,\iota}^T \dot{\boldsymbol{q}}. \tag{2.2}$$

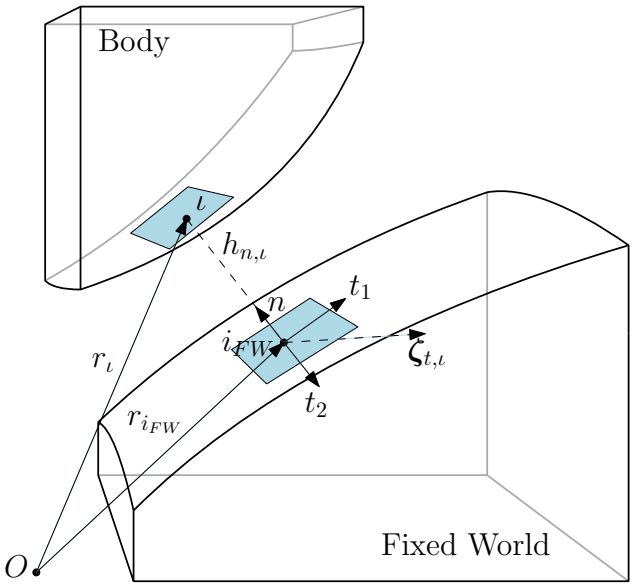

Figure 2.1: *An illustration of a body impacting the fixed world. A contact point ι is defined on the body, which can make contact with the fixed world at i_{FW}. The points ι and i_{FW} are connected by a line which is perpendicular to their respective bodies, which is used to define the contact distance $h_{n,\iota}$ and normal contact velocity $\zeta_{n,\iota}$. In the plane tangent to the body's surface, the tangential contact velocity $\boldsymbol{\zeta}_{tw,\iota}$ is defined.*

Then, the continuous dynamics of a mechanical system with unilateral constraints and spatial friction are of the form

$$\boldsymbol{M}(\boldsymbol{q})\dot{\boldsymbol{\xi}} + \boldsymbol{C}(\boldsymbol{q}, \boldsymbol{\xi}) = \boldsymbol{S}(\boldsymbol{q})\boldsymbol{u} + \sum_{\iota \in \mathcal{I}_{\mathrm{cl}}} \boldsymbol{w}_{n,\iota}(\boldsymbol{q})\lambda_{n,\iota} + \boldsymbol{W}_{t,\iota}(\boldsymbol{q})\boldsymbol{\lambda}_{t,\iota}, \tag{2.3}$$

(Contact Law),

(Friction Law),

with $\boldsymbol{q}, \boldsymbol{\xi} \in \mathbb{R}^n$ and $\boldsymbol{u} \in \mathbb{R}^m$. Here $\boldsymbol{M}(\boldsymbol{q}) \in \mathbb{R}^{n \times n}$ is the mass matrix of the system, $\boldsymbol{C}(\boldsymbol{q}, \boldsymbol{\xi}) \in \mathbb{R}^n$ contains the centripetal, Coriolis and gravitational forces in the system and $\boldsymbol{S}(\boldsymbol{q}) \in \mathbb{R}^{n \times m}$ represents the generalized directions of the forces. $\lambda_{n,\iota} \in \mathbb{R}$ and $\boldsymbol{\lambda}_{t,\iota} \in \mathbb{R}^2$ are the normal and tangential reaction forces, respectively, of contact point ι with $\boldsymbol{w}_{n,\iota} \in \mathbb{R}^n$ and $\boldsymbol{W}_{t,\iota} \in \mathbb{R}^{n \times 2}$ the corresponding reaction force Jacobians. When a contact point activates a unilateral constraint, impulsive dynamics can cause the state of the system to jump. These dynamics are of the form

$$\boldsymbol{M}(\boldsymbol{q})(\boldsymbol{\xi}^+ - \boldsymbol{\xi}^-) = \sum_{\iota \in \mathcal{I}_{\mathrm{cl}}} \boldsymbol{w}_{n,\iota}(\boldsymbol{q}) \Lambda_{n,\iota} + \boldsymbol{W}_{t,\iota}(\boldsymbol{q}) \boldsymbol{\Lambda}_{t,\iota}, \tag{2.4}$$

(Impulsive Contact Law),

(Impulsive Friction Law).

Here $\Lambda_{n,\iota}$ and $\boldsymbol{\Lambda}_{t,\iota}$ the normal and tangential impulsive reaction forces, respectively, of contact point ι. These dynamics are impulsive, and happen at one instance in time. The $^-$ superscript indicates the ante-event state and the $^+$ superscript indicates the post-event state. In the following sections three different methods of describing the contact and friction laws are presented. First a complementarity problem formulation of mechanical systems with unilateral constraints is given, from which later a proximal point formulation and a hybrid system formulation are derived. For more information on modeling of multibody systems one can refer to [22] and [61].

2.2 Complementarity problem formulation

2.2.1 Signorini's contact law and Poisson's impact law

To describe the normal contact between rigid bodies Signorini's contact law is used. Since the bodies are impenetrable and reaction forces caused by contact cannot prevent the bodies from seperating, both the contact distance $h_{n,\iota}$ and $\lambda_{n,\iota}$ cannot become negative. Two situations are possible

1. $h_{n,\iota} = 0 \ \wedge \ \lambda_{n,\iota} \geq 0$ (closed-contact)
2. $h_{n,\iota} > 0 \ \wedge \ \lambda_{n,\iota} = 0$ (open-contact)

These situations are illustrated in Figure 2.2a, where it can be seen that the two situations are orthogonal. This behavior can be summarized in the complementarity condition

$$0 \leq h_{n,\iota} \perp \lambda_{n,\iota} \geq 0, \tag{2.5}$$

where the symbol $\perp$ is used to express the orthogonality between $h_{n,\iota}$ and $\lambda_{n,\iota}$. The complementarity condition in (2.5) is called Signorini's contact law. When contact happens at nonzero velocity, impact occurs. Newton's impact law is used to describe this impact. Newton's law of impact is defined as

$$\zeta_{n,\iota}^+ = -e_{n,\iota} \zeta_{n,\iota}^-, \ \text{when } h_{n,\iota} = 0, \ \dot{h}_{n,\iota} < 0. \tag{2.6}$$

In this work the coefficient of restitution $e_{n,\iota}$ is assumed to be 0, describing a completely inelastic contact. For closed contacts, an impact law can be defined that relates the impulsive contact force $\Lambda_{n,\iota}$ to the post-impact normal velocity $\zeta_{n,\iota}$. Considering multi-contact systems, two situations can occur when a contact is closed:

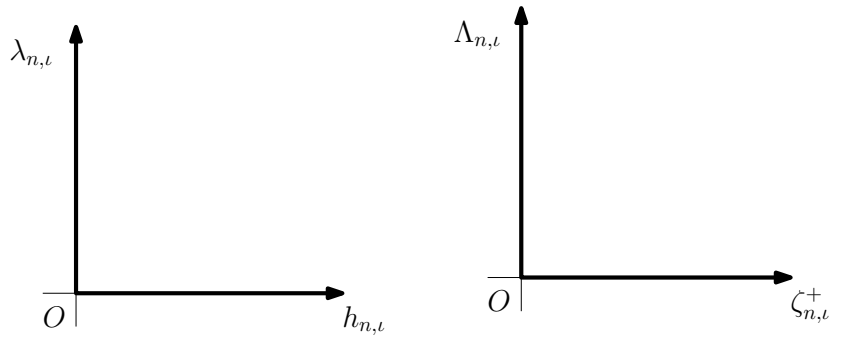

(a) *Signorini's contact law.*

(b) *Poisson's impact law without restitution.*

Figure 2.2

1. $\Lambda_{n,\iota} > 0 \ \wedge \ \zeta^+_{n,\iota} = 0$ (impact)
2. $\Lambda_{n,\iota} = 0 \ \wedge \ \zeta^+_{n,\iota} \geq 0$ (no impact)

The second case can occur when a contact point other than ι makes impact. The situations described above are illustrated in Figure 2.2b, where again the orthogonality can be observed. The behavior is written into the complementarity condition

$$0 \leq \zeta^+_{n,\iota} \perp \Lambda_{n,\iota} \geq 0, \qquad \forall \iota \in \mathcal{I}_{\text{cl}}, \tag{2.7}$$

with $\mathcal{I}_{\text{cl}}$ the set of closed contacts. The complementarity condition (2.7) is called Poisson's impact law. Note that the impact law is defined on velocity level, whereas the contact law is defined on position level.

2.2.2 Coulomb's friction law

Coulomb's friction law is often used to describe dry friction in mechanical systems. When considering 3-dimensional environments, Coulomb's friction law is defined as

$$||\boldsymbol{\lambda}_{t,\iota}|| \ \in \ \begin{cases} ||\boldsymbol{\lambda}_{t,\iota}|| \leq \mu_\iota \lambda_{n,\iota}, & \text{if } ||\boldsymbol{\zeta}_{t,\iota}|| = 0 \\ ||\boldsymbol{\lambda}_{t,\iota}|| = \mu_\iota \lambda_{n,\iota}, & \text{if } ||\boldsymbol{\zeta}_{t,\iota}|| > 0 \end{cases}, \tag{2.8}$$

with μ_ι the friction coefficient of contact point ι, and since friction is considered isotropic

$$\boldsymbol{\zeta}_{t,\iota} = -\kappa_\iota \, \text{SgnSp}(\boldsymbol{\lambda}_{t,\iota}), \tag{2.9}$$

with $\kappa_\iota > 0$ and

$$\text{SgnSp}(a) = \begin{cases} \frac{a}{||a||} & a \neq 0 \\ 0 & a = 0 \end{cases}, \tag{2.10}$$

for some vector a as defined in [62]. (2.8) can be considered as a relation between the magnitude of the tangential velocity $\boldsymbol{\zeta}_{t,\iota}$ and the reaction friction force $\boldsymbol{\lambda}_{t,\iota}$. (2.9) can be considered as a relation between the direction of $\boldsymbol{\zeta}_{t,\iota}$ and $\boldsymbol{\lambda}_{t,\iota}$, namely that $\boldsymbol{\zeta}_{t,\iota}$ and $\boldsymbol{\lambda}_{t,\iota}$ are always in opposite directions. The constant κ_ι can then be interpreted as the magnitude of the tangential velocity. Coulomb's friction law is illustrated in Figure 2.3a. In Figure 2.3b the same law is illustrated, but now as orthogonal vectors. As mentioned before, this is convenient for writing the law in a complementarity form.

The complementarity formulation of the Coulomb's law is therefore defined as

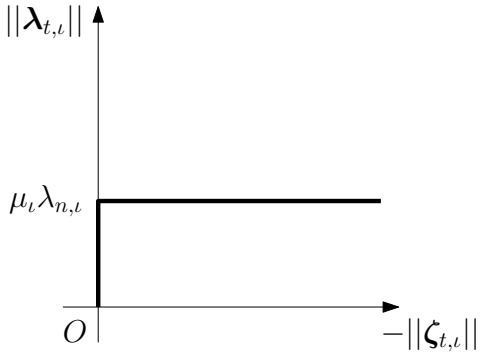

(a) *Coulomb's friction law.*

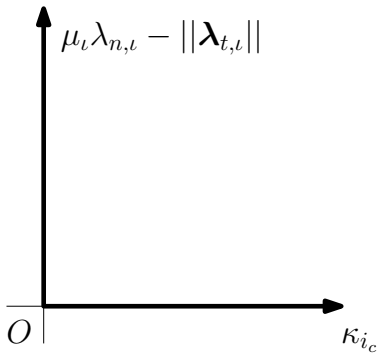

(b) *Coulomb's friction law as orthogonal vectors. κ_ι is defined as the magnitude of the tangential velocity $\boldsymbol{\zeta}_{t,\iota}$.*

Figure 2.3

$$0 \leq \mu_\iota \lambda_{n,\iota} - ||\boldsymbol{\lambda}_{t,\iota}|| \perp \kappa_\iota \geq 0, \tag{2.11}$$
$$\boldsymbol{\zeta}_{t,\iota} = -\kappa_\iota \operatorname{SgnSp}(\boldsymbol{\lambda}_{t,\iota}). \tag{2.12}$$

(2.9) is rewritten to (2.12) to avoid singularity problems for $||\boldsymbol{\lambda}_{t,\iota}|| = 0$. For the impulsive behavior of the friction law Newton's impact law is used to define the tangential post-impact velocity as

$$\boldsymbol{\zeta}^+_{t,\iota} = -e_{t,\iota} \boldsymbol{\zeta}^-_{t,\iota}, \tag{2.13}$$

where in this work $e_{t,\iota} = 0$ is assumed. Then, similarly to the non-impulsive case, the impulsive Coulomb's friction law can be defined as

$$0 \leq \mu \Lambda_{n,\iota} - ||\boldsymbol{\Lambda}_{t,\iota}|| \perp \kappa_\iota \geq 0. \qquad \forall \iota \in \mathcal{I}_{\mathrm{cl}}, \tag{2.14}$$
$$\boldsymbol{\zeta}^+_{t,\iota} = \kappa_\iota \operatorname{SgnSp}(\boldsymbol{\Lambda}_{t,\iota}), \qquad \forall \iota \in \mathcal{I}_{\mathrm{cl}}. \tag{2.15}$$

Note that just as the contact case, the impulsive friction law only holds for closed contacts.

2.2.3 System dynamics with contact and friction law

The flow dynamics are then described by

$$\boldsymbol{M}(\boldsymbol{q})\dot{\boldsymbol{\xi}} + \boldsymbol{C}(\boldsymbol{q}, \boldsymbol{\xi}) = \boldsymbol{S}(\boldsymbol{q})\boldsymbol{u} + \sum_{\iota \in \mathcal{I}_{\mathrm{cl}}} \boldsymbol{w}_{n,\iota}(\boldsymbol{q})\lambda_{n,\iota} + \boldsymbol{W}_{t,\iota}(\boldsymbol{q})\boldsymbol{\lambda}_{t,\iota}, \tag{2.16}$$
$$0 \leq h_{n,\iota} \perp \lambda_{n,\iota} \geq 0, \tag{2.17}$$
$$0 \leq \mu \lambda_{n,\iota} - ||\boldsymbol{\lambda}_{t,\iota}|| \perp \kappa_\iota \geq 0, \tag{2.18}$$
$$\boldsymbol{\zeta}_{t,\iota} = -\kappa_\iota \operatorname{SgnSp}(\boldsymbol{\lambda}_{t,\iota}), \tag{2.19}$$

with

$$h_{n,\iota} = \boldsymbol{w}^T_{n,\iota}(\boldsymbol{q})\boldsymbol{q}, \tag{2.20}$$
$$\zeta_{n,\iota}(\boldsymbol{q}) = \boldsymbol{w}^T_{n,\iota}(\boldsymbol{q})\boldsymbol{\xi}, \tag{2.21}$$
$$\boldsymbol{\zeta}_{t,\iota}(\boldsymbol{q}) = \boldsymbol{W}^T_{t,\iota}(\boldsymbol{q})\boldsymbol{\xi}. \tag{2.22}$$

The discrete dynamics, which take place when a contact point goes through an event, are described by

$$\boldsymbol{M}(\boldsymbol{q})(\boldsymbol{\xi}^{+}-\boldsymbol{\xi}^{-})=\sum_{\iota\in\mathcal{I}_{\mathrm{cl}}}\boldsymbol{w}_{n,\iota}(\boldsymbol{q})\Lambda_{n,\iota}+\boldsymbol{W}_{t,\iota}(\boldsymbol{q})\boldsymbol{\Lambda}_{t,\iota}, \tag{2.23}$$

$$0\leq\zeta_{n,\iota}^{+}\perp\Lambda_{n,\iota}\geq 0,\qquad\forall\iota\in\mathcal{I}_{\mathrm{cl}}, \tag{2.24}$$

$$0\leq\mu\Lambda_{n,\iota}-||\boldsymbol{\Lambda}_{t,\iota}||\perp\kappa_{\iota}\geq 0.\qquad\forall\iota\in\mathcal{I}_{\mathrm{cl}}, \tag{2.25}$$

$$\boldsymbol{\zeta}_{t,\iota}^{+}=-\kappa_{\iota}\,\mathrm{SgnSp}(\boldsymbol{\Lambda}_{t,\iota}),\qquad\forall\iota\in\mathcal{I}_{\mathrm{cl}}, \tag{2.26}$$

with

$$\zeta_{n,\iota}^{+}(\boldsymbol{q})=\boldsymbol{w}_{n,\iota}^{T}(\boldsymbol{q})\boldsymbol{\xi}^{+}, \tag{2.27}$$

$$\boldsymbol{\zeta}_{t,\iota}^{+}(\boldsymbol{q})=\boldsymbol{W}_{t,\iota}^{T}(\boldsymbol{q})\boldsymbol{\xi}^{+}. \tag{2.28}$$

2.3 Hybrid system formulation

In this section the dynamics of the complementarity system defined in Section 2.2 is written to a hybrid formulation, resulting in a hybrid framework for mechanical systems with unilateral constraints and spatial friction. In [63, p. 222] event driven numerical methods are presented for mechanical systems with spatial friction. However, these methods do not apply to the hybrid system framework. To the best of our knowledge, this work is first in presenting a model suitable for event driven simulation methods for the hybrid system framework with spatial friction.

2.3.1 Hybrid systems with impulsive effects

According to [64], an impulsive dynamical system can be described by a hybrid system with impulsive effects. This makes it a valid framework for mechanical systems with unilateral constraints and spatial friction. The notation given in [64] is convenient from a tracking point-of-view, considering that only the dynamics encountered during the trajectory need to be described. A hybrid system with impulsive effects consists of three elements:

1. Continuous dynamics, a continuous-time differential equation which defines the behavior of the system in between events
2. Discrete dynamics, which defines the way the state of the system is reset during events
3. Reset sets, which is a criterion to decide when the state of the system is to be reset

Therefore, a hybrid system with impulsive effects is given by

$$\begin{aligned}\dot{\boldsymbol{x}}(t,j)&=\boldsymbol{f}(\boldsymbol{x}(t,j),\boldsymbol{u}(t,j),t,j), &&\boldsymbol{x}(t,j),\boldsymbol{u}(t,j)\in\mathcal{C}^{j}\\ \boldsymbol{x}(t,j+1)&=\boldsymbol{g}(\boldsymbol{x}(t,j),\boldsymbol{u}(t,j),t,j), &&\boldsymbol{x}(t,j),\boldsymbol{u}(t,j)\in\mathcal{D}^{j+1}\end{aligned} \tag{2.29}$$

with $\boldsymbol{x}(t,j)\in\mathbb{R}^{n(j)}$, $\boldsymbol{u}(t,j)\in\mathbb{R}^{m(j)}$, $\boldsymbol{f}:\mathbb{R}^{n(j)}\times\mathbb{R}^{m(j)}\times\mathbb{R}\to\mathbb{R}^{n(j)}$. Note that the state dimension $n(j)$ and the input dimension $m(j)$ can vary in different modes j. For the difference equation we have $\boldsymbol{g}:\mathbb{R}^{n(j-1)}\times\mathbb{R}^{m(j-1)}\times\mathbb{R}\to\mathbb{R}^{n(j)}$. $\mathcal{C}^{j}$ is the flow set of the system, and $\mathcal{D}^{j}(t)\subseteq\partial\mathcal{C}^{j}:=\{\boldsymbol{x}(t,j)\in\mathbb{R}^{n(j)},\ \boldsymbol{u}(t,j)\in\mathbb{R}^{m(i)}\mid\gamma_{=}^{j}(\boldsymbol{x}^{\wedge},\boldsymbol{u}^{\wedge},t)=0,\ \gamma_{\geq}^{j}(\boldsymbol{x}^{\wedge},\boldsymbol{u}^{\wedge},t)\geq 0\}$, where $\gamma_{=}^{j}$ and $\gamma_{\geq}^{j}$ are some sets of guard functions that are activated at event j, $\boldsymbol{x}^{\wedge}$,$\boldsymbol{u}^{\wedge}$ are some virtual state and input that are not necessarily physically realistic, and $\partial\mathcal{C}^{j}$ indicates the border of $\mathcal{C}^{j}$.

The dynamics given in (2.29) will be used to describe a tracking problem for mechanical systems with unilateral constraints and spatial friction. A nominal state-input trajectory is considered consisting of absolutely continuous segments $(\boldsymbol{\alpha}(t,j), \boldsymbol{\mu}(t,j))$, with $t \in \left[\tau^j, \tau^{j+1}\right]$ and $j \in \{0,1,...,N\}$ the event counter. The nominal state and input, $\boldsymbol{\alpha}(t,j)$ and $\boldsymbol{\mu}(t,j)$ respectively, define the nominal trajectory with N events. The nominal event time of event j is denoted by τ^j and regular time is denoted by t. Every segment of the nominal trajectory $(\boldsymbol{\alpha}(t,j), \boldsymbol{\mu}(t,j))$ and every event $j \in \{1,2,...,N\}$ satisfy the dynamics in (2.29), where an event happens when $(\boldsymbol{\alpha}(t,j), \boldsymbol{\mu}(t,j))$ enters $\mathcal{D}^{j+1}$. Such a nominal trajectory existing of absolutely continuous segments experiencing events according to (2.29) is illustrated in Figure **??**.

In 2.4 an example trajectory of a block pushing towards a surface is illustrated. The block has two contact points on its edges ι_1 and ι_2. It starts with both contact points in open contact as can be seen in Figure 2.4a. The flow is described by $\dot{\boldsymbol{\alpha}}(t,0) = \boldsymbol{f}^0(\boldsymbol{\alpha}(t,0), \boldsymbol{\mu}(t,0), t)$ for $t \in [t_0, \tau^1]$. Then i_2 makes impact with the surface at τ^1, causing a jump in the state and a change in continuous dynamics $\dot{\boldsymbol{\alpha}}(t,1) = \boldsymbol{f}^1(\boldsymbol{\alpha}(t,1), \boldsymbol{\mu}(t,1), t)$ for $t \in [\tau^1, \tau^2]$. This is illustrated in Figure 2.4b, where i_2 is in closed contact and slipping over the contact surface. At τ^2, i^1 makes impact as well causing another jump and another change in continuous dynamics. The block now has both contact points slipping over the contact surface. After this both contact points release contact one by one. Since there are no impulsive forces present in this transition, the state does not jump when a contact point releases. However, a jump in the time-derivate of the state is possible, which makes these transitions continuous but nonsmooth.

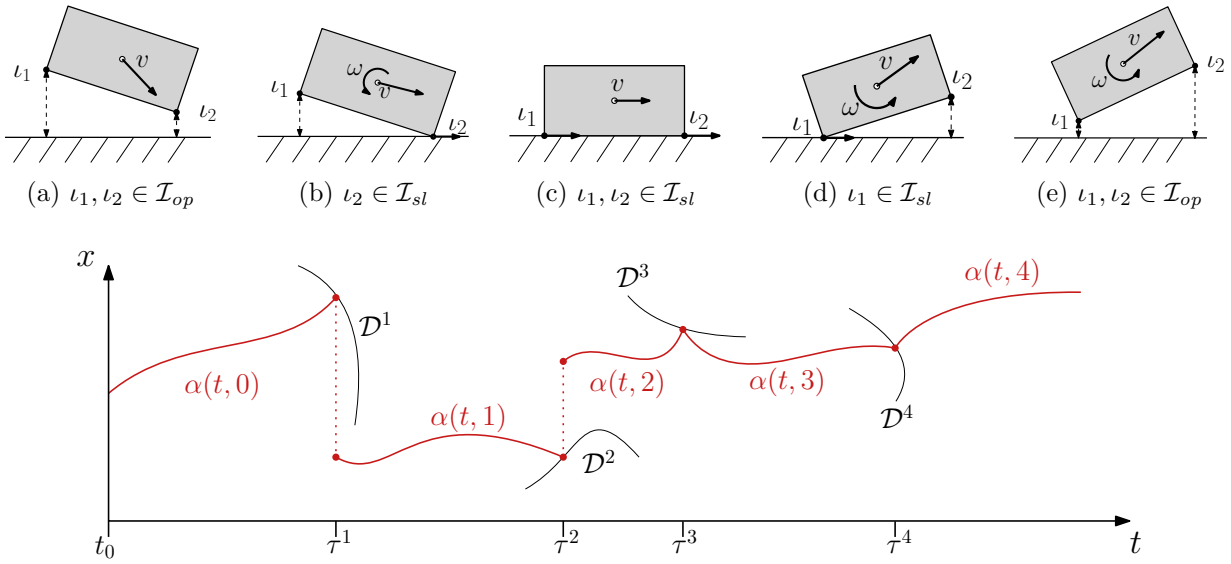

Figure 2.4: *An example trajectory, which satisfies the dynamics* (2.29)*, of a block pushing towards and withdrawing from a surface with velocity v. Note that the sets D besides being dependent on $\boldsymbol{x}$, are also dependent on $\boldsymbol{u}$. Also, although not depicted in this image, the state space of the system varies with every event.*

The following sections will be used to write the complementarity system defined in Section 2.2 into a hybrid system with impulsive effects as in (2.29). In 2.3.2 the continuous dynamics $\boldsymbol{f}^j$ will be derived for mechanical systems with unilateral constraints and spatial friction. Then, in Section 2.3.3 the reset set $\mathcal{D}^j$ will be defined. Finally, in Section 2.3.4 the discrete dynamics $\boldsymbol{g}^j$ will be derived. This will fully define the hybrid system with impulsive effects formulation of mechanical systems with unilateral constraints and spatial friction.

2.3.2 Continuous dynamics

When describing mechanical systems, we take

$$\boldsymbol{x} = \begin{bmatrix} \boldsymbol{q} \\ \dot{\boldsymbol{q}} \end{bmatrix}, \quad \dot{\boldsymbol{x}} = \begin{bmatrix} \dot{\boldsymbol{q}} \\ \ddot{\boldsymbol{q}} \end{bmatrix}, \tag{2.30}$$

where $\boldsymbol{q}$ and $\dot{\boldsymbol{q}}$ are the joint positions, velocities and accelerations respectively. As described in Section 2.2, for mechanical systems a set of contact points $\iota \in \{\iota_1, \iota_2, ..., \iota_c\}$ is defined. Here c is the number of considered contact points. A set $\mathcal{I}_{\text{cl}}$ is defined as the set of closed contact points, such that a contact $\iota \in \mathcal{I}_{\text{cl}}$ has closed a unilateral constraint. The set of contact points in open contact is defined as $\mathcal{I}_{\text{op}} := \{\iota \mid \iota \notin \mathcal{I}_{\text{cl}}\}$. The set $\mathcal{I}_{\text{cl}}$ is subdivided in two subsets $\mathcal{I}_{\text{sl}}$ and $\mathcal{I}_{\text{st}}$, where $\mathcal{I}_{\text{sl}}$ is the set of closed contact points in slip and $\mathcal{I}_{\text{st}}$ the set of closed contact points in stick. Here $\mathcal{I}_{\text{cl}} = \mathcal{I}_{\text{sl}} \cup \mathcal{I}_{\text{st}}$ and $\mathcal{I}_{\text{sl}} \cup \mathcal{I}_{\text{st}} = \emptyset$.

The equations of motion, given in (2.3), can be rewritten to

$$\ddot{\boldsymbol{q}} = \boldsymbol{M}^{-1}(\boldsymbol{q}) \left[\boldsymbol{S}(\boldsymbol{q})\boldsymbol{u} - \boldsymbol{C}(\boldsymbol{q}, \dot{\boldsymbol{q}}) + \boldsymbol{W}_n(\boldsymbol{q})\boldsymbol{\lambda}_n + \boldsymbol{W}_t(\boldsymbol{q})\boldsymbol{\lambda}_t \right], \tag{2.31}$$

with

$$\boldsymbol{W}_n = \left[\boldsymbol{w}_{n,i_1}, \boldsymbol{w}_{n,i_2}, ..., \boldsymbol{w}_{n,\iota} \right] \in \mathbb{R}^{n \times c}, \tag{2.32}$$

$$\boldsymbol{W}_t = \left[\boldsymbol{W}_{t,i_1}, \boldsymbol{W}_{t,i_2}, ..., \boldsymbol{W}_{t,\iota} \right] \in \mathbb{R}^{n \times 2c}, \tag{2.33}$$

$$\boldsymbol{\lambda}_n = \left[\lambda_{n,\iota_1}; \lambda_{n,\iota_2}; ...; \lambda_{n,\iota_c} \right] \in \mathbb{R}^{c}, \tag{2.34}$$

$$\boldsymbol{\lambda}_t = \left[\boldsymbol{\lambda}_{t,\iota_1}; \boldsymbol{\lambda}_{t,\iota_2}; ...; \boldsymbol{\lambda}_{t,\iota_c} \right] \in \mathbb{R}^{2c}, \tag{2.35}$$

Note that since $\boldsymbol{f}^j$ is only defined on $\boldsymbol{x}(t,j), \boldsymbol{u}(t,j) \notin \mathcal{D}^j$, it is not necessary to use $\boldsymbol{\xi}$ to define the equations of motion as done in (2.3). Now $\boldsymbol{f}^j$ can be written as

$$\dot{\boldsymbol{x}}(t,j) = \begin{bmatrix} \dot{\boldsymbol{q}} \\ \boldsymbol{M}^{-1}(\boldsymbol{q}) \left[\boldsymbol{S}(\boldsymbol{q})\boldsymbol{u} - \boldsymbol{C}(\boldsymbol{q}, \dot{\boldsymbol{q}}) + \boldsymbol{W}_n(\boldsymbol{q})\boldsymbol{\lambda}_n + \boldsymbol{W}_t(\boldsymbol{q})\boldsymbol{\lambda}_t \right] \end{bmatrix}. \tag{2.36}$$

The closed contact points in $\mathcal{I}_{\text{cl}}$ experience reaction forces $\lambda_{n,\iota}$ and $\boldsymbol{\lambda}_{t,\iota}$, as can be seen in (2.31). Therefore for all closed contact points $\iota \in \mathcal{I}_{\text{cl}}$ constraints are given which define these reaction forces. These constraints are given by

$$\boldsymbol{w}_{n,\iota}^T(\boldsymbol{q})\ddot{\boldsymbol{q}} + \dot{\boldsymbol{w}}_{n,\iota}^T(\boldsymbol{q})\dot{\boldsymbol{q}} = 0, \qquad \forall \iota \in \mathcal{I}_{\text{cl}}, \tag{2.37}$$

$$\boldsymbol{\lambda}_{t,\iota} + \mu_\iota \lambda_{n,\iota} \operatorname{SgnSp}(\boldsymbol{W}_{t,\iota}^T \dot{\boldsymbol{q}}) = 0, \qquad \forall \iota \in \mathcal{I}_{\text{sl}}, \tag{2.38}$$

$$\boldsymbol{W}_{t,\iota}^T(\boldsymbol{q})\ddot{\boldsymbol{q}} + \dot{\boldsymbol{W}}_{t,\iota}^T(\boldsymbol{q})\dot{\boldsymbol{q}} = 0, \qquad \forall \iota \in \mathcal{I}_{\text{st}}, \tag{2.39}$$

where $\mathcal{I}_{\text{sl}}$ and $\mathcal{I}_{\text{st}}$ are the sets of closed contacts in slip and closed contacts in stick respectively. Now, with (2.36) and (2.37)-(2.39), the continuous dynamics of the hybrid system with impulsive dynamics are correctly defined. A more thorough derivation of these dynamics can be found in Appendix A.1.

System mode descriptor

A system will have different flow dynamics as the system mode changes, as can be seen in (2.37)-(2.39). Also the guard functions that can be activated will change with the mode, as will be shown in Section 2.3.3. Therefore it is necessary to keep track of the mode the system is in. The system mode descriptor σ^j is introduced to conveniently describe the current system mode. Each contact

point can either be in open-contact, closed-contact slip or closed-contact stick. The system mode descriptor is therefore defined as the ordered set

$$\sigma = (\sigma_1, \sigma_2, ..., \sigma_\iota), \tag{2.40}$$

where σ_ι is the mode of contact point ι. σ_ι can either have the value 'op' for a contact point in open-contact, 'sl' for a contact point in closed-contact slip, or 'st' for a contact point in closed-contact stick. For example, the system mode descriptor of the mode in Figure 2.4b is $\sigma = \{\text{op}, \text{sl}\}$.

2.3.3 Discrete event sets

When the continuous dynamics enter an event set $\mathcal{D}$, an event will take place. Such an event can cause a contact point to enter a different set. This will lead to different post-event continuous dynamics, and it can cause the state to reinitialize according to the discrete dynamics presented in Section 2.3.4. For each set of contact points these sets are defined differently. In this section the sets $\mathcal{D}$ are defined for each set of contact points. The derivation of the discrete event sets can be found in Appendix A.1.

Discrete events sets in open contact
For all contact points $\iota \in \mathcal{I}_{\text{op}}$ the discrete event sets are defined as

$$\mathcal{D}_\iota^{\text{op}\to\text{cl}} = \{\boldsymbol{q} \mid \gamma_\iota^{\text{op}\to\text{cl}} = 0,\ \dot{\gamma}_\iota^{\text{op}\to\text{cl}} < 0\}, \tag{2.41}$$

with

$$\gamma_\iota^{\text{op}\to\text{cl}} = h_{n,\iota}(\boldsymbol{q}). \tag{2.42}$$

Discrete events sets in closed contact slip
For all contact points $\iota \in \mathcal{I}_{\text{sl}}$ the discrete event sets are defined as

$$\mathcal{D}_\iota^{\text{sl}\to\text{st}} = \{\boldsymbol{q} \mid \gamma_\iota^{\text{sl}\to\text{st}} = 0,\ \dot{\gamma}_\iota^{\text{sl}\to\text{st}} < 0\}, \tag{2.43}$$
$$\mathcal{D}_\iota^{\text{cl}\to\text{op}} = \{\boldsymbol{q}, \boldsymbol{u} \mid \gamma_\iota^{\text{cl}\to\text{op}} = 0,\ \dot{\gamma}_\iota^{\text{cl}\to\text{op}} < 0\}, \tag{2.44}$$

with

$$\gamma_\iota^{\text{sl}\to\text{st}} = \sqrt{\boldsymbol{\zeta}_{t,\iota}\boldsymbol{\zeta}_{t,\iota}^T}, \tag{2.45}$$
$$\gamma_\iota^{\text{cl}\to\text{op}} = \lambda_{n,\iota}. \tag{2.46}$$

Discrete events sets in closed contact stick
For all contact points $\iota \in \mathcal{I}_{\text{st}}$ the discrete event sets are defined as

$$\mathcal{D}_\iota^{\text{st}\to\text{sl}} = \{\boldsymbol{q}, \boldsymbol{u} \mid \gamma_\iota^{\text{st}\to\text{sl}} = 0,\ \dot{\gamma}_\iota^{\text{sl}\to\text{st}} < 0\}, \tag{2.47}$$
$$\mathcal{D}_\iota^{\text{cl}\to\text{op}} = \{\boldsymbol{q}, \boldsymbol{u} \mid \gamma_\iota^{\text{cl}\to\text{op}} = 0,\ \dot{\gamma}_\iota^{\text{cl}\to\text{op}} < 0\}, \tag{2.48}$$

with

$$\gamma_\iota^{\text{st}\to\text{sl}} = \mu^2\lambda_{n,\iota}^2 - \boldsymbol{\lambda}_{t,\iota}\boldsymbol{\lambda}_{t,\iota}^T, \tag{2.49}$$
$$\gamma_\iota^{\text{cl}\to\text{op}} = \lambda_{n,\iota}. \tag{2.50}$$

These event sets lead to a non-impulsive event, which is described in Section 2.3.4.

2.3.4 Discrete dynamics

A contact point entering a discrete event set $\mathcal{D}$ indicates that the system in its current mode is infeasible. The system should therefore go through a discrete event, in which the state can be reinitialized and the mode can be changed to a feasible system. One contact point entering a discrete event set can lead to other contact points experiencing infeasible reaction forces, making it difficult to determine in what mode each contact point should be. The reinitialization of the state and selection of a post-event mode is described by the discrete dynamics in this section. First a *nonlinear complementarity problem* (NCP) is solved to reinitialize the state. The NCP generates a unique feasible solution [65], which for simple systems can be found by iterating over all solutions until the feasible solution is found. Then a mode selection algorithm is presented to find a feasible post-event mode, which defines the continuous dynamics to be integrated after the event.

State reinitialization
From the impulsive dynamics (2.23)-(2.26), the discrete dynamics for an impulsive event which determine the post-event state $\boldsymbol{q}^+$ can be derived as

$$\dot{\boldsymbol{q}}^+ = \boldsymbol{M}^{-1}\left[\boldsymbol{W}_n\boldsymbol{\Lambda}_n + \boldsymbol{W}_t\boldsymbol{\Lambda}_t\right] + \dot{\boldsymbol{q}}^-, \tag{2.51}$$

$$\boldsymbol{w}_{n,\iota}^T\dot{\boldsymbol{q}}^+ = 0, \qquad \forall \iota \in \mathcal{I}_{\mathrm{cl}}, \tag{2.52}$$

$$\boldsymbol{\Lambda}_{t,\iota} + \mu\Lambda_{n,\iota}\,\mathrm{SgnSp}(\boldsymbol{\zeta}_{t,\iota}^-) = 0, \qquad \forall \iota \in \mathcal{I}_{\mathrm{sl}}, \tag{2.53}$$

$$\boldsymbol{W}_{t,\iota}^T\dot{\boldsymbol{q}}^+ = 0, \qquad \forall \iota \in \mathcal{I}_{\mathrm{st}}. \tag{2.54}$$

Here the unknown variables are $\dot{\boldsymbol{q}}^+ \in \mathbb{R}^n$, $\boldsymbol{\Lambda}_n \in \mathbb{R}^{c_{\mathrm{cl}}}$ and $\boldsymbol{\Lambda}_t \in \mathbb{R}^{2c_{\mathrm{cl}}}$, which means that there are $n + 3c_{\mathrm{cl}}$ unknown variables. From (2.51) we get n equations, from (2.52) we get c_{cl} equations and since $\mathcal{I}_{\mathrm{sl}} \cup \mathcal{I}_{\mathrm{st}} = \mathcal{I}_{\mathrm{cl}}$, $\boldsymbol{\lambda}_{t,\iota} \in \mathbb{R}^2$, and $\boldsymbol{W}_{t,\iota}^T\ddot{\boldsymbol{q}}^+ + \dot{\boldsymbol{W}}_{t,\iota}^T\dot{\boldsymbol{q}}^+ \in \mathbb{R}^2$ we get $2c_{\mathrm{cl}}$ equations from (2.53)-(2.54). Since we have $n + 3c_{\mathrm{cl}}$ unknown variables and $n + 3c_{\mathrm{cl}}$ equations, the system is solvable.

The problem that remains is that it is not straightforward to know which dynamics to solve, because the dynamics change as the system-mode changes. The set of equations that should be solved is the set of equations that corresponds to the system-mode which generates a feasible post-event state. When a contact point enters a discrete event set, and thus generates an infeasible state, it can be concluded that the system will go through an event because in it's current mode the system is infeasible. However, it is not guaranteed that the contact point which entered the event set will change their mode. Actually any contact point, or even several contact points, can change their mode. Therefore the dynamics should be solved for several modes, until a feasible post-event state is found. A feasible post-event state is a post-event state solved for a certain system-mode σ, such that the all corresponding guard functions are in its unactivated state, i.e., all $\Gamma_\iota > 0$. As mentioned earlier, there will exist a unique system-mode where the system has a feasible post-impact state. Similar to the non-impulsive guard functions defined in Section 2.3.3, the impulsive guard functions are given by

$$\Gamma_\iota^{\mathrm{cl}\to\mathrm{op}} = \Lambda_{n,\iota}, \tag{2.55}$$

$$\Gamma_\iota^{\mathrm{sl}\to\mathrm{st}} = \boldsymbol{\zeta}_{t,\iota}^+(\boldsymbol{\zeta}_{t,\iota}^+)^T, \tag{2.56}$$

$$\Gamma_\iota^{\mathrm{st}\to\mathrm{sl}} = \mu^2\Lambda_{n,\iota}^2 - \boldsymbol{\Lambda}_{t,\iota}\boldsymbol{\Lambda}_{t,\iota}^T. \tag{2.57}$$

Note that all guard functions are defined at velocity level during the state reinitialization. The NCP is defined at velocity level, meaning that only guard functions on velocity level need to be considered. For example, it is impossible for the state reinitialization to generate an infeasible position because the position of the system is not updated during the state reinitialization. When $\Lambda_{n,\iota} = 0$ and $\boldsymbol{\Lambda}_{t,\iota} = 0$ during an event, one speaks of a non-impulsive event. In this case the state

is not reinitialized during the event. However, the system will enter a different mode however. For both impulsive and non-impulsive events the post-event mode is determined during the mode selection, which is described below.

Mode selection
The mode σ of a system is determined by the guard functions defined in Section 2.3.3. All guard functions γ_ι should be greater than zero for the system to be in a feasible mode. Because some of these guard functions are defined on acceleration level and the post-event acceleration is not constrained by the NCP, we should first find a post-event mode σ^+ where the accelerations $\ddot{\boldsymbol{q}}$ and reaction forces $\boldsymbol{\lambda}_n, \boldsymbol{\lambda}_t$ are feasible before we know which continuous dynamics describe a feasible system. From the continuous dynamics (2.16)-(2.19), post-event accelerations and reaction forces are defined by

$$\ddot{\boldsymbol{q}}^+ = \boldsymbol{M}^{-1}\left[\boldsymbol{S}\boldsymbol{u}^+ - \boldsymbol{C} + \boldsymbol{W}_n\boldsymbol{\lambda}_n^+ + \boldsymbol{W}_t\boldsymbol{\lambda}_t^+\right], \tag{2.58}$$

$$\boldsymbol{w}_{n,\iota}^T\ddot{\boldsymbol{q}}^+ + \dot{\boldsymbol{w}}_{n,\iota}^T\dot{\boldsymbol{q}}^+ = 0, \qquad \forall \iota \in \mathcal{I}_{\mathrm{cl}}, \tag{2.59}$$

$$\boldsymbol{\lambda}_{t,\iota}^+ + \mu\lambda_{n,\iota}^+ \operatorname{SgnSp}(\boldsymbol{W}_{t,\iota}^T\dot{\boldsymbol{q}}^+) = 0, \qquad \forall \iota \in \mathcal{I}_{\mathrm{sl}}, \tag{2.60}$$

$$\boldsymbol{W}_{t,\iota}^T\ddot{\boldsymbol{q}}^+ + \dot{\boldsymbol{W}}_{t,\iota}^T\dot{\boldsymbol{q}}^+ = 0, \qquad \forall \iota \in \mathcal{I}_{\mathrm{st}}, \tag{2.61}$$

where $\boldsymbol{M}$, $\boldsymbol{S}$, $\boldsymbol{C}$, $\boldsymbol{w}_{n,\iota}$ and $\boldsymbol{W}_{t,\iota}$ are evaluated at the post-event state $\boldsymbol{q}^+$ and state time-derivative $\dot{\boldsymbol{q}}^+$. Because we are interested in whether the accelerations and reaction forces are feasible, the guard functions defined on acceleration level are evaluated. The guard functions that determine the feasibility of a post-event mode are given by

$$\gamma_\iota^{\mathrm{cl}\to\mathrm{op}}(\ddot{\boldsymbol{q}}) = \lambda_{n,\iota}, \qquad \forall \iota \in \mathcal{I}_{\mathrm{cl}}, \tag{2.62}$$

$$\gamma_\iota^{\mathrm{st}\to\mathrm{sl}}(\ddot{\boldsymbol{q}}) = \mu_\iota^2\lambda_{n,\iota}^2 - \boldsymbol{\lambda}_{t,\iota}\boldsymbol{\lambda}_{t,\iota}^T, \qquad \forall \iota \in \mathcal{I}_{\mathrm{st}}, \tag{2.63}$$

with $\mathcal{I}_{\mathrm{sl}} \cup \mathcal{I}_{\mathrm{st}} = \mathcal{I}_{\mathrm{cl}}$. Note that the guard functions $\gamma_\iota^{\mathrm{op}\to\mathrm{cl}}$ and $\gamma_\iota^{\mathrm{sl}\to\mathrm{st}}$ are not evaluated. This is unnecessary, because contact points in open contact can only activate guard functions defined at position level. Since the non-impulsive dynamics only update the acceleration, it is impossible for a contact point in open contact to change mode during an impulsive event. This also holds for the guard function from slip to stick, which is defined on velocity level.

The process of solving a hybrid system with impulsive effects is illustrated in Figure 2.5. The system first flows according to some continuous dynamics. When an event set $\mathcal{D}$ is entered, the system gives a ante-event state $\boldsymbol{x}^-$. Then during the state reinitialization an NCP is solved using the ante-event state, which determines the post-event state $\boldsymbol{x}^+$. Finally, the mode selection is solved, which finds a feasible post-event mode σ^+ for that post-event state $\boldsymbol{x}^+$. The continuous dynamics for the next flow segment is defined by σ^+ with $\boldsymbol{x}^+$ the initial condition.

2.4 Summary

The modeling of mechanical systems with unilateral constraints and spatial friction is presented in this chapter. First a complementarity problem formulation of such systems is presented, using Signorini's contact law, Poisson's impact law and Coulomb's friction law. This system fully defines the dynamics of mechanical systems with unilateral constraints and spatial friction. From the complementarity problem formulation a hybrid system with impulsive effects is derived. This system is defined with a control point-of-view in mind, and its compatibility with the control strategy that will be presented in the following chapters. The hybrid system is defined in three parts. First the continuous dynamics are presented. Then the discrete event sets are given, which are state-input

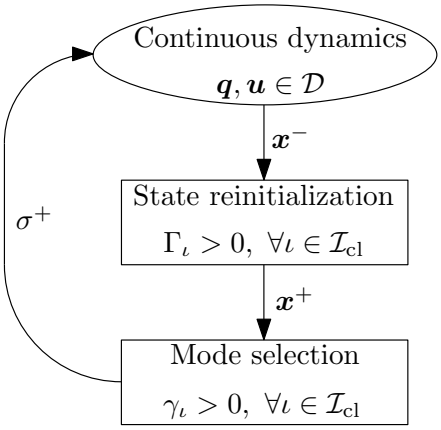

Figure 2.5: *The algorithm used to solve a hybrid system with impulsive effects depicted in a flowchart.*

sets that trigger a discrete event when the state and input enters such a set. Finally the dynamics of such an event are presented, which consist of a state reinitialization and a mode selection.

Chapter 3

Tracking for Hybrid Systems: Isolated State-and-Input-Triggered Events

In this chapter, a control strategy is presented for trajectories of hybrid systems which, due to the introduction of perturbations, experience isolated state-and-input-triggered events. Such systems are called *nonlinear state-and-input-triggered hybrid systems* (NSITHS). Isolated state-and-input-triggered events are considered, which means that the guard functions are activated separately, such that there is always flow between the events. The perturbations are assumed small enough that they can cause the state trajectory to jump at a different time than the nominal reference trajectory, but not cause the system to activate other guards or experience other events. The mismatch in event time between the nominal trajectory and state trajectory can result in *peaking behavior* of the tracking error [41, 42]. First, a notion of error is presented, which is used to avoid peaking behavior. After that a first-order approximation of the NSITHS is presented in the form of a *linear time triggered hybrid system* (LTTHS). A proof is given in [55], which shows that the stability of the LTTHS can be used to asses the local stability of the original NSITHS. Consequentially, conventional stability analysis tools for LTTHS can be used to asses the local stability of te NSITHS. Finally, a short summary of the findings in this chapter is given. The work in this chapter is an extension to [55], where the sensitivity analysis in this chapter is suitable for input-dependent guard functions.

3.1 State-input perturbations in trajectories with state-jumps

This section presents *reference-spreading* (RS) for ordered guard activations. First the tracking problem is presented. The perturbations introduced in the state trajectory cause the state trajectory and reference trajectory to have non-coinciding event-times. This mismatch in event-times results in peaking behavior in the tracking error, meaning that two relatively large jumps can be observed. Using reference-spreading this peaking behavior can be avoided, resulting in a tracking error where only one relatively smaller jump is observed.

3.1.1 Nonlinear state-and-input-triggered hybrid systems

As presented in Section 2.3.1, a mechanical system can be described by the hybrid system with impulsive effects framework. Such a system is a nonlinear state-and-input-triggered hybrid system. The NSITHS is now formally defined.

Definition 1 (NSITHS)**.** *The nonlinear state-and-input-triggered hybrid system is given by*

$$\begin{aligned} \dot{\boldsymbol{x}}(t,j) &= \boldsymbol{f}^j(\boldsymbol{x}(t,j),\boldsymbol{u}(t,j),t), && \boldsymbol{x}(t,j),\boldsymbol{u}(t,j) \in \mathcal{C}^j \\ \boldsymbol{x}(t,j+1) &= \boldsymbol{g}^{j+1}(\boldsymbol{x}(t,j),\boldsymbol{u}(t,j),t), && \boldsymbol{x}(t,j),\boldsymbol{u}(t,j) \in \mathcal{D}^{j+1} \end{aligned} \tag{3.1}$$

where $\boldsymbol{f}^j$ is a nonlinear Lipschitz continuous function. $\mathcal{C}^j$ is the flow set after event j, and $\mathcal{D}^{j+1}$ a state-input set, where when $\boldsymbol{x}(t,j),\boldsymbol{u}(t,j) \in \mathcal{D}^{j+1}$ a state reinitialization is triggered according to $\boldsymbol{x}(t,j+1) = \boldsymbol{g}^{j+1}(\boldsymbol{x}(t,j),\boldsymbol{u}(t,j),t)$.

The nominal trajectory of an NSITHS is illustrated in Figure 3.1 in red. Some minimal regularity conditions on the NSITHS are defined, which are necessary for the sensitivity analysis presented later. Formally, the following assumptions are made.

Assumption 1 (t-completeness and non-Zeno behavior of $\boldsymbol{\alpha}$)**.** *The reference trajectory $\boldsymbol{\alpha}$ is defined for all $t > t_0$. Also, the reference trajectory segments $\boldsymbol{\alpha}(t,j)$ have non-vanishing time-domains $I^j_{\boldsymbol{\alpha}}$.*

Assumption 1 guarantees that the number of events N will only go to infinity if time t goes to infinity as well. This assumption is often made in analysis using hybrid systems. It can then be guaranteed that there is non-zero time between events, if $\boldsymbol{g}(\boldsymbol{\alpha}(\tau^{j+1},j),\boldsymbol{\mu}(\tau^{j+1},j),j+1) \notin \mathcal{D}^{j+1}$. The t-completeness of $\boldsymbol{\alpha}$ guarantees that there is always a trajectory defined for the system to track.

Now an initial state and input perturbation ϵ is introduced, which causes the state trajectory $\boldsymbol{x}$ to differ from the reference trajectory $\boldsymbol{\alpha}$. The goal is to write a control strategy, such that the perturbed state trajectory $\boldsymbol{x}$ will converge to the reference trajectory $\boldsymbol{\alpha}$. Now an initial state-input perturbation $z_0 = \frac{\partial \boldsymbol{x}}{\partial \epsilon}$ is introduced, where ϵ is a scalar perturbation parameter. The initial state $\boldsymbol{\alpha}_0$ and input $\boldsymbol{\mu}_0$ of the reference trajectory $\boldsymbol{\alpha}$ is perturbed, resulting in $\boldsymbol{x}_0(\epsilon) = \boldsymbol{\alpha}_0 + \epsilon \boldsymbol{z}_0$ and $\boldsymbol{u}(t,j,\epsilon) = \boldsymbol{\mu}(t,j) + \epsilon \boldsymbol{v}(t,j)$. This generates a trajectory close to the reference trajectory $\boldsymbol{\alpha}$, which is also dependent on the initial state and input perturbation ϵ, i.e., $\boldsymbol{x}(t,j,\epsilon)$.

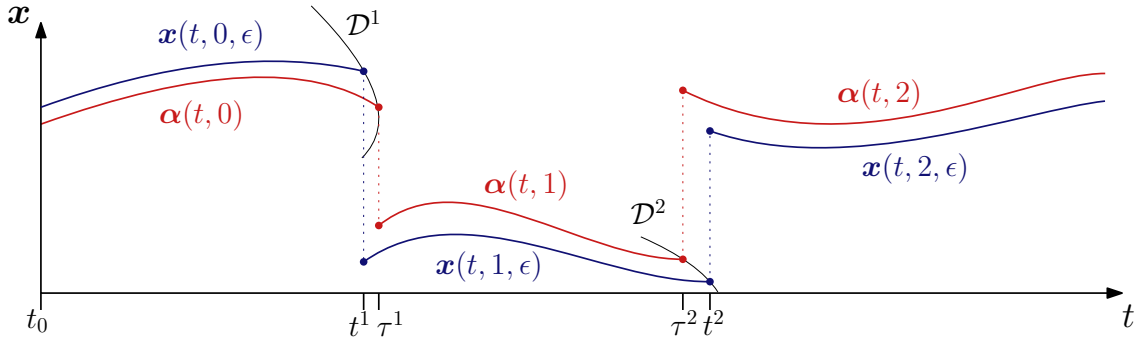

Figure 3.1: *in orange the nominal (unperturbed) and in cyan the perturbed trajectory of a hybrid system with impulsive effects. Due to the perturbation in the cyan trajectory, a mismatch between the perturbed and the nominal event times arises.*

For the nominal trajectory the state and input are known over the entire time-domain, meaning that the event-times are also known. For the perturbed trajectory this is not the case. Due to the uncertainty in the state and input, there is an uncertainty in the event-times as well. This uncertainty can cause a mismatch between the nominal event times τ^1,τ^2 and the perturbed event times t^1,t^2. Now we take a closer look at the first event, to illustrate the peaking behavior as a result of a jump mismatch. In Figure 3.2 the state evolution x of the first event is depicted besides the tracking error $||\boldsymbol{x} - \boldsymbol{\alpha}||$. Here on can clearly see that a peak arises in the tracking error when the jump times do not coincide. At t^1 the state trajectory jumps, while the reference trajectory

does not. At τ^1 the reference trajectory jumps as well. This means that in $[t^1, \tau^1]$, a post-event state trajectory is compared to a ante-event reference trajectory, resulting in a large peak in the tracking error. This is undesirable, as it will lead to large and unnecessary actuation forces.

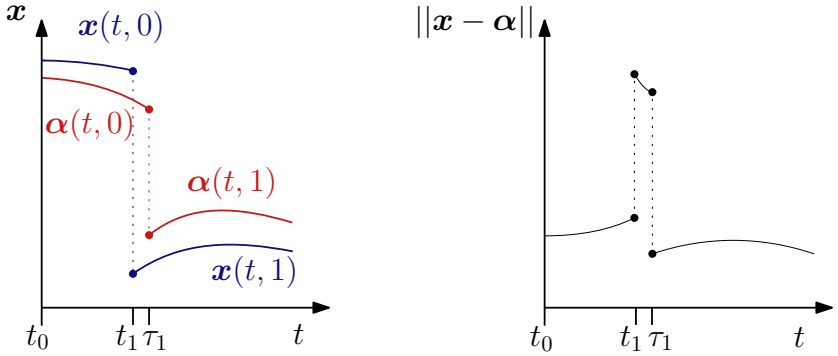

Figure 3.2: *A closer look at the first event of the trajectory in Figure 3.1. On the left the state-evolution x is depicted and on the right the tracking error $||\boldsymbol{x}-\boldsymbol{\alpha}||$. A clear peak can be noticed in the tracking error as a result from the event-time mismatch.*

In the next section a solution to the peaking behavior is presented.

3.1.2 Reference-spreading

To avoid peaking behavior in the tracking error, in [49] a novel notion of error is presented which is named reference spreading in [53]. This control strategy uses reference trajectories which are extended beyond event-times, such that an ante-event state trajectories can always be compared to an ante-event reference trajectory and a post-event state trajectories can always be compared to a post-event reference trajectory. This is illustrated in Figure 3.3, where the reference trajectory segments $\boldsymbol{\alpha}(t,j)$ are all extended resulting in $\overline{\boldsymbol{\alpha}}(t,j)$. Adopting the notation of [16], the hybrid domain of $\boldsymbol{\alpha}$ is defined by segments $I^j_{\boldsymbol{\alpha}} = [\tau^j, \tau^{j+1}]$, which together form the entire domain of $\boldsymbol{\alpha}$ as

$$\operatorname{dom} \boldsymbol{\alpha} = \bigcup_{j=0}^{N} I^j_{\boldsymbol{\alpha}} \times \{j\}. \tag{3.2}$$

Similarly the state segments $x(t,j)$ are defined on the domain $I^j_{\boldsymbol{x}} = [t^j, t^{j+1}]$ with the entire domain defined as

$$\operatorname{dom} \boldsymbol{x} = \bigcup_{j=0}^{N} I^j_{\boldsymbol{x}} \times \{j\}. \tag{3.3}$$

The domain of the extended reference trajectory segments is extended such that $I^j_{\boldsymbol{x}} \subseteq I^j_{\overline{\boldsymbol{\alpha}}}$. The set of jump times of $\boldsymbol{\alpha}(t,j)$ and $\boldsymbol{x}(t,j,\epsilon)$ are denoted as

$$\operatorname{eve} \boldsymbol{\alpha} = \bigcup_{j=1}^{N} \{\tau^j\} \times \{j-1\}, \tag{3.4}$$

$$\operatorname{eve} \boldsymbol{x} = \bigcup_{j=1}^{N} \{t^j\} \times \{j-1\}, \tag{3.5}$$

respectively.

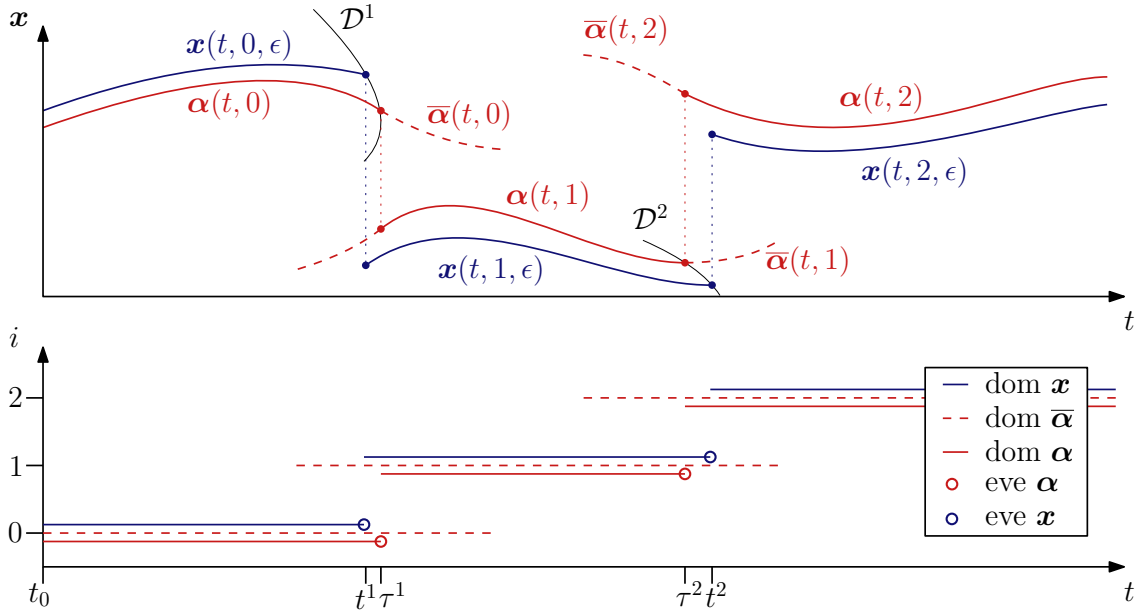

Figure 3.3: *An illustration of the nominal reference trajectory (orange) and the perturbed trajectory (cyan), where the nominal reference trajectory is extended such that* $\operatorname{dom} x \subseteq \operatorname{dom} \overline{\alpha}$.

Now a continuity based assumption on the vector field $\boldsymbol{f}$ is defined. This assumption uses the extended reference trajectory $\overline{\boldsymbol{\alpha}}$ illustrated in Figure 3.3.

Assumption 2 (Lipschitz continuity of $\boldsymbol{f}$)**.** *We assume that in a neighborhood of the reference trajectory* $\boldsymbol{\alpha}$*,* $\boldsymbol{f}$ *is Lipschitz with respect to* $\boldsymbol{x}$ *uniformly in* t *and* j*. I.e.,* $\exists \varepsilon_{\boldsymbol{f}} > 0$ *and* $\exists L$*, independent of* t, j*, such that* $\forall i$*,* $||\boldsymbol{f}(\boldsymbol{a},t,j) - \boldsymbol{f}(\boldsymbol{b},t,j)|| < L||a-b||$*,* $\forall t \in (\tau^j - \varepsilon_{\boldsymbol{f}}, \tau^{j+1} + \varepsilon_{\boldsymbol{f}})$ *and* $\forall \boldsymbol{a},\boldsymbol{b} \in B_{\varepsilon_{\boldsymbol{f}}}(\overline{\boldsymbol{\alpha}}(t,j))$*, where* $B_{\varepsilon_{\boldsymbol{f}}}(\overline{\boldsymbol{\alpha}}(t,j))$ *is a ball with radius* $\epsilon_{\boldsymbol{f}}$ *around* $\overline{\boldsymbol{\alpha}}(t,j)$*).*

In Assumption 2 it is clear why the extended reference trajectory $\overline{\boldsymbol{\alpha}}$ is necessary. The Lipschitz continuity condition is defined on the interval $t \in (\tau^j - \varepsilon_{\boldsymbol{f}}, \tau^{j+1} + \varepsilon_{\boldsymbol{f}}) \supset \operatorname{dom} \boldsymbol{\alpha}$, which means that an extension of $\boldsymbol{\alpha}$ is necessary to be able to define this assumption.

In the lower plot of Figure 3.3 the domains of $\boldsymbol{x}$, $\boldsymbol{\alpha}$ and $\overline{\boldsymbol{\alpha}}$ are illustrated for each segment. Note that for every segment, $I^j_{\boldsymbol{x}} \subseteq I^j_{\overline{\boldsymbol{\alpha}}}$. This means that when the tracking error is defined as $||\boldsymbol{x} - \overline{\boldsymbol{\alpha}}||$, we can keep tracking the error $||\boldsymbol{x}(t,j) - \overline{\boldsymbol{\alpha}}(t,j)||$ until an event is detected. Even if the event-time $t^j > \tau^j$. When an event is detected, the error $||\boldsymbol{x}(t,j+1) - \overline{\alpha}(t,j+1)||$ can be tracked. Again, because $I^{j+1}_{\boldsymbol{x}} \subseteq I^{j+1}_{\overline{\boldsymbol{\alpha}}}$, this is also possible for the case where $t^j < \tau^j$. Using this notion of error leaves only one jump in the tracking error, even under the presence of event-time mismatches. More importantly, the peak in the tracking error is avoided, an ante-event state trajectory will not be compared to a post-event reference trajectory (and vice versa) anymore. In Figure 3.4 the tracking error with and without reference spreading are compared. Here it is clear that the tracking defined using reference spreading does not have the peak which the normal notion of error does have. It also jumps only once at the perturbed event-time t_1.

In the next section the error defined using reference spreading is used to make a first-order approximation of perturbed trajectories with ordered guard-activation.

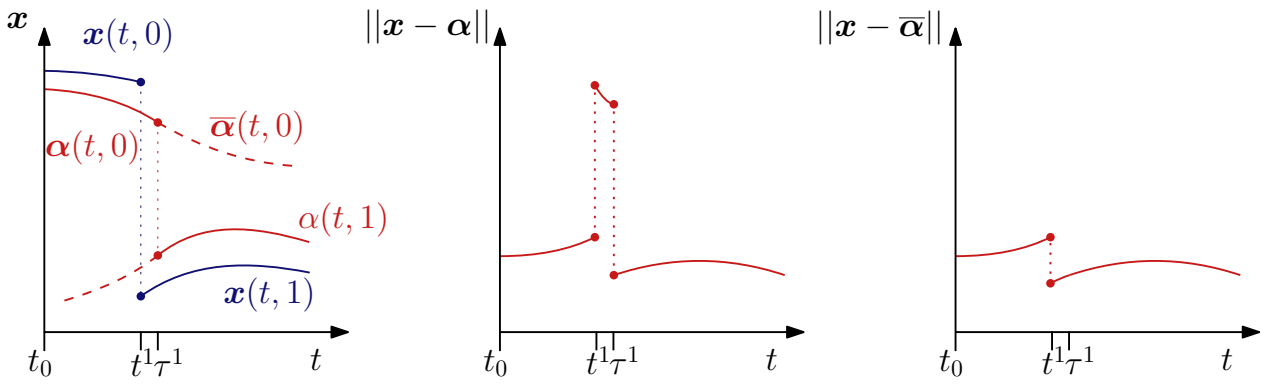

Figure 3.4: *A close up of the first event of the reference trajectory, in which the peaking behavior is cleary removed by evaluating the extended reference trajectory.*

3.2 First-order approximation of trajectories with ordered guard-activations

In [51] a sensitivity analysis is presented, where so-called sensitivity functions are used to provide first-order approximations of the effects of parameter variations on solutions. These sensitivity functions can also be used to approximate the solution under parameter variations, when the variations are close enough to zero. In the case of mechanical systems experiencing perturbations, the sensitivity equations describe the system's response the initial state-input perturbations. These perturbation dynamics can be used to formulate a first-order approximation of the perturbed state of the system. To find a first-order approximation of state reinitializations in nonsmooth trajectories, an extension to this sensitivity analysis is necessary in the form of a linearized jump gain. The linearized jump gain and the linearized perturbation dynamics together define an LTTHS, which can guarantee local asymptotic stability of the NSITHS when the LTTHS is stable [55]. For a more thorough derivation of the analysis performed in this section, Appendix C should be consulted. Now some assumptions are defined, which are necessary to be able to perform the sensitivity analysis.

Assumption 3 (Existence of a guard function)**.** *We assume that there exist constants ε_γ, and real valued guard function $\gamma(\boldsymbol{x},\boldsymbol{u},t,j)$ which is continuously differentiable with respect to $\boldsymbol{x}$, $\boldsymbol{u}$, and t, for each $j \in \{1,2,...,N\}$, such that*

$$\begin{aligned}
&\gamma(\boldsymbol{x},\boldsymbol{u},t,j) > 0 \qquad && (\boldsymbol{x},\boldsymbol{u},t) \in B_{\varepsilon_\gamma}(\boldsymbol{\alpha}(\tau,j),\boldsymbol{\mu}(\tau,j),\tau) \cap \mathcal{C}^j \setminus \partial\mathcal{C}^j \\
&\gamma(\boldsymbol{x},\boldsymbol{u},t,j) = 0 \qquad && (\boldsymbol{x},\boldsymbol{u},t) \in B_{\varepsilon_\gamma}(\boldsymbol{\alpha}(\tau,j),\boldsymbol{\mu}(\tau,j),\tau) \cap \mathcal{D}^{j+1} \\
&\gamma(\boldsymbol{x},\boldsymbol{u},t,j) < 0 \qquad && (\boldsymbol{x},\boldsymbol{u},t) \in B_{\varepsilon_\gamma}(\boldsymbol{\alpha}(\tau,j),\boldsymbol{\mu}(\tau,j),\tau) \cap (\mathbb{R}^n \times \mathbb{R}^m \times \mathbb{R}) \setminus \mathcal{C}^j
\end{aligned} \tag{3.6}$$

where $B_{\varepsilon_\gamma}(\boldsymbol{\alpha}(\tau,j),\tau)$ is a ball with radius ε_γ around $\boldsymbol{\alpha}(\tau,j)$ with $\tau = \tau^{j+1}$. $\mathcal{C}^j$ is the flow set of a trajectory after event j and $\mathcal{D}^{j+1}$ is the event set which triggers event $j+1$, which is defined as $\partial\mathcal{C}^j$, where $\partial\mathcal{C}^j$ represents the boundary of flow set $\mathcal{C}^j$ (existence of a guard function).

Assumption 4 (Transversal guard activations)**.** *Under Assumption 3, we assume there exists a constant $c > 0$, such that*

$$\begin{aligned}
D_1\gamma(\boldsymbol{\alpha}(t,j),\boldsymbol{\mu}(t,j),t,j)\cdot\boldsymbol{f}(\boldsymbol{\alpha}(t,j),\boldsymbol{\mu}(t,j),t,j) + D_2\gamma(\boldsymbol{\alpha}(t,j),\boldsymbol{\mu}(t,j),t,j)\cdot\boldsymbol{f}(\boldsymbol{\alpha}(t,j),\boldsymbol{\mu}(t,j),t,j) + \\
D_3\gamma(\boldsymbol{\alpha}(t,j),\boldsymbol{\mu}(t,j),t,j) \leq -c,
\end{aligned} \tag{3.7}$$

for every event time $(t,j) \in E_{\boldsymbol{\alpha}}$.

Remark 1. *The guard function time derivative of* $\gamma^{sl\to st} = \sqrt{\boldsymbol{\zeta}_t^T \boldsymbol{\zeta}_t}$*, i.e.* $\dot{\gamma}^{sl\to st} =$ *is undefined for* $\gamma^{sl\to st}$*. Therefore a Taylor expansion is used to create a first order approximation of the left limit of* $\dot{\gamma}^{sl\to st}$ *at* $t = \tau^j$*, to check whether the guard is activated transversally. More information on this can be found in Appendix A.1.2.*

Assumption 5 (Perturbation-independent guard-event pairs)**.** *With the set of all participating guard functions* γ_{part}*, we assume that there exist a constant* ε_γ*, and set of nominal activated guard functions* γ^j_{nom}*, such that*

$$\gamma_{\text{part}} \setminus \gamma^j_{\text{nom}} > 0, \quad \forall \boldsymbol{x}, \boldsymbol{u} \in B_{\varepsilon_\gamma}(\boldsymbol{\alpha}(\tau, j), \boldsymbol{\mu}(\tau, j), \tau), \tag{3.8}$$

where $\gamma^j = \gamma(\boldsymbol{x}, \boldsymbol{u}, t, j)$*, and* $B_{\varepsilon_\gamma}(\boldsymbol{\alpha}(\tau, j), \boldsymbol{\mu}(\tau, j), \tau)$ *is a ball with radius* ε_γ *centered around the ante-event state and input* $\boldsymbol{\alpha}(\tau, j), \boldsymbol{\mu}(\tau, j)$ *of event* j*.*

Assumption 3 guarantees that the guard function exists in a ball around the nominal ante-event state. In other words, it assumes that the properties of a guard function, i.e., $\gamma > 0$ in the flow set, $\gamma = 0$ in the event set, and $\gamma < 0$ outside of the flow set, are maintained in a ball around the nominal ante-event state $B_{\varepsilon_\gamma}(\boldsymbol{\alpha}(\tau, j), \tau)$. $\gamma(\boldsymbol{x}, \boldsymbol{u}, t, j) = 0$ represents the set where an event will happen, which together with Assumption 4 guarantees that an event will happen, even under perturbations. Assumption 4 assumes that the vector field pushes the reference trajectory out of the flow set $\mathcal{C}^j$, and that grazing incidents are avoided. The combination of the existence of a guard function in an area around the nominal ante-event state and the transversal guard activation guarantees that there exists a range of perturbations where the guard is activated as well. Assumption 5 makes sure that the perturbed trajectory will activate the same guard functions as the reference trajectory. Now an assumption of the jump maps $\boldsymbol{g}$ is defined.

Assumption 6 (Locally differentiable jump map)**.** *We assume that for all* $i \in [1, 2, ..., N]$ *the jump map* $\boldsymbol{g}(\boldsymbol{x}, \boldsymbol{u}, j)$ *is locally differentiable, in the sense that* $D_1\boldsymbol{g}(\boldsymbol{x}, \boldsymbol{u}, j)$ *and* $D_2\boldsymbol{g}(\boldsymbol{x}, \boldsymbol{u}, j)$ *exist in the ball* $B_{\varepsilon_\gamma}(\boldsymbol{\alpha}(\tau, j), \tau)$*, where* B_{ε_γ} *is the ball in which* γ *exist and* $\tau = \tau^{j+1}$*.*

The differentiability of the jump map is necessary to make a first-order approximation of the perturbed state trajectory. This is explained in more detail in the next section.

3.2.1 Sensitivity analysis

The sensitivity analysis for the continuous segments of a perturbed trajectory, gives a set of equations which describe the systems reaction to an initial state-input perturbation. The perturbed state is defined as

$$\boldsymbol{x}(t, j, \epsilon) = \boldsymbol{x}(t_0, j, \epsilon) + \int_{t_0}^{t} \boldsymbol{f}^j(\boldsymbol{x}(s, j, \epsilon), \boldsymbol{u}(s, j, \epsilon), s)ds, \tag{3.9}$$

with the input chosen as $\boldsymbol{u}(t, j, \epsilon) = \overline{\boldsymbol{\mu}} - \boldsymbol{K}\left(\boldsymbol{x}(t, j, \epsilon) - \boldsymbol{\alpha}(t, j)\right)$, where $\overline{\boldsymbol{\mu}}$ is a feedforward term that generates the reference trajectory $\boldsymbol{\alpha}$ and $\boldsymbol{K}\left(\boldsymbol{x}(t, j, \epsilon) - \boldsymbol{\alpha}(t, j)\right)$ is a feedback term to achieve tracking of the reference. To find a first-order approximation of the perturbed state, the perturbed state direction $\boldsymbol{z}(t)$ and the perturbed input direction $\boldsymbol{v}(t)$ are defined as

$$\boldsymbol{z}(t, j) = \left.\frac{\partial \boldsymbol{x}(t, j, \epsilon)}{\partial \epsilon}\right|_{\epsilon=0}, \text{ and } \boldsymbol{v}(t, j) = \left.\frac{\partial \boldsymbol{u}(t, j, \epsilon)}{\partial \epsilon}\right|_{\epsilon=0} = -\boldsymbol{K}(t)\boldsymbol{z}(t). \tag{3.10}$$

Then the sensitivity analysis in [51] gives a first-order approximation of the state based on a Taylor series of $\boldsymbol{x}^j(t,\epsilon)$ with respect to ϵ as

$$\boldsymbol{x}(t,j,\epsilon) = \boldsymbol{x}(t,j,0) + \epsilon \left.\frac{\partial \boldsymbol{x}(t,j,\epsilon)}{\partial \epsilon}\right|_{\epsilon=0} + o(\epsilon), \tag{3.11}$$

$$= \boldsymbol{\alpha}(t,j) + \epsilon \boldsymbol{z}(t,j) + o(\epsilon), \tag{3.12}$$

with $o(\epsilon)$ indicating the little-o notation of ϵ which represents higher order terms. To find a first order approximation of the $\dot{\boldsymbol{x}}(t,j,\epsilon)$, an expression for $\dot{\boldsymbol{z}}(t,j)$ should be found. By first taking the partial derivative with respect to ϵ and then with respect to t of (3.9), the perturbation dynamics are found to be

$$\dot{\boldsymbol{z}}(t,j) = \boldsymbol{A}(t,j)\boldsymbol{z}(t,j) + \boldsymbol{B}(t,j)\boldsymbol{v}(t,j), \tag{3.13}$$

with

$$\boldsymbol{A}(t,j) = D_1\boldsymbol{f}(\boldsymbol{\alpha}(t,j), \boldsymbol{\mu}(t,j), t, j), \tag{3.14}$$

$$\boldsymbol{B}(t,j) = D_2\boldsymbol{f}(\boldsymbol{\alpha}(t,j), \boldsymbol{\mu}(t,j), t, j), \tag{3.15}$$

where D_a is defined as the partial derivative of the function that follows with respect to the a^{th} argument of that function evaluated at $\epsilon = 0$. The first order approximation of the perturbed state dynamics in continuous time is then defined as

$$\dot{\boldsymbol{x}}(t,j,\epsilon) \approx \dot{\boldsymbol{\alpha}}(t,j) + \epsilon\dot{\boldsymbol{z}}(t,j), \tag{3.16}$$

where $\dot{\boldsymbol{\alpha}}(t,j)$ is known from the tracked reference trajectory and $\dot{\boldsymbol{z}}(t,j)$ is known from the sensitivity analysis performed on the system. Now the first-order approximation is defined for the continuous segments of a trajectory. What remains is that the state reinitializations should be linearized as well. The reinitialization of the nominal trajectory is described by

$$\boldsymbol{\alpha}(\tau^j, j) = \boldsymbol{g}(\boldsymbol{\alpha}(\tau^j, j-1), \boldsymbol{\mu}(\tau^j, j-1), \tau^j, j), \tag{3.17}$$

and the reinitialization of the perturbed state is described by (due to Assumption 2, 5, and 6)

$$\boldsymbol{x}(t^j, j, \epsilon) = \boldsymbol{g}(\boldsymbol{x}(t^j, j-1, \epsilon), \boldsymbol{u}(t^j, j-1, \epsilon), t^j, j). \tag{3.18}$$

Similar to the Taylor expansion used in (3.11), the state and input of the next segment evaluated at the perturbed event time t^j can be expanded to

$$\boldsymbol{x}(t^j, j, \epsilon) = \overline{\boldsymbol{\alpha}}(t^j, j) + \epsilon\boldsymbol{z}(t^j, j) + o(\epsilon), \tag{3.19}$$

$$\boldsymbol{u}(t^j, j, \epsilon) = \overline{\boldsymbol{\mu}}(t^j, j) + \epsilon\boldsymbol{v}(t^j, j) + o(\epsilon). \tag{3.20}$$

The same can be done for $\boldsymbol{\alpha}(t^j, j)$, $\boldsymbol{\mu}(t^j, j)$, $\boldsymbol{z}(t^j, j)$, and $\boldsymbol{v}(t^j, j)$, which when substituted into (3.19) and (3.20) result in

$$\boldsymbol{x}(t^j, j, \epsilon) = \boldsymbol{\alpha}(\tau^j, j) + \epsilon\dot{\boldsymbol{\alpha}}(\tau^j, j)\Delta + \epsilon\boldsymbol{z}(\tau^j, j) + o(\epsilon), \tag{3.21}$$

$$\boldsymbol{u}(t^j, j, \epsilon) = \boldsymbol{\mu}(\tau^j, j) + \epsilon\dot{\boldsymbol{\mu}}(\tau^j, j)\Delta + \epsilon\boldsymbol{v}(\tau^j, j) + o(\epsilon), \tag{3.22}$$

with

$$\Delta^j = \left.\frac{\partial t^j}{\partial \epsilon}\right|_{\epsilon=0}. \tag{3.23}$$

To find Δ^j we evaluate the ante-event guard function

$$\gamma(\boldsymbol{x}(t^j, j-1, \epsilon), \boldsymbol{u}(t^j, j-1, \epsilon), t^j, j) = 0, \tag{3.24}$$

where γ is evaluated at the left limit of event j. Due to Assumptions 2, 3, and 4 it is guaranteed that the solution of (3.24) is close to the nominal solution. Note that γ is dependent on the input $\boldsymbol{u}$, whereas in [58] the sensitivity analysis is performed for guard functions which solely depend on state $\boldsymbol{x}$ and time t. From (3.24) the expression for Δ^j is found to be

$$\Delta^j = -\frac{D_1\gamma^- \cdot \boldsymbol{z}^- + D_2\gamma^- \cdot \boldsymbol{v}^-}{\dot{\gamma}^-}, \tag{3.25}$$

with

$$\gamma^- = \gamma(\boldsymbol{\alpha}(\tau^j, j-1), \boldsymbol{\mu}(\tau^j, j-1), \tau^j, j), \tag{3.26}$$
$$\dot{\gamma}^- = D_1\gamma^- \cdot \dot{\boldsymbol{\alpha}}(\tau^j, j-1) + D_2\gamma^- \cdot \dot{\boldsymbol{\mu}}(\tau^j, j-1) + D_3\gamma^-, \tag{3.27}$$
$$\boldsymbol{z}^- = \boldsymbol{z}(\tau^j, j-1), \tag{3.28}$$
$$\boldsymbol{v}^- = \boldsymbol{v}(\tau^j, j-1), \tag{3.29}$$

where the $-$ superscript indicates a left limit of event j. Now (3.17) is expanded and substituted into (3.21) to find

$$\boldsymbol{z}^+ = D_1\boldsymbol{g}^- \cdot \left(\boldsymbol{z}^- + \dot{\boldsymbol{\alpha}}^-\Delta^j\right) + D_2\boldsymbol{g}^- \cdot \left(\boldsymbol{v}^- + \dot{\boldsymbol{\mu}}^-\Delta^j\right) + D_3\boldsymbol{g}^- \cdot \Delta^j - \dot{\boldsymbol{\alpha}}^+\Delta^j, \tag{3.30}$$

with

$$\boldsymbol{g}^- = \boldsymbol{g}(\boldsymbol{\alpha}(\tau^j, j-1), \boldsymbol{\mu}(\tau^j, j-1), \tau^j, j), \tag{3.31}$$
$$\boldsymbol{z}^+ = \boldsymbol{z}(\tau^j, j), \tag{3.32}$$
$$\boldsymbol{\alpha}^- = \boldsymbol{\alpha}(\tau^j, j-1), \tag{3.33}$$
$$\boldsymbol{\alpha}^+ = \boldsymbol{\alpha}(\tau^j, j), \tag{3.34}$$
$$\boldsymbol{\mu}^- = \boldsymbol{\mu}(\tau^j, j-1). \tag{3.35}$$

Here the $+$ superscript indicates the right limit of event j. This can finally be rewritten to

$$\boldsymbol{z}^+ = \boldsymbol{L}(\tau^j, j) \begin{bmatrix} \boldsymbol{z}^- \\ \boldsymbol{v}^- \end{bmatrix}, \tag{3.36}$$

with

$$\boldsymbol{L}(\tau^j, j) = \begin{bmatrix} \boldsymbol{G}(\tau^j, j) & \boldsymbol{J}(\tau^j, j) \end{bmatrix}, \tag{3.37}$$
$$\boldsymbol{G}(\tau^j, j) = D_1\boldsymbol{g}^- - \left(\dot{\boldsymbol{g}}^- - \boldsymbol{f}^+\right)\frac{D_1\gamma^-}{\dot{\gamma}^-}, \tag{3.38}$$
$$\boldsymbol{J}(\tau^j, j) = D_2\boldsymbol{g}^- - \left(\dot{\boldsymbol{g}}^- - \boldsymbol{f}^+\right)\frac{D_2\gamma^-}{\dot{\gamma}^-}, \tag{3.39}$$

where

$$\boldsymbol{f}^- = \boldsymbol{f}(\boldsymbol{\alpha}(\tau^j, j-1), \boldsymbol{\mu}(\tau^j, j-1), \tau^j, j-1), \tag{3.40}$$
$$\boldsymbol{f}^+ = \boldsymbol{f}(\boldsymbol{\alpha}(\tau^j, j), \boldsymbol{\mu}(\tau^j, j), \tau^j, j), \tag{3.41}$$
$$\dot{\boldsymbol{g}}^- = D_1\boldsymbol{g}^- \cdot \boldsymbol{f}^- + D_2\boldsymbol{g}^- \cdot \dot{\boldsymbol{\mu}}^- + D_3\boldsymbol{g}^-. \tag{3.42}$$

Due to Assumptions 3 and 6, the derivatives of the jump map $\boldsymbol{g}$ and the guard function γ exist locally. Therefore, the linearized jump gains $\boldsymbol{G}$ and $\boldsymbol{L}$ are defined locally as well.

3.2.2 Linear time triggered hybrid system

Now the sensitivity analysis performed in previous section is used to define the LTTHS associated to reference trajectory $\boldsymbol{\alpha}$ and the NSITHS defined in Definition 1. The LTTHS converts the state-triggered behavior of the NSITHS to a time-triggered behavior using a first order approximation of the state jumps. Where the jump times for NSITHS are unknown for perturbed trajectories, the LTTHS jumps at the same event-times as the nominal trajectory $\boldsymbol{\alpha}$. In [55] a proof is given that stability of the LTTHS implies local asymptotic stability of the NSITHS. Since the stability assessment of LTTHS is well established in literature, the LTTHS can be used to conveniently assess the local asymptotic stability of the NSITHS. Now the LTTHS is formally defined.

Definition 2 (LTTHS)**.** *The linear time-triggered hybrid system associated with the reference trajectory α and the NSITHS is given by*

$$\dot{\boldsymbol{z}}(t,j) = \boldsymbol{A}(t,j)\boldsymbol{z}(t,j) + \boldsymbol{B}(t,j)\boldsymbol{v}(t,j) \qquad (t,j) \in \text{dom } \boldsymbol{\alpha} \tag{3.43}$$

$$\boldsymbol{z}^+ = \boldsymbol{G}(t,j)\boldsymbol{z}^- + \boldsymbol{J}(t,j)\boldsymbol{v}^- \qquad (t,j) \in \text{eve } \boldsymbol{\alpha} \tag{3.44}$$

with initial condition $\boldsymbol{z}(t_0,0) = z_0$, $\boldsymbol{z}^+ = \boldsymbol{z}(\tau^j, j)$, $\boldsymbol{z}^- = \boldsymbol{z}(\tau^j, j-1)$,

$$\boldsymbol{A}(t,j) = D_1\boldsymbol{f}(\boldsymbol{\alpha}(t,j), \boldsymbol{\mu}(t,j), t, j) \tag{3.45}$$

$$\boldsymbol{B}(t,j) = D_2\boldsymbol{f}(\boldsymbol{\alpha}(t,j), \boldsymbol{\mu}(t,j), t, j) \tag{3.46}$$

$$\boldsymbol{G}(t,j) = D_1\boldsymbol{g}^- - \left(\dot{\boldsymbol{g}}^- - \boldsymbol{f}^+\right)\frac{D_1\gamma^-}{\dot{\gamma}^-}, \tag{3.47}$$

$$\boldsymbol{J}(t,j) = D_2\boldsymbol{g}^- - \left(\dot{\boldsymbol{g}}^- - \boldsymbol{f}^+\right)\frac{D_2\gamma^-}{\dot{\gamma}^-}, \tag{3.48}$$

and

$$\boldsymbol{f}^- = \boldsymbol{f}(\boldsymbol{\alpha}(\tau^j, j-1), \boldsymbol{\mu}(\tau^j, j-1), \tau^j, j-1), \tag{3.49}$$

$$\boldsymbol{f}^+ = \boldsymbol{f}(\boldsymbol{\alpha}(\tau^j, j), \boldsymbol{\mu}(\tau^j, j), \tau^j, j), \tag{3.50}$$

$$\boldsymbol{g}^- = \boldsymbol{g}(\boldsymbol{\alpha}(\tau^j, j-1), \boldsymbol{\mu}(\tau^j, j-1), \tau^j, j), \tag{3.51}$$

$$\dot{\boldsymbol{g}}^- = D_1\boldsymbol{g}^- \cdot \boldsymbol{f}^- + D_2\boldsymbol{g}^- \cdot \dot{\boldsymbol{\mu}}^- + D_3\boldsymbol{g}^-, \tag{3.52}$$

$$\gamma^- = \gamma(\boldsymbol{\alpha}(\tau^j, j-1), \boldsymbol{\mu}(\tau^j, j-1), \tau^j, j), \tag{3.53}$$

$$\dot{\gamma}^- = D_1\gamma^- \cdot \dot{\boldsymbol{\alpha}}(\tau^j, j-1) + D_2\gamma^- \cdot \dot{\boldsymbol{\mu}}(\tau^j, j-1) + D_3\gamma^-. \tag{3.54}$$

The LTTHS defined in Definition 2 gives a first order approximation of a perturbed trajectory of the NSITHS. With a nominal trajectory $\boldsymbol{\alpha}$ with input $\boldsymbol{\mu}$, the perturbed trajectory $\boldsymbol{x}(t,j,\epsilon)$ is the trajectory generated by initial condition $\boldsymbol{x}_0(\epsilon) = \boldsymbol{\alpha}_0 + \epsilon\boldsymbol{z}_0$ and input $\boldsymbol{u}(t,j,\epsilon) = \boldsymbol{\mu}(t,j) + \epsilon\boldsymbol{v}(t,j)$. The first order approximation is then defined as $\boldsymbol{x}(t,j,\epsilon) \approx \boldsymbol{\alpha}(t,j) + \epsilon\boldsymbol{z}(t,j)$, with $\boldsymbol{z}$ defined by the LTTHS. Note that the approximation jumps at the same time instants as the nominal trajectory, with $(t,j) \in \text{eve } \boldsymbol{\alpha}$. This results in a trajectory which is generally infeasible around the jump times. However, due to the short timescales of the events, we are more interested in finding a good approximation of the continuous segments between the events, which is what the LTTHS achieves. Since $\boldsymbol{z} = \frac{\partial \boldsymbol{x}}{\partial \epsilon}$, an LTTHS with an equilibrium at $\boldsymbol{z} = 0$ implies tracking of $\boldsymbol{\alpha}$. Therefore, the feedback gains for the input $\boldsymbol{v}(t,j) = -\boldsymbol{K}(t,j)\boldsymbol{z}(t,j)$ should be chosen in such a way that this is achieved. Straightforward stability analysis tools for LTTHS are available in the literature, about which more can be read in Appendix C.3. Finally, one should realize that the term $\boldsymbol{v}^-$ is not an input that can be freely chosen. $\boldsymbol{v}^-$ is directly related to $\boldsymbol{v}(t,j)$, as it is a result of the feedback law implemented during the continuous segment before the event.

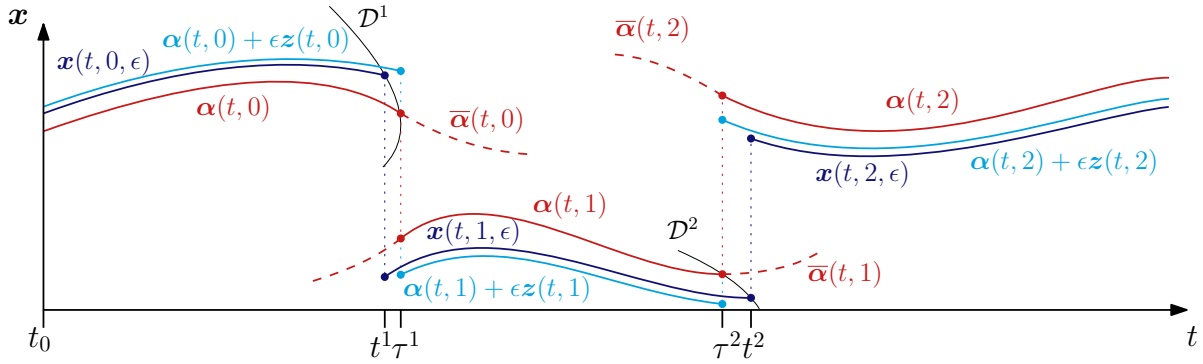

Figure 3.5: *The first order approximation $\boldsymbol{\alpha}+\epsilon\boldsymbol{z}$ (cyan) generated by the LTTHS is illustrated besides the perturbed trajectory $\boldsymbol{x}$ (blue) and the nominal trajectory $\boldsymbol{\alpha}$ (red). Note that the event times of the approximation are the same as those of the nominal trajectory.*

3.3 Summary

In this chapter a control strategy is presented to achieve tracking of trajectories with single guard activations for nonlinear state input triggered hybrid systems. The NSITHS is formally defined, which is a framework suitable for the dynamics defined in Chapter 2. An initial state and input perturbation is introduced into this system, generating perturbed trajectories of which the perturbed event times differ from the nominal event times, and are not known beforehand. This mismatch in event time leads to a behavior called peaking, generating undesirable actuation forces. Reference spreading is then presented to avoid peaking behavior, which leads to less and smaller jumps in the tracking error. Then, under certain assumptions, a sensitivity analysis is performed. The sensitivity analysis leads to a LTTHS describing the tracking error dynamics, which is used to generate a first order approximation of the perturbed state. This LTTHS can be evaluated using conventional stability analysis tools, considering that stability of the LTTHS implies tracking of the nominal reference trajectory.

Chapter 4

Tracking for Hybrid Systems: Simultaneous State-and-Input-Triggered Events

In this chapter the control strategy presented in Chapter 3 is extended to be suitable for trajectories with simultaneous guard activations. Simultaneous guard activations are activations where a trajectory triggers two guard functions at the same time-instant. Take for example a box with two contact points, where the contact points make contact with a surface at the same time. When perturbations are introduced in these trajectories, the simultaneity of the event can get lost. Also, the order of activations can change depending on the perturbation. The box can first make contact with one contact point and then with the other, or the other way around. This complicates the definition of the first-order approximation. In this chapter, a novel notation from [66] is presented to describe trajectories with simultaneous guard functions. Reference spreading is applied to trajectories with simultaneous events, which is used as basis to define a positive homogeneous jump gain which approximates the jump behavior of the perturbed trajectory. The positive homogeneous jump gain defines the *positive homogeneous time-triggered hybrid system* (PTHHS), whose stability implies local asymptotic stability of the NSITHS. This chapter extends the work presented in [66] to being suitable for input-dependent guard functions, and therefore mechanical systems experiencing dry friction and releasing motions.

4.1 Simultaneous guard-activation

To be able to perform the sensitivity analysis presented in Chapter 3 for trajectories with simultaneous guard activations, some adjustments need to be made to the notation. In this section a new notation, introduced in [66], is presented, namely: the event character, micro- and macro-events, multiscale hybrid time, guard function index, mode descriptor, phantom segments, and historical notation. After this, reference spreading for simultaneous guard-activations is discussed.

4.1.1 Adopted notation

In a simultaneous event, more than one guard function is activated in one event. In Figure 4.1 an example of a simultaneous activation is illustrated. The ante-event reference trajectory, $\boldsymbol{\alpha}(t, 0)$, activates two guard functions, γ^1 and γ^2. The number of guard functions that are activated in a

single nominal event is called the *event character*. In the example in Figure 4.1, the event character $c = 2$.

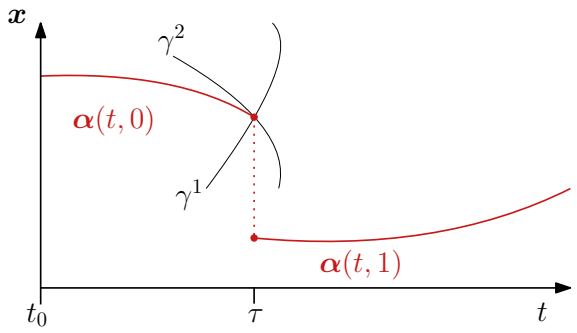

Figure 4.1: *An illustration of a trajectory going through a simultaneous event. At $t = \tau$, the trajectory activates two guard functions, γ^1 and γ^2.*

When perturbations are introduced in an event with simultaneous activations, the number of events the system goes through can change. Instead of a simultaneous activation of a c guards, the guards can be activated in rapid succession. These events that are the result of loss of simultaneity are called *micro-events*, where several micro-events form one *macro event*. Micro-events will generate extra segments in the state trajectory in comparison to the reference trajectory. To keep track of these segments, *multiscale hybrid time* is introduced. Multiscale hybrid time is denoted by (t, i, k), where t is regular time, i the macro-event counter, and k the micro-event counter. The micro-event counter k is incremented everytime an event occurs, except when a macro event is completed by reaching the nominal post-event mode. The micro-event counter k then resets to 0, and the macro-event counter i is incremented. One can now write $\boldsymbol{x}(t, i, k)$ to make a distinction between all the segments that generated as a result of loss of simultaneity. Multiscale hybrid is directly related to the regular hybrid time, according to

$$j(i,k) = k + \sum_{I=0}^{i} l_I, \tag{4.1}$$

where l_I is the number of micro-events in macro-event I. The perturbed event times of micro-events are denoted by t_k^i, which is event time of the k^{th} micro-event of macro-event i. A guard function index η is introduced to identify the several guard functions that are involved with a macro-event. The guard functions of macro-event i are given by γ_η^i, with

$$\eta = 2^\nu, \quad \text{with } \nu \in \{0, 1, ..., c^i\}. \tag{4.2}$$

η is written in the binary numeral system for a more intuitive notation of the different guard functions. The modes that the system is in, is indicated using the *mode descriptor* s_k^i. The mode descriptor s_k^i is associated to event i, similar to τ^i. It should no be confused with the hybrid time i, which defines a segment rather than a point. The micro-segments around contact point i can be described using

$${}^{s_k^i}\boldsymbol{x}(t) = \boldsymbol{x}(t, i-1, k), \tag{4.3}$$

with s_k^i the mode of the k^{th} micro-event associated to macro-event i. Similar to η, the mode descriptor is written in the binary numeral system. For example, when the event character $c^i = 2$, the guard functions that are involved with that macro event are γ_{10}^i and γ_{01}^i. The system begins in mode $s_0^i = 00$, where $\gamma_{10}^i, \gamma_{01}^i > 0$. When the state activates one of the guard functions, for

example $\gamma_{01}^i = 0$, the next mode becomes $s_1^i = 01$. When the other guard function is activated as well, $\gamma_{10}^i = 0$, the system completes its macro-event with $s_2^i = 0$. This is illustrated in Figure 4.2. **MAKE EXAMPLE MORE CLEAR WITH BLOCK**

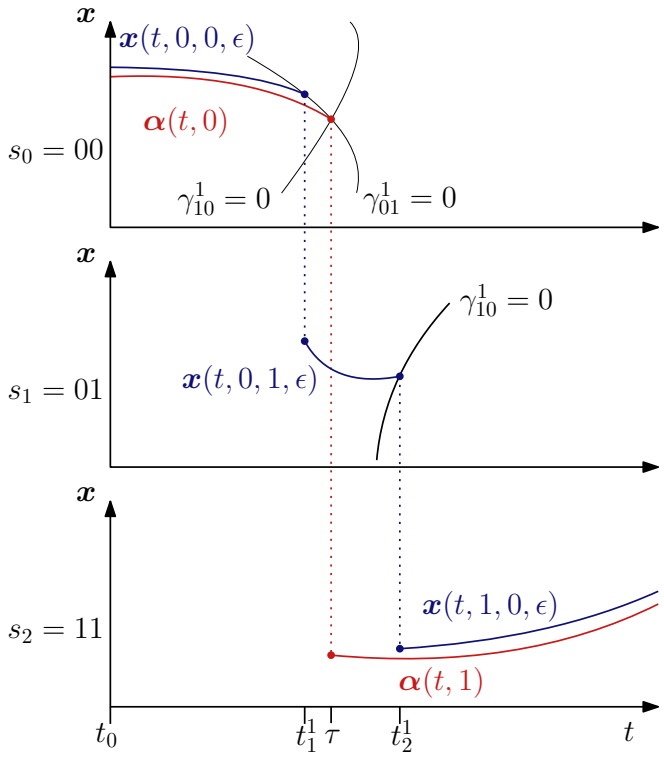

Figure 4.2: *A reference trajectory going through a simultaneous event and a state trajectory experiencing loss of simultaneity are illustrated in this figure. Where the reference trajectory activates γ^{10} and γ^{01} simultaneously, the state trajectory first activates γ^{01} at $t = t_1^1$, flows for $t \in [t_1^1, t_2^2]$, and then activates γ^{10} at $t = t_2^1$.*

Depending on the perturbation, several mode sequences can achieve the expected nominal end mode when simultaneity is lost. The different mode sequences can generate a different post-event state, since the differential equation that describes the micro-segments in between the micro-events change with their mode. Therefore, it is useful to be able to indicate an entire mode sequence with one variable. We call this notation the *historical notation*. We define the growing sequence S_k^i as

$$S_k^i = s_k^i \leftarrow s_{k-1}^i \leftarrow ... \leftarrow s_0^i, \tag{4.4}$$

where $s_0^i = 00...0$ with length c^i. A growing mode sequence is a sequence of micro-events, where at eacht micro-event another guard function is activated and no guard functions deactivated. We can now define ${}^{S_k^i}\boldsymbol{x}(t)$ as ${}^{s_k^i}\boldsymbol{x}(t)$ that is a result of the growing sequence S_k^i. The jump maps that are applied during such a sequence are given by

$${}^{p}\boldsymbol{x} = {}^{p \leftarrow a}\boldsymbol{g}({}^{a}\boldsymbol{x}, {}^{a}\boldsymbol{u}, t), \tag{4.5}$$

where p represents the post-event mode descriptor, and a the ante-event mode descriptor. For example, the state jump from s_k^i to s_{k+1}^i is given by ${}^{s_{k+1}^i}\boldsymbol{x} = {}^{s_{k+1}^i \leftarrow s_k^i}\boldsymbol{g}({}^{s_k^i}\boldsymbol{x}, {}^{s_k^i}\boldsymbol{u}, t)$. To denote growing sequences with a particular order of events, we define

$${}^{\nu_k \nu_{k-1} ... \nu_1}S_k = s_k \leftarrow s_{k-1} \leftarrow ... \leftarrow s_0, \tag{4.6}$$

where all mode descriptor entries are defined as $s_\kappa = s_{\kappa-1} + \eta_\kappa$, with $\eta_\kappa = 2^{\nu_\kappa}$ **mistake in ACC paper? Check again.** Now that the notation for trajectories with simultaneous guard activations is in place, the analysis of these systems can be discussed.

4.1.2 Reference-spreading for simultaneous events

For trajectories with simultaneous activations, the perturbed state can experience more events than the reference trajectory. The perturbed state will enter micro-modes and micro-segments, which are undefined in the reference trajectory. To be able to define a physically realistic comparison between the reference trajectory and the state trajectory, the reference trajectory needs to be adjusted. This is done in the form of *nominal phantom modes* and *nominal phantom segments*. Phantom modes are modes defined in the reference trajectory, that do not physically exist. (phantom modes and segments, do not exist in reference, but they are necessary because state can make more jumps. Same idea behind RS, we want to compare reference and state that are in the same mode)

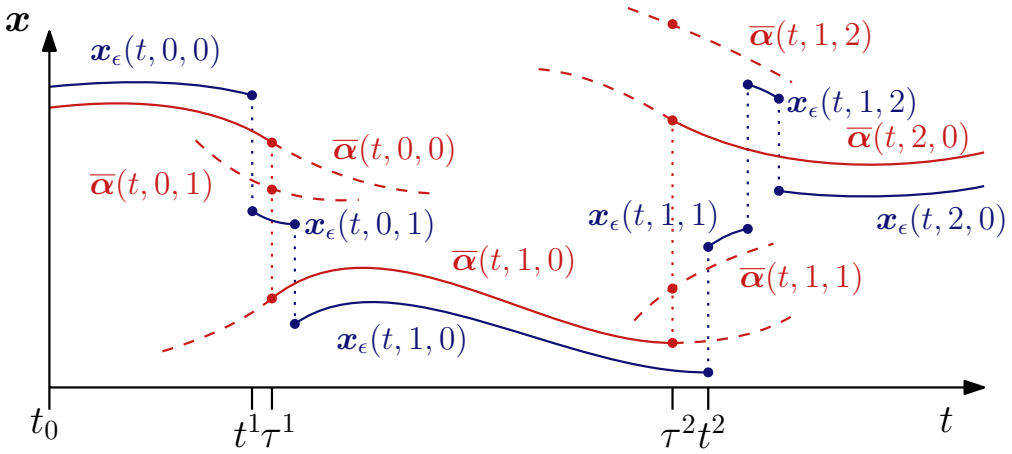

Figure 4.3: *The state evolution of the reference trajectory and state trajectory. Phantom segments are added to the reference trajectory, to which the micro-segments of the state trajectory can be compared.*

4.2 First-order approximation for trajectories with simultaneous guard-activation

- Positive homogeneity
- Growing mode sequences assumption
- Associativity assumption
- Positive homogeneous jump gain derivation
- Pushing and withdrawing segments, and effect of pos hom jump gain (v during event is 0)
- PTTHS (Positive homogeneous time-triggered hybrid system)

- Note that the sensitivity analysis does take micro-events into consideration, but resulting controller does not

4.3 Summary

Chapter 5

Numerical Validation

Chapter 6

Conclusions and Recommendations

Bibliography

[1] Virginia Tech Robotics and Mechatronics Lab. Simlab quadruped. `http://www.me.vt.edu/research/laboratories/rmlab/`, 2018.

[2] ABB Robotics. Irb 360 flexpicker. `https://new.abb.com/products/robotics/industrial-robots/irb-360`, 2018.

[3] Remco I. Leine and Henk Nijmeijer. *Dynamics and Bifurcations of Non-Smooth Mechanical Systems*. Springer-Verlag, Berlin, Heidelberg, 1st edition, 2004.

[4] A. F. Fillippov. *Differential Equations with Discontinuous Righthand Sides*. Springer-Science, Dordrecht, 1st edition, 1988.

[5] Remco I. Leine and Nathan Van De Wouw. Uniform Convergence of Monotone Measure Differential Inclusions: With Application To the Control of Mechanical Systems With Unilateral Constraints. *International Journal of Bifurcation and Chaos*, 18(5):1435–1457, 2008.

[6] J. J. Moreau and P. O. Panagiotopoulos. *Nonsmooth Mechanics and Applications*. Springer-Verlag, Wien, 1st edition, 1988.

[7] Bernard Brogliato. *Nonsmooth Mechanics*. Springer, 3rd edition, 1999.

[8] N Van De Wouw. An introduction to Time-Stepping: a Numerical Technique for Mechanical Systems with Unilateral Constraints. pages 1–27, 2004.

[9] A. J. Van Der Schaft and J. M. Schumacher. Complementarity modeling of hybrid systems. *IEEE Transactions on Automatic Control*, 43(4):483–490, 1998.

[10] W. Heemels. *Linear complementarity systems: a study in hybrid dynamics*. PhD thesis, Eindhoven University of Technology, 1999.

[11] Christoph Glocker. *Set-Valued Force Laws: Dynamics of Non-Smooth Systems*, volume 1. Springer, Zürich, 1 edition, 2001.

[12] Jean-Matthieu Bourgeot and Bernard Brogliato. Passivity-based tracking control of multiconstraint complementarity Lagrangian systems. *International Journal of Bifurcation and Chaos*, 15(6):1839–1866, 2005.

[13] Irinel-Constantin Morarescu and Bernard Brogliato. Tracking Control of Multiconstraint Complementarity Lagrangian Systems. *International Journal of Bifurcation and Chaos*, 55(6):1300–1313, 2010.

[14] Dong Jin Hyun, Sangok Seok, Jongwoo Lee, and Sangbae Kim. High speed trot-running: Implementation of a hierarchical controller using proprioceptive impedance control on the MIT Cheetah. *International Journal of Robotics Research*, 33(11):1417–1445, 2014.

[15] Benjamin Morris and Jessy W. Grizzle. Hybrid invariant manifolds in systems with impulse effects with application to periodic locomotion in bipedal robots. *IEEE Transactions on Automatic Control*, 54(8):1751–1764, 2009.

[16] Rafal Goebel, Ricardo G. Sanfelice, and Andrew R. Teel. Hybrid dynamical systems. *IEEE Control Systems Magazine*, 29(2):28–93, 2009.

[17] Jerry Ding, Jeremy H Gillula, Haomiao Huang, Michael P Vitus, Wei Zhang, and Claire J Tomlin. Hybrid Systems in Robotics: Toward Reachability-Based Controller Design. *IEEE Robotics & Automation Magazine*, 18(3):33–43, 2011.

[18] Hui Ye and a. N. Michel. Stability theory for hybrid dynamical systems. *IEEE Transactions on Automatic Control*, 43(4):461–474, 1998.

[19] J. Lygeros, K.H. Johansson, S.N. Simic, and S.S. Sastry. Dynamical properties of hybrid automata. *IEEE Transactions on Automatic Control*, 48(1):2–17, 2003.

[20] F. L. Pereira and G. N. Silva. Lyapunov stability of measure driven impulsive systems. *Differential Equations*, 40(8):1122–1130, 2004.

[21] Bernard Brogliato. Absolute stability and the Lagrange-Dirichlet theorem with monotone multivalued mappings. *Systems and Control Letters*, 51(5):343–353, 2004.

[22] R.I. Leine and N. van de Wouw. *Stability and Convergence of Mechanical Systems with Unilateral Constraints*, volume 36. Springer, 2008.

[23] M Kanat Camlibel, Jong-Shi Pang, and Jinglai Shen. Lyapunov Stability of Complementarity and Extended Systems. *SIAM Journal on Optimization*, 17(4):1056–1101, 2007.

[24] M. Kanat Camlibel and Nathan Van De Wouw. On the Convergence of Linear Passive Complementarity Systems. *IEEE Conference on Decision and Control*, 46th:5886–5891, 2007.

[25] Marc H. Raibert. Hopping in Legged Systems - Modeling and Simulation for the Two-Dimensional One-Legged Case. *IEEE Transactions on Systems, Man and Cybernetics*, SMC-14(3):451–463, 1984.

[26] Andrés Lebaudy, Joseph Prosser, and Moshe Kam. Control Algorithms for a Vertically-Constrained One-Legged Hopping Machine. *Proceedings of the 32nd Conference on Decision and Control*, pages 2688–2693, 1993.

[27] H. Michalska, M. Ahmadi, and M. Buehler. Vertical motion control of a hopping robot. *Proceedings of IEEE International Conference on Robotics and Automation*, 3(April):2712–2717, 1996.

[28] Pedro Gregorio, Mojtaba Ahmadi, and Martin Buehler. Design, control, and energetics of an electrically actuated legged robot. *IEEE Transactions on Systems, Man, and Cybernetics, Part B: Cybernetics*, 27(4):626–634, 1997.

[29] Jesse W. Grizzle, Gabriel Abba, and Franck Plestan. Asymptotically stable walking for biped robots: Analysis via systems with impulse effects. *IEEE Transactions on Automatic Control*, 46(1):51–64, 2001.

[30] Aaron D. Ames. Human-inspired control of Bipedal walking robots. *IEEE Transactions on Automatic Control*, 59(5):1115–1130, 2014.

[31] Jacob Reher, Eric A. Cousineau, Ayonga Hereid, Christian M. Hubicki, and Aaron D. Ames. Realizing dynamic and efficient bipedal locomotion on the humanoid robot DURUS. *Proceedings - IEEE International Conference on Robotics and Automation*, 2016-June:1794–1801, 2016.

[32] Agility Robotics. Cassie. `http://www.agilityrobotics.com/robots/#cassie`, 2018.

[33] Jessy W. Grizzle, Christine Chevallereau, Ryan W. Sinnet, and Aaron D. Ames. Models, feedback control, and open problems of 3D bipedal robotic walking. *Automatica*, 50(8):1955–1988, 2014.

[34] Nathan van de Wouw and Remco I Leine. Tracking control for a class of measure differential inclusions. *Proceedings IEEE Conference on Decision and Control*, pages 2526–2532, 2008.

[35] Nathan Van De Wouw and Remco I Leine. Stability and Control of Lur'e-type Measure Differential Inclusions. pages 129–151, 2010.

[36] Roberto Naldi and Ricardo G. Sanfelice. Passivity-based control for hybrid systems with applications to mechanical systems exhibiting impacts. *Automatica*, 49(5):1104–1116, 2013.

[37] Ricardo G. Sanfelice, J. J. Benjamin Biemond, Nathan Van De Wouw, and W. P. Maurice H. Heemels. Tracking control for hybrid systems via embedding of known reference trajectories. *Proceedings of the 2011 American Control Conference*, pages 869–874, 2011.

[38] Ricardo G. Sanfelice, J. J.Benjamin Biemond, Nathan Van De Wouw, and W. P. Maurice H. Heemels. An embedding approach for the design of state-feedback tracking controllers for references with jumps. *International Journal of Robust and Nonlinear Control*, 24:1585–1608, 2014.

[39] Michael Posa, Mark Tobenkin, and Russ Tedrake. Stability Analysis and Control of Rigid Body Systems with Impacts and Friction. *IEEE TRANSACTIONS ON AUTOMATIC CONTROL*, 61(6):1423–1437, 2016.

[40] Ye Zhao, Benito R. Fernandez, and Luis Sentis. A Framework for Planning and Controlling Non-Periodic Bipedal Locomotion. 2015.

[41] J J B Biemond, N Van De Wouw, W P M H Heemels, and H Nijmeijer. Tracking Control for Hybrid Systems with State-Triggered Jumps. *IEEE Transactions on Automatic Control*, 58(257462):876–890, 2013.

[42] Laura Menini and Antonia Tornambè. Asymptotic tracking of periodic trajectories for a simple mechanical system subject to nonsmooth impacts. *IEEE Transactions on Automatic Control*, 46(7):1122–1126, 2001.

[43] S. Galeani, L. Menini, A. Potini, and A. Tornambè. Trajectory tracking for a particle in elliptical billiards. *International Journal of Control*, 81(2):189–213, 2008.

[44] Fulvio Forni, Andrew R. Teel, and Luca Zaccarian. Follow the bouncing ball: Global results on tracking and state estimation with impacts. *IEEE Transactions on Automatic Control*, 58(6):1470–1485, 2013.

[45] J. J.Benjamin Biemond, W. P.Maurice H. Heemels, Ricardo G. Sanfelice, and Nathan van de Wouw. Distance function design and Lyapunov techniques for the stability of hybrid trajectories. *Automatica*, 73:38–46, 2016.

[46] Michael Baumann, J. J.Benjamin Biemond, Remco I. Leine, and Nathan van de Wouw. Synchronization of impacting mechanical systems with a single constraint. *Physica D: Nonlinear Phenomena*, 362:9–23, 2018.

[47] Jisu Kim, Hyungbo Shim, and Jin Heon Seo. Tracking control for hybrid systems with state jumps using gluing function. *2016 IEEE 55th Conference on Decision and Control, CDC 2016*, pages 3006–3011, 2016.

[48] Ting Yang, Fen Wu, and Lixian Zhang. Tracking control of hybrid systems with state-triggered jumps and stochastic events and its application. *IET Control Theory & Applications*, 11(7):1024–1033, 2017.

[49] Alessandro Saccon, Nathan van de Wouw, and Henk Nijmeijer. Sensitivity analysis of hybrid systems with state jumps with application to trajectory tracking. *Proceedings of the 53rd IEEE Conference on Decision and Control*, pages 3065–3070, 2014.

[50] Mark Rijnen, Alessandro Saccon, and Henk Nijmeijer. On Optimal Trajectory Tracking for Mechanical Systems with Unilateral Constraints. *2015 IEEE 54th Annual Conference on Decision and Control (CDC)*, pages 2561–2566, 2015.

[51] Hassan K. Khalil. *Nonlinear Systems*. Prentice-Hall, Englewood Cliffs, NJ, 3rd edition, 1996.

[52] Gian Paolo Incremona, Alessandro Saccon, Antonella Ferrara, and Henk Nijmeijer. Trajectory tracking of mechanical systems with unilateral constraints: Experimental results of a recently introduced hybrid PD feedback controller. *Proceedings of the IEEE Conference on Decision and Control*, 54rd IEEE(Cdc):920–925, 2015.

[53] M. W.L.M. Rijnen, A. T. van Rijn, H. Dallali, A. Saccon, and H. Nijmeijer. Hybrid Trajectory Tracking for a Hopping Robotic Leg. *IFAC-PapersOnLine*, 49(14):107–112, 2016.

[54] N. G. Tsagarakis, S. Morfey, H. Dallali, G. A. Medrano-Cerda, and D. G. Caldwell. An asymmetric compliant antagonistic joint design for high performance mobility. *IEEE International Conference on Intelligent Robots and Systems*, pages 5512–5517, 2013.

[55] M.W.L.M. Rijnen, J.J.B. Biemond, N. van de Wouw, A. Saccon, and H. Nijmeijer. Hybrid Systems with State-Triggered Jumps: Sensitivity-Based Stability Analysis with Application to Trajectory Tracking. pages 1–16, 2017.

[56] Mark Rijnen, Eric De Mooij, Silvio Traversaro, Francesco Nori, Nathan Van De Wouw, Alessandro Saccon, and Henk Nijmeijer. Control of humanoid robot motions with impacts: Numerical experiments with reference spreading control. *Proceedings - IEEE International Conference on Robotics and Automation*, pages 4102–4107, 2017.

[57] Huihua Zhao, Jonathan Horn, Jacob Reher, Victor Paredes, and Aaron D. Ames. A hybrid systems and optimization-based control approach to realizing multi-contact locomotion on transfemoral prostheses. *Proceedings of the IEEE Conference on Decision and Control*, 54(2):1607–1612, 2015.

[58] Hao Liang Chen. *Trajectory tracking control for mechanical systems experiencing simultaneous impacts*. Master's thesis, Eindhoven University of Technology, 2018.

[59] Christoph Glocker. Energetic consistency conditions for standard impacts: Part I: Newton-type inequality impact laws and Kane's example. *Multibody System Dynamics*, 32(4):445–509, 2014.

[60] Anthom van Rijn. *Hybrid trajectory tracking for hopping robots.* Master's thesis, Eindhoven University of Technology, 2016.

[61] N. van de Wouw. *Multibody and Nonlinear Dynamics Lecture Notes.* University of Technology Eindhoven, Eindhoven, 2016.

[62] C. Studer and Ch Glocker. Representation of normal cone inclusion problems in dynamics via non-linear equations. *Archive of Applied Mechanics*, 76(5-6):327–348, 2006.

[63] Vincent Acary and Bernard Brogliato. *Numerical Methods for Nonsmooth Dynamical Systems: Applications in Mechanics and Electronics*, volume 35. Springer, Montbonnot, 2008.

[64] Wassim M Haddad, VijaySekhar Chellaboina, and Sergey G. Nersesov. *Impulsive and Hybrid Dynamical Systems.* Princeton University Press, New Jersey, 1st edition, 2006.

[65] Étienne Delassus. Mémoire sur la théorie des liaisons finies unilatérales. *Annales scientifiques de l'É.N.S.*, 34(3rd):95–179, 1917.

[66] Mark Rijnen, Hao Liang Chen, Nathan Van De Wouw, Alessandro Saccon, and Henk Nijmeijer. Sensitivity analysis for trajectories of nonsmooth mechanical systems with simultaneous impacts : a hybrid systems perspective. 2018.

Appendix A

Nonsmooth modeling

A.1 Hybrid system formulation for mechanical systems

A.1.1 Continuous dynamics derivation

A.1.2 Discrete event set derivation

In this section the discrete event sets D are defined. When the state or input of the system enters a discrete event set, contact points can change set and a reinitialization of the state can take place. In this work the assumption is made that all contact points in closed contact are in the same set, i.e., in either $\mathcal{I}_{\text{sl}}$ or $\mathcal{I}_{\text{st}}$.

More elaboration on why the conditions that are chosen are chosen (i.e., why $||\boldsymbol{\zeta}_{t,i}|| = 0$)

Recap each paragraph using section D and mentioning γ's again.

Open to stick/slip
When a contact point is "open", it can trigger a guard function $\gamma_{\text{op}\to\text{cl}}$ to go from open to closed. This guard is defined using the contact distance h_{n,i_c}. When $h_{n,i_c} > 0$, the contact point is in open-contact. When $h_{n,i_c} = 0$ with $\dot{h}_{n,i_c} < 0$, the contact point enters the closed-contact mode with a non-zero ante-impact velocity. Therefore the guard function $\gamma_{\text{op}\to\text{cl}}$ is given by

$$\gamma_{\text{op}\to\text{cl}} = h_{n,i_c}(\boldsymbol{q}). \tag{A.1}$$

The plane that spans $\gamma = 0$ is divided in two regions: a region where the post-impact state is in slip and a region where the post-impact state is in stick. ***I*** This region is defined by Γ_{i_c}, where $\Gamma_{i_c} < 0$ in the region where the contact point goes to slip and $\Gamma_{i_c} > 0$ in the region where the contact point goes to stick. When $\Gamma_{i_c} = 0$ the system is right at the border between a slip post-impact state and a stick post-impact state. This is illustrated in Figure A.1.

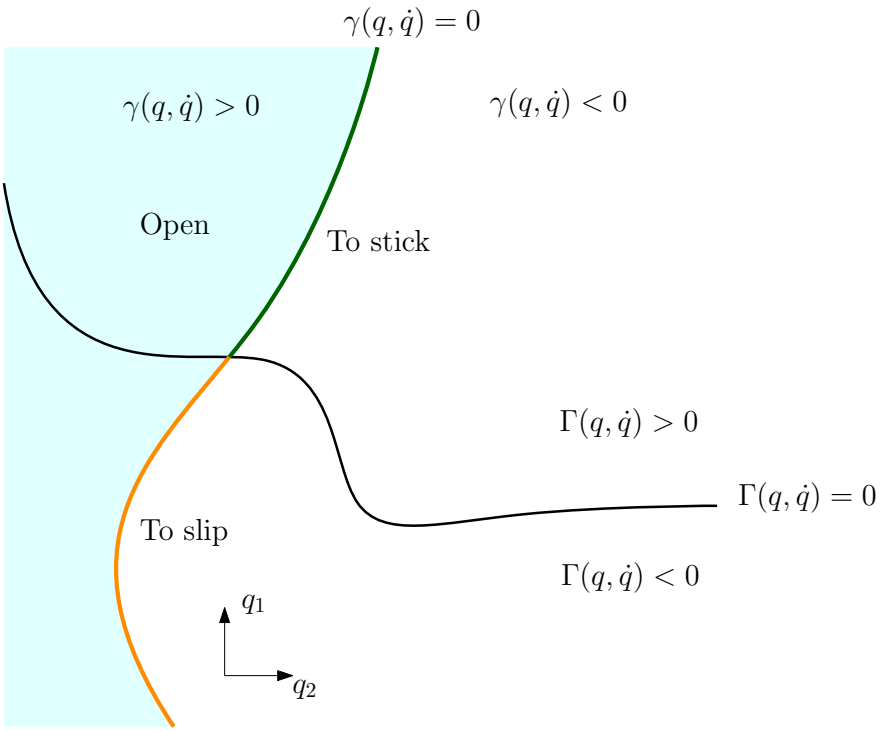

Figure A.1: *The functions* $\boldsymbol{\gamma}(\boldsymbol{q},\dot{\boldsymbol{q}})$ *and* $\boldsymbol{\Gamma}(\boldsymbol{q},\dot{\boldsymbol{q}})$ *illustrated in the state space of* $\boldsymbol{q} \in \mathbb{R}^2$*. The light blue area is the state space where the contact is open, and goes the closed when it triggers* $\gamma = 0$*. If it triggers* $\gamma = 0$ *in the area where* $\Gamma < 0$ *(orange), then the contact will go to slip. If it triggers* $\gamma = 0$ *in the area where* $\Gamma \geq 0$ *(green), then the contact will go to stick.*

For slip, we know that $\mu\Lambda_{n,i_c} - ||\boldsymbol{\Lambda}_{t,i_c}|| = 0$ and for stick, we know that $\mu\Lambda_{n,i_c} - ||\boldsymbol{\Lambda}_{t,i_c}|| \geq 0$. From this we can derive the guard function

$$\Gamma_{i_c} = \mu^2 \underline{\Lambda}^2_{n,i_c}(\underline{\boldsymbol{q}},\underline{\dot{\boldsymbol{q}}}) - \underline{\boldsymbol{\Lambda}}_{t,i_c}(\underline{\boldsymbol{q}},\underline{\dot{\boldsymbol{q}}})\underline{\boldsymbol{\Lambda}}^T_{t,i_c}(\underline{\boldsymbol{q}},\underline{\dot{\boldsymbol{q}}}). \tag{A.2}$$

The underlined variables are virtual states, meaning that they do not necessarily have a physical meaning. The way (A.2) is given, it is defined in both open and closed contact. This map is only physically realistic during an event from open to closed contact. However, by using virtual states we obtain a differentiable guard function Γ_{i_c}. This guard function Γ_{i_c} satisfies the requirements that $\Gamma_{i_c} < 0$ in the region where the contact point goes to slip, $\Gamma_{i_c} > 0$ in the region where the contact point goes to stick and $\Gamma_{i_c} = 0$ at the border. We now find expressions for Λ_{n,i_c} and $\boldsymbol{\Lambda}_{t,i_c}$ by looking at the jump map to stick, given in (**??**) to (**??**).

We can rewrite (**??**) to

$$\dot{\boldsymbol{q}} = \boldsymbol{M}^{-1}\boldsymbol{W}_n\underline{\boldsymbol{\Lambda}}_n + \boldsymbol{M}^{-1}\boldsymbol{W}_t\underline{\boldsymbol{\Lambda}}_t + \underline{\dot{\boldsymbol{q}}}, \tag{A.3}$$

and (**??**), (**??**) to

$$\boldsymbol{W}_n^T\underline{\dot{\boldsymbol{q}}} = 0, \tag{A.4}$$
$$\boldsymbol{W}_t^T\underline{\dot{\boldsymbol{q}}} = 0, \tag{A.5}$$

with

$$\boldsymbol{W}_n = \left[\boldsymbol{w}_{n,i_1}, \boldsymbol{w}_{n,i_2}, ..., \boldsymbol{w}_{n,i_c}\right] \in \mathbb{R}^{n\times C}, \tag{A.6}$$
$$\boldsymbol{W}_t = \left[\boldsymbol{W}_{t,i_1}, \boldsymbol{W}_{t,i_2}, ..., \boldsymbol{W}_{t,i_c}\right] \in \mathbb{R}^{n\times 2C}, \tag{A.7}$$
$$\underline{\boldsymbol{\Lambda}}_n = \left[\underline{\Lambda}_{n,i_1}; \underline{\Lambda}_{n,i_2}; ...; \underline{\Lambda}_{n,i_c}\right] \in \mathbb{R}^{C}, \tag{A.8}$$
$$\underline{\boldsymbol{\Lambda}}_t = \left[\underline{\boldsymbol{\Lambda}}_{t,i_1}; \underline{\boldsymbol{\Lambda}}_{t,i_2}; ...; \underline{\boldsymbol{\Lambda}}_{t,i_c}\right] \in \mathbb{R}^{2C}. \tag{A.9}$$

Substituting (A.3) into (A.4) and (A.5) leads to

$$\boldsymbol{W}_n^T\boldsymbol{M}^{-1}\boldsymbol{W}_n\underline{\boldsymbol{\Lambda}}_n + \boldsymbol{W}_n^T\boldsymbol{M}^{-1}\boldsymbol{W}_t\underline{\boldsymbol{\Lambda}}_t + \underline{\boldsymbol{\zeta}}_n = 0 \tag{A.10}$$
$$\boldsymbol{W}_t^T\boldsymbol{M}^{-1}\boldsymbol{W}_n\underline{\Lambda}_n + \boldsymbol{W}_t^T\boldsymbol{M}^{-1}\boldsymbol{W}_t\underline{\boldsymbol{\Lambda}}_t + \underline{\boldsymbol{\zeta}}_t = 0, \tag{A.11}$$

respectively, with

$$\underline{\boldsymbol{\zeta}}_n = \boldsymbol{W}_n^T\underline{\dot{\boldsymbol{q}}}, \tag{A.12}$$
$$\underline{\boldsymbol{\zeta}}_t = \boldsymbol{W}_t^T\underline{\dot{\boldsymbol{q}}}. \tag{A.13}$$

This is now rewritten to

$$\begin{bmatrix}\boldsymbol{W}_n^T\boldsymbol{M}^{-1}\boldsymbol{W}_n & \boldsymbol{W}_n^T\boldsymbol{M}^{-1}\boldsymbol{W}_t\\ \boldsymbol{W}_t^T\boldsymbol{M}^{-1}\boldsymbol{W}_n & \boldsymbol{W}_t^T\boldsymbol{M}^{-1}\boldsymbol{W}_t\end{bmatrix}\begin{bmatrix}\underline{\boldsymbol{\Lambda}}_n\\ \underline{\boldsymbol{\Lambda}}_t\end{bmatrix} + \begin{bmatrix}\underline{\boldsymbol{\zeta}}_n\\ \underline{\boldsymbol{\zeta}}_t\end{bmatrix} = 0, \tag{A.14}$$

which is in turn rewritten to

$$\begin{bmatrix}\underline{\boldsymbol{\Lambda}}_n\\ \underline{\boldsymbol{\Lambda}}_t\end{bmatrix} = -\boldsymbol{D}^{-1}\begin{bmatrix}\underline{\boldsymbol{\zeta}}_n\\ \underline{\boldsymbol{\zeta}}_t\end{bmatrix}, \quad \text{with } \boldsymbol{D} = \begin{bmatrix}\boldsymbol{W}_n^T\boldsymbol{M}^{-1}\boldsymbol{W}_n & \boldsymbol{W}_n^T\boldsymbol{M}^{-1}\boldsymbol{W}_t\\ \boldsymbol{W}_t^T\boldsymbol{M}^{-1}\boldsymbol{W}_n & \boldsymbol{W}_t^T\boldsymbol{M}^{-1}\boldsymbol{W}_t\end{bmatrix}. \tag{A.15}$$

The matrix $\boldsymbol{D}$ is often called a Delassus-matrix. We now have expressions for $\underline{\boldsymbol{\Lambda}}_n$ and $\underline{\boldsymbol{\Lambda}}_t$ which are continuous and differentiable in $(\boldsymbol{q}, \dot{\boldsymbol{q}})$. It is straightforward that $\Gamma(\boldsymbol{q}, \dot{\boldsymbol{q}})$ is continuous and differentiable as well. In this work only trajectories where all closed contacts are in the same mode are considered. This means that when (A.2) is smaller than zero, i.e., the reaction forces are infeasible for a stick post-impact mode, all contact points have a feasible slip post-impact mode. For trajectories where different contact points can be in slip and in stick at the same time, this conclusion can not be drawn. One should then iterate over all possible post-impact modes until a post-impact mode is found which has feasible reaction forces.

Slip to stick/open

When a contact point is in closed-contact slip, it can transition to closed-contact stick and it can transition to open-contact. A slipping contact transitions to sticking when the tangential velocity of the contact point is zero, i.e.,

$$||\boldsymbol{\zeta}_{t,\iota}|| = 0. \tag{A.16}$$

A guard function that can be used to describe this set is

$$\gamma_{\text{sl}\to\text{st}} = \boldsymbol{\zeta}_{t,\iota}^T\boldsymbol{\zeta}_{t,\iota}, \tag{A.17}$$

which is equal to zero when $||\boldsymbol{\zeta}_{t,i_c}|| = 0$, greater than zero when $||\boldsymbol{\zeta}_{t,i_c}|| > 0$, smaller than zero when $||\boldsymbol{\zeta}_{t,i_c}|| < 0$, and it is globally differentiable. The time derivative of the guard function is then given by

$$\dot{\gamma}^{\text{sl}\to\text{st}} = \frac{\dot{\boldsymbol{\zeta}}_{t,1} + \dot{\boldsymbol{\zeta}}_{t,2}}{\sqrt{\boldsymbol{\zeta}_{t,1}^2 + \boldsymbol{\zeta}_{t,2}^2}}. \tag{A.18}$$

For $\gamma^{\text{sl}\to\text{st}} = 0$, $\dot{\gamma}^{\text{sl}\to\text{st}}$ is undefined because of a division by zero. But we can take the left limit of $\dot{\gamma}^{\text{sl}\to\text{st}}$ to find the direction at which the guard is activated. Using a Taylor expansion w.r.t. the time we can define the limits

$$\dot{\boldsymbol{\zeta}}_{t,1}(\tau + s) = a_1 s + o(s), \tag{A.19}$$

$$\dot{\boldsymbol{\zeta}}_{t,2}(\tau + s) = a_2 s + o(s), \tag{A.20}$$

where τ is the event time where $\gamma = 0$. Note that the Taylor expansions are only physically realistic for $s < 0$. We can then write

$$\dot{\gamma}^{\text{sl}\to\text{st}}(\tau + s) = \frac{(a_1 + a_2)s + o(s)}{\sqrt{(a_1^2 + a_2^2)s^2 + o(s^2)}} \approx \text{Sign}(s)(a_1 + a_2). \tag{A.21}$$

Since we're interested in the left limit, we get

$$\lim_{s\to 0^-} \dot{\gamma}^{\text{sl}\to\text{st}}(\tau + s) = -(a_1^2 + a_2^2), \tag{A.22}$$

which will be non-zero when the guard is activated transversally. This guard function can be used to perform the positive homogenization. For simulations we have to find another solution, because $\gamma^{\text{sl}\to\text{st}}$ cannot become negative. This will lead to problems when we use zero-border crossing detection.

For a slipping contact transitioning to open-contact an acceleration based guard function is necessary, since the normal velocity of the contact point is constrained in the continuous dynamics of a slipping contact. Therefore, a slipping contact point transitions to open-contact when

$$\lambda_{n,i_c} = 0. \tag{A.23}$$

Similarly to the expression found for $\boldsymbol{\Lambda}_n$ and $\boldsymbol{\Lambda}_t$, we can use (2.31) and (**??**) to define the vector $\boldsymbol{\lambda}_n$. With

$$\underline{\boldsymbol{\lambda}}_n = \left[\underline{\lambda}_{n,i_1}; \underline{\lambda}_{n,i_2}; ...; \underline{\lambda}_{n,i_C}\right] \in \mathbb{R}^C, \tag{A.24}$$

$$\underline{\boldsymbol{\lambda}}_t = \left[\underline{\boldsymbol{\lambda}}_{t,i_1}; \underline{\boldsymbol{\lambda}}_{t,i_2}; ...; \underline{\boldsymbol{\lambda}}_{t,i_C}\right] \in \mathbb{R}^{2C}, \tag{A.25}$$

the dynamics and constraints for a system with all closed contact points in slip are defined as

$$\ddot{\boldsymbol{q}} = \boldsymbol{M}^{-1}\left[\boldsymbol{S}\boldsymbol{u} - \boldsymbol{H} + \boldsymbol{W}_n\boldsymbol{\lambda}_n + \boldsymbol{W}_t\boldsymbol{\lambda}_t\right], \tag{A.26}$$

$$\boldsymbol{W}_n^T\ddot{\boldsymbol{q}} + \dot{\boldsymbol{W}}_n^T\dot{\boldsymbol{q}} = 0, \tag{A.27}$$

$$\boldsymbol{\lambda}_t = -\mu\boldsymbol{Z}_t\boldsymbol{\lambda}_n, \tag{A.28}$$

with

$$\boldsymbol{Z}_t = \begin{bmatrix} \langle\boldsymbol{\zeta}_{t,i_1}\rangle & \boldsymbol{0} & \cdots & \boldsymbol{0} \\ \boldsymbol{0} & \langle\boldsymbol{\zeta}_{t,i_2}\rangle & \cdots & \boldsymbol{0} \\ \vdots & \vdots & \ddots & \vdots \\ \boldsymbol{0} & \boldsymbol{0} & \cdots & \langle\boldsymbol{\zeta}_{t,i_C}\rangle \end{bmatrix}, \quad \in \mathbb{R}^{2C\times C} \tag{A.29}$$

where $\langle\boldsymbol{\zeta}_t\rangle = \left[\langle\boldsymbol{\zeta}_{t,i_1}\rangle, \langle\boldsymbol{\zeta}_{t,i_2}\rangle, ..., \langle\boldsymbol{\zeta}_{t,i_C}\rangle\right]^T$, with $\langle\boldsymbol{\zeta}_{t,i_c}\rangle$ the unit vector $\boldsymbol{\zeta}_{t,i_c}$. (A.26)-(A.28) can be rewritten into

$$\boldsymbol{\lambda}_n = -\left[\boldsymbol{W}_n^T\boldsymbol{M}^{-1}\left(\boldsymbol{W}_n - \mu\boldsymbol{W}_t\boldsymbol{Z}_t\right)\right]^{-1}\boldsymbol{W}_n^T\boldsymbol{M}^{-1}\left[\boldsymbol{S}\boldsymbol{u} - \boldsymbol{H}\right] - \dot{\boldsymbol{W}}_n^T\dot{\boldsymbol{q}}, \tag{A.30}$$

which can be used to define the guard function (A.23).

Stick to slip/open
When a contact point is in closed-contact stick, it can transition to closed-contact slip and it can transition to open-contact. A slipping contact transitions to sticking when the tangential reaction force becomes equal to the normal reaction force at that contact point times the friction coefficient, i.e.,

$$\mu\lambda_{n,i_c} = ||\boldsymbol{\lambda}_{t,i_c}||. \tag{A.31}$$

A guard function that can be used to describe this set is

$$\gamma_{\text{st}\to\text{sl}} = \mu^2\lambda_{n,i_c}^2 - \boldsymbol{\lambda}_{t,i_c}\boldsymbol{\lambda}_{t,i_c}^T, \tag{A.32}$$

which is equal to zero when $\mu^2\lambda_{n,i_c}^2 = ||\boldsymbol{\lambda}_{t,i_c}||$, greater than zero when $\mu^2\lambda_{n,i_c}^2 > ||\boldsymbol{\lambda}_{t,i_c}||$, and it is globally differentiable. It is physically impossible that $\mu^2\lambda_{n,i_c}^2 < ||\boldsymbol{\lambda}_{t,i_c}||$, meaning that $\gamma_{\text{st}\to\text{sl}}$ will never be smaller than zero. The dynamics and constraints of a system with all contact points in stick are defined as

$$\ddot{\boldsymbol{q}} = \boldsymbol{M}^{-1}\left[\boldsymbol{S}\boldsymbol{u} - \boldsymbol{H} + \boldsymbol{W}_n\boldsymbol{\lambda}_n + \boldsymbol{W}_t\boldsymbol{\lambda}_t\right], \tag{A.33}$$
$$\boldsymbol{W}_n^T\ddot{\boldsymbol{q}} + \dot{\boldsymbol{W}}_n^T\dot{\boldsymbol{q}} = 0, \tag{A.34}$$
$$\boldsymbol{W}_t^T\ddot{\boldsymbol{q}} + \dot{\boldsymbol{W}}_t^T\dot{\boldsymbol{q}} = 0,, \tag{A.35}$$

Substituting (A.33) into (A.34) and (A.35) leads to

$$\boldsymbol{W}_n^T\boldsymbol{M}^{-1}\boldsymbol{W}_n\boldsymbol{\lambda}_n + \boldsymbol{W}_n^T\boldsymbol{M}^{-1}\boldsymbol{W}_t\boldsymbol{\lambda}_t = \boldsymbol{W}_n^T\boldsymbol{M}^{-1}\left[\boldsymbol{S}\boldsymbol{u} - \boldsymbol{H}\right] - \dot{\boldsymbol{W}}_n^T\dot{\boldsymbol{q}}, \tag{A.36}$$
$$\boldsymbol{W}_t^T\boldsymbol{M}^{-1}\boldsymbol{W}_n\boldsymbol{\lambda}_n + \boldsymbol{W}_t^T\boldsymbol{M}^{-1}\boldsymbol{W}_t\boldsymbol{\lambda}_t = \boldsymbol{W}_t^T\boldsymbol{M}^{-1}\left[\boldsymbol{S}\boldsymbol{u} - \boldsymbol{H}\right] - \dot{\boldsymbol{W}}_t^T\dot{\boldsymbol{q}}, \tag{A.37}$$

which can be rewritten to

$$\begin{bmatrix}\boldsymbol{\lambda}_n\\ \boldsymbol{\lambda}_t\end{bmatrix} = -\boldsymbol{D}^{-1}\begin{bmatrix}\boldsymbol{W}_n^T\boldsymbol{M}^{-1}\left[\boldsymbol{S}\boldsymbol{u} - \boldsymbol{H}\right] - \dot{\boldsymbol{W}}_n^T\dot{\boldsymbol{q}}\\ \boldsymbol{W}_t^T\boldsymbol{M}^{-1}\left[\boldsymbol{S}\boldsymbol{u} - \boldsymbol{H}\right] - \dot{\boldsymbol{W}}_t^T\dot{\boldsymbol{q}}\end{bmatrix}. \tag{A.38}$$

Using (A.38) the guard function (A.32) is defined.

A.1.3 Discrete dynamics derivation

In this section the discrete dynamics are defined, describing the state reinitialization when a discrete event set is entered. These dynamics are defined by a jump map $\boldsymbol{g}$, which is defined differently for each post-event mode.

Slip post-impact mode $\dot{\boldsymbol{q}}^+ = \boldsymbol{g}_{\to\text{sl}}(\dot{\boldsymbol{q}}^-)$
The discrete dynamics of a transition with a slip post-impact mode are given by

$$\boldsymbol{M}[\dot{\boldsymbol{q}}^+ - \dot{\boldsymbol{q}}^-] = \boldsymbol{W}_n\boldsymbol{\Lambda}_n + \boldsymbol{W}_t\boldsymbol{\Lambda}_t, \tag{A.39}$$
$$\boldsymbol{W}_n^T\dot{\boldsymbol{q}}^+ = 0, \tag{A.40}$$
$$\boldsymbol{\Lambda}_t = -\mu\boldsymbol{Z}_t^-\boldsymbol{\Lambda}_n, \tag{A.41}$$

with $\boldsymbol{Z}_t^-$ defined as in (A.29) using the unit vector of the ante-impact tangential velocity $\langle\boldsymbol{\zeta}_t^-\rangle$. After substituting (A.41) intro (A.39) and rewriting to

$$\dot{\boldsymbol{q}}^+ = \left[\boldsymbol{M}^{-1}\boldsymbol{W}_n - \mu\boldsymbol{M}^{-1}\boldsymbol{W}_t\boldsymbol{Z}_t^-\right]\boldsymbol{\Lambda}_n + \dot{\boldsymbol{q}}^-, \tag{A.42}$$

and expression for $\boldsymbol{\Lambda}_n$ can be found by substituting this into (A.40), which is

$$\boldsymbol{\Lambda}_n = -\left[\boldsymbol{W}_n^T\boldsymbol{M}^{-1}\boldsymbol{W}_n - \mu\boldsymbol{W}_n^T\boldsymbol{M}^{-1}\boldsymbol{W}_t\boldsymbol{Z}_t^-\right]^{-1}\boldsymbol{W}_n^T\dot{\boldsymbol{q}}^-, \tag{A.43}$$

The jump map $\dot{\boldsymbol{q}}^+ = \boldsymbol{g}_{\to\mathrm{sl}}(\dot{\boldsymbol{q}}^-)$ is then found by substituting (A.43) into (A.42),

$$\dot{\boldsymbol{q}}^+ = -\left[\boldsymbol{M}^{-1}\boldsymbol{W}_n - \mu\boldsymbol{M}^{-1}\boldsymbol{W}_t\boldsymbol{Z}_t^-\right]\left[\boldsymbol{W}_n^T\boldsymbol{M}^{-1}\boldsymbol{W}_n - \mu\boldsymbol{W}_n^T\boldsymbol{M}^{-1}\boldsymbol{W}_t\boldsymbol{Z}_t^-\right]^{-1}\boldsymbol{W}_n^T\dot{\boldsymbol{q}}^- + \dot{\boldsymbol{q}}^-. \tag{A.44}$$

Note that when there is a transition from stick to slip, i.e., there is no impact, the post-event velocity is $\dot{\boldsymbol{q}}^+ = \dot{\boldsymbol{q}}^-$.

Stick post-impact mode $\dot{\boldsymbol{q}}^+ = \boldsymbol{g}_{\to\mathrm{st}}(\dot{\boldsymbol{q}}^-)$
The discrete dynamics of a transition with a stick post-impact mode are given by

$$\boldsymbol{M}[\dot{\boldsymbol{q}}^+ - \dot{\boldsymbol{q}}^-] = \boldsymbol{W}_n\Lambda_n + \boldsymbol{W}_t\boldsymbol{\Lambda}_t, \tag{A.45}$$
$$\boldsymbol{W}_n^T\dot{\boldsymbol{q}}^+ = 0, \tag{A.46}$$
$$\boldsymbol{W}_t^T\dot{\boldsymbol{q}}^+ = 0. \tag{A.47}$$

After rewriting (A.45) into

$$\dot{\boldsymbol{q}}^+ = \boldsymbol{M}^{-1}\boldsymbol{W}_n\boldsymbol{\Lambda}_n + \boldsymbol{M}^{-1}\boldsymbol{W}_t\boldsymbol{\Lambda}_t + \dot{\boldsymbol{q}}^-, \tag{A.48}$$

substituting this into (A.46) and (A.47) results in

$$\boldsymbol{W}_n^T\boldsymbol{M}^{-1}\boldsymbol{W}_n\boldsymbol{\Lambda}_n + \boldsymbol{W}_n^T\boldsymbol{M}^{-1}\boldsymbol{W}_t\boldsymbol{\Lambda}_t + \boldsymbol{W}_n^T\dot{\boldsymbol{q}}^- = 0 \tag{A.49}$$
$$\boldsymbol{W}_t^T\boldsymbol{M}^{-1}\boldsymbol{W}_n\boldsymbol{\Lambda}_n + \boldsymbol{W}_t^T\boldsymbol{M}^{-1}\boldsymbol{W}_t\boldsymbol{\Lambda}_t + \boldsymbol{W}_t^T\dot{\boldsymbol{q}}^- = 0. \tag{A.50}$$

This can be rewritten into a definition of $\boldsymbol{\Lambda}_n$ and $\boldsymbol{\Lambda}_t$, given by

$$\begin{bmatrix}\boldsymbol{\Lambda}_n\\ \boldsymbol{\Lambda}_t\end{bmatrix} = -\boldsymbol{D}^{-1}\begin{bmatrix}\boldsymbol{W}_n^T\dot{\boldsymbol{q}}^-\\ \boldsymbol{W}_t^T\dot{\boldsymbol{q}}^-\end{bmatrix}, \quad \text{with } \boldsymbol{D} = \begin{bmatrix}\boldsymbol{W}_n^T\boldsymbol{M}^{-1}\boldsymbol{W}_n & \boldsymbol{W}_n^T\boldsymbol{M}^{-1}\boldsymbol{W}_t\\ \boldsymbol{W}_t^T\boldsymbol{M}^{-1}\boldsymbol{W}_n & \boldsymbol{W}_t^T\boldsymbol{M}^{-1}\boldsymbol{W}_t\end{bmatrix}. \tag{A.51}$$

Substituting $\boldsymbol{\Lambda}_n$ and $\boldsymbol{\Lambda}_t$ into (A.48) results in the jump map $\dot{\boldsymbol{q}}^+ = \boldsymbol{g}_{\to\mathrm{st}}(\dot{\boldsymbol{q}}^-)$,

$$\dot{\boldsymbol{q}}^+ = \boldsymbol{M}^{-1}\boldsymbol{W}_n\boldsymbol{\Lambda}_n + \boldsymbol{M}^{-1}\boldsymbol{W}_t\boldsymbol{\Lambda}_t + \dot{\boldsymbol{q}}^-, \tag{A.52}$$

Similarly to the stick to slip case, note that when there is a transition from slip to stick the post-event velocity is $\dot{\boldsymbol{q}}^+ = \dot{\boldsymbol{q}}^-$.

Open-contact post-impact mode $\dot{\boldsymbol{q}}^+ = \boldsymbol{g}_{\to\mathrm{op}}(\dot{\boldsymbol{q}}^-)$
The discrete dynamics of a transition with a slip post-impact mode are given by

$$\boldsymbol{M}(\dot{\boldsymbol{q}}^+ - \dot{\boldsymbol{q}}^-) = 0. \tag{A.53}$$

In this case there are no impulsive reaction forces, and it is trivial to see that the jump map $\dot{\boldsymbol{q}}^+ = \boldsymbol{g}_{\to\mathrm{op}}(\dot{\boldsymbol{q}}^-)$ is given by

$$\dot{\boldsymbol{q}}^+ = \dot{\boldsymbol{q}}^-. \tag{A.54}$$

A.2 Proximal Point Formulation

The contact law and friction law defined in the complementarity condition formulation can be redefined to a proximal point formulation. This makes the system compatible with simulation methods as timestepping [63, Chapter 10]. More information on the definition of the proximal point formulation of contact laws and friction laws can be found in [22, Section 5.3].

A.2.1 Signorini's contact law and Poisson's impact law

In Figure A.2 a convex set C is illustrated. The normal cone $N_C(\boldsymbol{x})$ of a point $\boldsymbol{x}$ is $N_C(\boldsymbol{x}) = 0$ if $\boldsymbol{x} \in \text{int}(C)$, where int(.) is the interior of a set. An example of this is point $\boldsymbol{x}_3$ in Figure A.2. Defining bd(.) as the boundary of the set, when $\boldsymbol{x} \in \text{bd}(C)$ there are two options. When $\boldsymbol{x}$ is on a smooth part of bd(C), then $N_C(\boldsymbol{x})$ is a ray normal to bd(C) at point $\boldsymbol{x}$ as depicted in at point $\boldsymbol{x}_1$. When $\boldsymbol{x}$ is on a nonsmooth part of bd(C), then $N_C(\boldsymbol{x})$ is a cone starting on the point $\boldsymbol{x}$ whose sides are normal to the left and right approximation of the point $\boldsymbol{x}$ on bd(C). This is illustrated at point $\boldsymbol{x}_2$. The proximal point $\text{prox}_C(\boldsymbol{z})$ of a point $\boldsymbol{z}$, is the point in C closest to the point $\boldsymbol{z}$. The point $\boldsymbol{x}$ is the proximal point to all points $\boldsymbol{z} \in N_C(\boldsymbol{x})$. For a point $\boldsymbol{z} \in C$, $\text{prox}_C(\boldsymbol{z}) = \boldsymbol{z}$ i.e. $\boldsymbol{x}_3$ in Figure A.2.

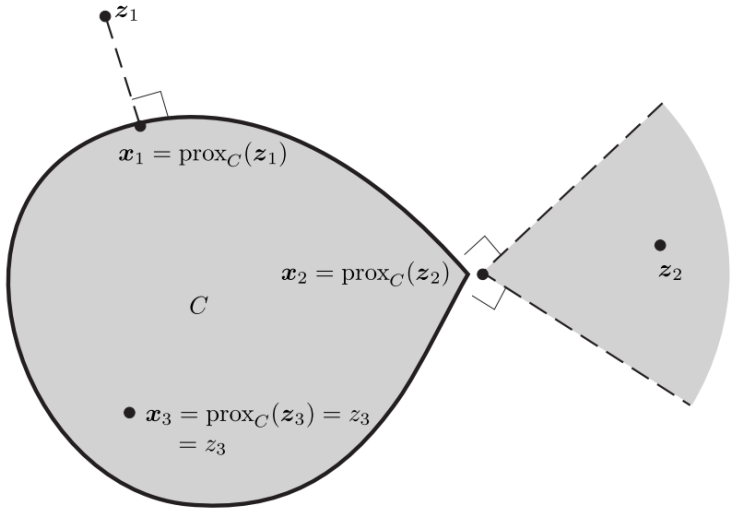

Figure A.2

This formulation can be used to define Signorini's contact law, which is defined as (2.17). The normal cone formulation, as illustrated in Figure A.2, of the contact is given by

$$-h_{n,i} \in N_{C_{n,i}}(\lambda_{n,i}), \quad \text{with } C_{n,i} = (\mathbb{R}^n)^+. \tag{A.55}$$

The set $C_{n,i}$ is the set of admissible normal forces according to Signorini's law. See Figure 2.2a for an illustration of the set $C_{n,i}$ with $\lambda_{n,i} \in C_{n,i}$ and $h_{n,i} \in N_{C_{n,i}}(\lambda_{n,i})$. Now using the fact that

$$\boldsymbol{x} = \text{prox}_C(\boldsymbol{x} - r\boldsymbol{y}), r > 0 \iff -\boldsymbol{y} \in N_C(\boldsymbol{x}), \tag{A.56}$$

rewriting (A.55) to a proximal point formulation gives

$$\lambda_{n,i} = \text{prox}_{C_{n,i}}(\lambda_{n,i} - rh_{n,i}), \quad \text{with } C_{n,i} = (\mathbb{R}^n)^+ \text{ and } r > 0. \tag{A.57}$$

Similarly for the Poisson's impact law illustrated in Figure 2.2b, we find the proximal point formulation

$$\Lambda_{n,i} = \text{prox}_{C_{n,i}}(\Lambda_{n,i} - r\zeta^+_{n,i}), \quad \text{with } C_{n,i} = (\mathbb{R}^n)^+ \text{ and } r > 0. \tag{A.58}$$

A.2.2 Coulomb's friction law

Now we define the normal cone formulation of Coulomb's friction law

$$-\boldsymbol{\zeta}_{t,i} \in N_{C_{t,i}}(\boldsymbol{\lambda}_{t,i}) \quad \forall i \in \mathcal{I}_a, \quad \text{with } C_{t,i}(\lambda_{n,i}) = \{\boldsymbol{\lambda}_{t,i} \mid ||\boldsymbol{\lambda}_{t,i}|| \leq \mu\lambda_{n,i}\}, \tag{A.59}$$

which is illustrated in Figure A.3.

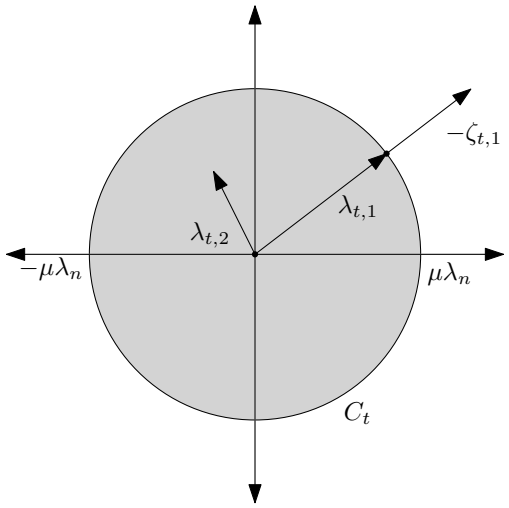

Figure A.3: *The friction disk with two seperate friction forces* $\boldsymbol{\lambda}_{t,1}$ *and* $\boldsymbol{\lambda}_{t,2}$. $\boldsymbol{\lambda}_{t,1} = \mu\lambda_{n,1}$, *resulting in a tangential velocity* $\boldsymbol{\zeta}_{t,i} > 0$. $\boldsymbol{\lambda}_{t,2} < \mu\lambda_{n,2}$, *leading to a tangential velocity* $\boldsymbol{\zeta}_{t,i} = 0$.

C_t is the set of all admitted friction forces. The tangential velocity $\boldsymbol{\zeta}_{t,i}$ is directed opposite to the friction force $\boldsymbol{\lambda}_{t,i}$ for isotropic friction.

Now using the fact that

$$\boldsymbol{x} = \text{prox}_C(\boldsymbol{x} - r\boldsymbol{y}), r > 0 \iff -\boldsymbol{y} \in N_C(\boldsymbol{x}), \tag{A.60}$$

we can rewrite the normal cone to a proximal point formulation

$$\boldsymbol{\lambda}_{t,i} = \text{prox}_{C_{t,i}}(\boldsymbol{\lambda}_{t,i} - r\boldsymbol{\zeta}_{t,i}) \quad \text{with } C_{t,i}(\lambda_{n,i}) = \{\boldsymbol{\lambda}_{t,i} \mid ||\boldsymbol{\lambda}_{t,i}|| \leq \mu\lambda_{n,i}\} \text{ and } r > 0. \tag{A.61}$$

Similarly, for the impact dynamics we can formulate

$$\boldsymbol{\Lambda}_{t,i} = \text{prox}_{C_{t,i}}(\boldsymbol{\Lambda}_{t,i} - r\boldsymbol{\zeta}^+_{t,i}) \quad \text{with } C_{t,i}(\lambda_{n,i}) = \{\boldsymbol{\Lambda}_{t,i} \mid ||\boldsymbol{\Lambda}_{t,i}|| \leq \mu\Lambda_{n,i}\} \text{ and } r > 0. \tag{A.62}$$

A.2.3 System dynamics with contact law and friction law

The flow dynamics is then described by

$$\boldsymbol{M}(\boldsymbol{q})\dot{\boldsymbol{\xi}} + \boldsymbol{H}(\boldsymbol{q}, \boldsymbol{\xi}) = \boldsymbol{S}(\boldsymbol{q})\boldsymbol{u} + \sum_{i \in \mathcal{I}_c} (\boldsymbol{w}_{n,i}(\boldsymbol{q})\lambda_{n,i} + \boldsymbol{W}_{t,i}(\boldsymbol{q})\boldsymbol{\lambda}_{t,i}), \tag{A.63}$$

$$\lambda_{n,i} = \text{prox}_{C_{n,i}}(\lambda_{n,i} - rh_{n,i}), \tag{A.64}$$

$$\boldsymbol{\lambda}_{t,i} = \text{prox}_{C_{t,i}}(\boldsymbol{\lambda}_{t,i} - r\boldsymbol{\zeta}_{t,i}), \tag{A.65}$$

with

$$C_{n,i} = (\mathbb{R}^n)^+ \text{ and } r > 0, \tag{A.66}$$

$$C_{t,i}(\lambda_{n,i}) = \{\boldsymbol{\lambda}_{t,i} \mid ||\boldsymbol{\lambda}_{t,i}|| \leq \mu\lambda_{n,i}\} \text{ and } r > 0. \tag{A.67}$$

The impulsive dynamics that take place when a contact point opens or closes contact is described by

$$\boldsymbol{M}(\boldsymbol{q})(\boldsymbol{\xi}^{+} - \boldsymbol{\xi}^{-}) = \sum_{i \in \mathcal{I}_c} \left(\boldsymbol{w}_{n,i}(\boldsymbol{q}) \Lambda_{n,i} + \boldsymbol{W}_{t,i}(\boldsymbol{q}) \boldsymbol{\Lambda}_{t,i} \right), \tag{A.68}$$

$$\Lambda_{n,i} = \operatorname{prox}_{C_{n,i}}(\Lambda_{n,i} - r\zeta_{n,i}^{+}), \tag{A.69}$$

$$\boldsymbol{\Lambda}_{t,i} = \operatorname{prox}_{C_{t,i}}(\boldsymbol{\Lambda}_{t,i} - r\boldsymbol{\zeta}_{t,i}^{+}) \tag{A.70}$$

with

$$C_{n,i} = (\mathbb{R}^n)^{+} \text{ and } r > 0, \tag{A.71}$$

$$C_{t,i}(\lambda_{n,i}) = \{\boldsymbol{\Lambda}_{t,i} \mid ||\boldsymbol{\Lambda}_{t,i}|| \leq \mu \Lambda_{n,i}\} \text{ and } r > 0. \tag{A.72}$$

Appendix B

Spatial Friction in Mechanical Systems with Unilateral Constraints

B.1 Reference trajectories with impact away from slip-stick border

Now we look at the case where a contact point goes from open to closed, away from $\mathbf{\Gamma} = 0$. This is illustrated in Figure B.1. The goal is to prove that for an event away from $\mathbf{\Gamma}$, a sufficiently small perturbation cannot cause the trajectory to hit $\gamma = 0$ at a perturbed ante-impact state $\boldsymbol{x}_\epsilon^-(t_\epsilon)$ where $\mathbf{\Gamma}$ changes sign in comparison with the unperturbed ante-impact state $\boldsymbol{\alpha}^-(\tau)$. From [66, p. 6] we know that based on the continuity property of $\boldsymbol{\gamma}$ and $\boldsymbol{f}$, the perturbed impact state can be written as

$$\boldsymbol{x}_\epsilon(t_\epsilon) = \boldsymbol{\alpha}(\tau) + \epsilon\dot{\boldsymbol{\alpha}}(\tau)\frac{\partial t_\epsilon}{\partial \epsilon} + \epsilon \boldsymbol{z}(\tau) + o(\epsilon), \tag{B.1}$$

for sufficiently small ϵ. The shortest distance between $\mathbf{\Gamma} = \mathbf{\Gamma}(\boldsymbol{\alpha}(\tau))$ and $\mathbf{\Gamma} = 0$ on the plane where $\boldsymbol{\gamma} = 0$ is defined as the constant $\delta_{\mathbf{\Gamma}}$, which is also illustrated in Figure B.1.

Let's define a point in the state $\boldsymbol{x}_{\boldsymbol{\gamma}=0,\mathbf{\Gamma}=0}$ where $\boldsymbol{\gamma}(\boldsymbol{x}_{\boldsymbol{\gamma}=0,\mathbf{\Gamma}=0}) = 0$ and $\mathbf{\Gamma}(\boldsymbol{x}_{\boldsymbol{\gamma}=0,\mathbf{\Gamma}=0}) = 0$. We are evaluating nominal trajectories which impact away from $\mathbf{\Gamma} = 0$, i.e. $\mathbf{\Gamma}(\boldsymbol{\alpha}(\tau)) \neq \mathbf{\Gamma}(\boldsymbol{x}_{\boldsymbol{\gamma}=0,\mathbf{\Gamma}=0})$. From Section **??** we know that $\mathbf{\Gamma}$ is continuously differentiable, which implies that it is Lipschitz-continuous and therefore satisfies the Lipschitz-continuity condition

$$||\boldsymbol{f}(\boldsymbol{x}) - \boldsymbol{f}(\boldsymbol{y})|| \leq \kappa||\boldsymbol{x} - \boldsymbol{y}||, \quad \forall \boldsymbol{x}, \boldsymbol{y} \in \mathbb{R}^n, \tag{B.2}$$

where $\kappa > 0$ [22]. By applying (B.2) to the function value of $\mathbf{\Gamma}$ at impact for the nominal trajectory and the perturbed trajectory, we find

$$||\mathbf{\Gamma}(\boldsymbol{\alpha}(\tau)) - \mathbf{\Gamma}(\boldsymbol{x}_{\boldsymbol{\gamma}=0,\mathbf{\Gamma}=0})|| \leq \kappa||\boldsymbol{\alpha}(\tau) - \boldsymbol{x}_{\boldsymbol{\gamma}=0,\mathbf{\Gamma}=0}||. \tag{B.3}$$

Now, since $\mathbf{\Gamma}(\boldsymbol{\alpha}(\tau)) \neq \mathbf{\Gamma}(\boldsymbol{x}_{\boldsymbol{\gamma}=0,\mathbf{\Gamma}=0})$, we know that $||\mathbf{\Gamma}(\boldsymbol{\alpha}(\tau)) - \mathbf{\Gamma}(\boldsymbol{x}_{\boldsymbol{\gamma}=0,\mathbf{\Gamma}=0})|| > 0$ and therefore from (B.3) that $||\boldsymbol{\alpha}(\tau) - \boldsymbol{x}_{\boldsymbol{\gamma}=0,\mathbf{\Gamma}=0}|| > 0$, i.e. $\delta_{\mathbf{\Gamma}} > 0$. Finally, from (B.1), we find

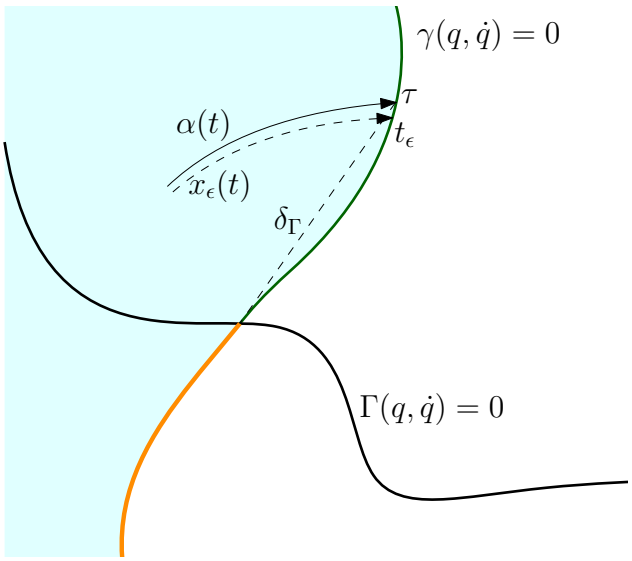

Figure B.1: *The guard functions $\boldsymbol{\gamma}$ and $\boldsymbol{\Gamma}$ in the state space of $\boldsymbol{q}$. A transition from open to closed is made away from $\boldsymbol{\Gamma}$. $\boldsymbol{\alpha}(t)$ is the nominal trajectory and $\boldsymbol{x}_\epsilon(t)$ a perturbed trajectory of the contact point up to the transition.*

$$||\boldsymbol{x}_\epsilon(t_\epsilon) - \boldsymbol{\alpha}(\tau)|| = ||\epsilon\dot{\boldsymbol{\alpha}}(\tau)\frac{\partial t_\epsilon}{\partial \epsilon} + \epsilon\boldsymbol{z}(\tau) + o(\epsilon)||. \tag{B.4}$$

Since $\delta_{\boldsymbol{\Gamma}} > 0$ and $\lim_{\epsilon\to 0} ||\boldsymbol{x}_\epsilon(t_\epsilon) - \boldsymbol{\alpha}(\tau)|| = 0$, there always exists an ϵ such that $||\boldsymbol{x}_\epsilon(t_\epsilon) - \boldsymbol{\alpha}(\tau)|| < \delta_{\boldsymbol{\Gamma}}$. In other words, this proves that if $\boldsymbol{f}$, $\boldsymbol{\gamma}$ and $\boldsymbol{\Gamma}$ are continuous and the nominal trajectory makes impact away from the slip-stick post-impact mode border $\boldsymbol{\Gamma} = 0$, then there always exists a range of ϵ such that the perturbed state will have the same post-impact mode as the nominal trajectory.

B.2 Reference trajectories with impact at the slip-stick border

- Consider as simultaneous trigger of open-closed guard and slip-stick guard. However, it is not entirely the same, as the slip-stick guard cannot be triggered before the open-closed guard.
- The trigger should be transversal, in both closed-open guard and slip-stick guard.
- If we can show continuity of post-impact state, then we can define a jump gain like H, which uses one jump map for the open to stick domain and another jump map for the open to slip domain.

B.3 Post-impact accelerations in open-to-stick transitions

The mode transition from stick to slip happens when a guard is triggered at acceleration level,

$$^{\text{slip}\leftarrow\text{stick}}\gamma = \mu^2\lambda_{n,i}^2 - \boldsymbol{\lambda}_{t,i}\boldsymbol{\lambda}_{t,i}^T, \tag{B.5}$$

and the post-impact mode is determined by the guard function defined at velocity level

$$\Gamma = \mu^2\Lambda_{n,i}^2(\boldsymbol{q},\dot{\boldsymbol{q}}^-) - \boldsymbol{\Lambda}_{t,i}(\boldsymbol{q},\dot{\boldsymbol{q}}^-)\boldsymbol{\Lambda}_{t,i}^T(\boldsymbol{q},\dot{\boldsymbol{q}}^-). \tag{B.6}$$

Since the jump map from open to stick is

$$\boldsymbol{M}(\boldsymbol{q})(\dot{\boldsymbol{q}}^+ - \dot{\boldsymbol{q}}^-) = \boldsymbol{w}_{n,i}(\boldsymbol{q})\Lambda_{n,i} + \boldsymbol{W}_{t,i}(\boldsymbol{q})\boldsymbol{\Lambda}_{t,i}, \tag{B.7}$$

$$\zeta_{n,i}^+ = 0, \tag{B.8}$$

$$\zeta_{t,i}^+ = 0, \tag{B.9}$$

which is on velocity level, the post-impact reaction forces of the open-to-stick event can be in the stick-to-slip jump set, causing an immediate transition to slip. This is demonstrated using the flow dynamics of the stick mode at the time-instant of the transition,

$$\boldsymbol{M}(\boldsymbol{q}^+)\ddot{\boldsymbol{q}}^+ + \boldsymbol{H}(\boldsymbol{q}^+, \dot{\boldsymbol{q}}^+) = \boldsymbol{S}(\boldsymbol{q}^+)\boldsymbol{u}^+ + \sum_{i\in\mathcal{I}_c}\left(\boldsymbol{w}_{n,i}(\boldsymbol{q}^+)\lambda_{n,i}^+ + \boldsymbol{W}_{t,i}(\boldsymbol{q}^+)\boldsymbol{\lambda}_{t,i}^+\right), \tag{B.10}$$

$$\boldsymbol{w}_{n,i}^T(\boldsymbol{q}^+)\ddot{\boldsymbol{q}}^+ + \dot{\boldsymbol{w}}_{n,i}^T(\boldsymbol{q}^+)\dot{\boldsymbol{q}}^+ = 0, \tag{B.11}$$

$$\boldsymbol{W}_{t,i}^T(\boldsymbol{q}^+)\ddot{\boldsymbol{q}}^+ + \dot{\boldsymbol{W}}_{t,i}^T(\boldsymbol{q}^+)\dot{\boldsymbol{q}}^+ = 0. \tag{B.12}$$

We can deduce from (B.8)-(B.9) and (B.11)-(B.12) that the normal acceleration of the transition contact point $\boldsymbol{w}_{n,i}^T(\boldsymbol{q}^+)\ddot{\boldsymbol{q}}^+$ and the tangential acceleration of the transitioning contact point $\boldsymbol{W}_{t,i}^T(\boldsymbol{q}^+)\ddot{\boldsymbol{q}}^+$ are both equal to zero. From (B.10) we then notice that $\lambda_{n,i}^+$ and $\boldsymbol{\lambda}_{t,i}^+$ depend continuously on $\boldsymbol{u}^+$ and can therefore instantly lead to $\mu^2\lambda_{n,i}^2 - \boldsymbol{\lambda}_{t,i}\boldsymbol{\lambda}_{t,i}^T > 0$ for certain $\boldsymbol{u}^+$. For these inputs the contact point will immediately start slipping after the open-to-stick transition. These areas are illustrated in Figure B.2

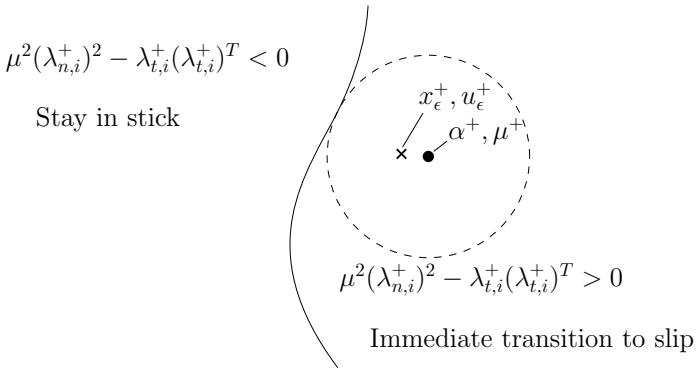

Figure B.2: *The border between an open-to-stick event that stays in stick and an open-to-stick event that immediately starts slipping is illustrated in this figure. The post event state and input indicated in the figure is in the* $\mu^2(\lambda_{n,i}^+)^2 - \boldsymbol{\lambda}_{t,i}^+(\boldsymbol{\lambda}_{t,i}^+)^T > 0$ *area, causing the contact point to immediately start slipping.*

Using the continuity of the system's flow dynamics and the function $\mu^2(\lambda_{n,i}^+)^2 - \boldsymbol{\lambda}_{t,i}^+(\boldsymbol{\lambda}_{t,i}^+)^T$, we can show that if we choose $\boldsymbol{\mu}^+$ such that $\boldsymbol{\alpha}^+, \boldsymbol{\mu}^+$ is not on $\mu^2(\lambda_{n,i}^+)^2 - \boldsymbol{\lambda}_{t,i}^+(\boldsymbol{\lambda}_{t,i}^+)^T = 0$ then there always exists a range of perturbations ϵ such that the perturbed post-impact is on the same side of $\mu^2(\lambda_{n,i}^+)^2 - \boldsymbol{\lambda}_{t,i}^+(\boldsymbol{\lambda}_{t,i}^+)^T = 0$ as the unperturbed trajectory similarly to Section B.1.

B.4 Slip-stick transition in closed-contact

Appendix C

Sensitivity Analysis for Input-Dependent Guards

C.1 Linearization for single jumps

The perturbed state is defined as

$$\boldsymbol{x}(t,\epsilon) = \boldsymbol{x}(t_0,\epsilon) + \int_{t_0}^{t} \boldsymbol{f}(\boldsymbol{x}(s,\epsilon),\boldsymbol{u}(s,\epsilon),s)ds. \tag{C.1}$$

Then

$$\frac{\partial \boldsymbol{x}(t,\epsilon)}{\partial \epsilon} = \frac{\partial \boldsymbol{x}_0}{\partial \epsilon} + \int_{t_0}^{t} \left(\frac{\partial \boldsymbol{f}}{\partial \boldsymbol{x}} \frac{\partial \boldsymbol{x}}{\partial \epsilon} + \frac{\partial \boldsymbol{f}}{\partial \boldsymbol{u}} \frac{\partial \boldsymbol{u}}{\partial \epsilon} \right) ds, \tag{C.2}$$

$$\frac{\partial^2 \boldsymbol{x}}{\partial t \partial \epsilon} = \frac{\partial \boldsymbol{f}}{\partial \boldsymbol{x}} \frac{\partial \boldsymbol{x}}{\partial \epsilon} + \frac{\partial \boldsymbol{f}}{\partial \boldsymbol{u}} \frac{\partial \boldsymbol{u}}{\partial \epsilon}, \tag{C.3}$$

which we can write as

$$\frac{\partial^2 \boldsymbol{x}}{\partial t \partial \epsilon} = D_1 \boldsymbol{f}(\boldsymbol{x}(t,\epsilon),\boldsymbol{u}(t,\epsilon),t) \cdot \frac{\partial \boldsymbol{x}}{\partial \epsilon} + D_2 \boldsymbol{f}(\boldsymbol{x}(t,\epsilon),\boldsymbol{u}(t,\epsilon),t) \cdot \frac{\partial \boldsymbol{u}}{\partial \epsilon}, \tag{C.4}$$

with $D_i \boldsymbol{f}$ the derivative of $\boldsymbol{f}$ wrt the ith term of $\boldsymbol{f}$. Evaluating (C.4) at $\epsilon = 0$ results in the flow dynamics of the positive homogenization

$$\dot{\boldsymbol{z}} = D_1 \boldsymbol{f}(\boldsymbol{\alpha}(t),\boldsymbol{\mu}(t),t) \cdot \boldsymbol{z}(t) + D_2 \boldsymbol{f}(\boldsymbol{\alpha}(t),\boldsymbol{\mu}(t),t) \cdot \boldsymbol{v}(t), \tag{C.5}$$

where

$$\boldsymbol{z}(t) = \left. \frac{\partial \boldsymbol{x}(t,\epsilon)}{\partial \epsilon} \right|_{\epsilon=0}, \text{ and } \boldsymbol{v}(t) = \left. \frac{\partial \boldsymbol{u}(t,\epsilon)}{\partial \epsilon} \right|_{\epsilon=0}. \tag{C.6}$$

When we consider a single jump

$$\boldsymbol{x}_\epsilon^+(t_\epsilon,\epsilon) = \boldsymbol{g}(\boldsymbol{x}_\epsilon^-(t_\epsilon,\epsilon),t_\epsilon), \tag{C.7}$$

using a Taylor approximation (**Under what conditions is this approximation valid? γ continuous, α continuous, $\boldsymbol{f}$ continuous?**) with respect to ϵ and around $\epsilon = 0$, we can write

$$\boldsymbol{x}_\epsilon^+(t_\epsilon,\epsilon) = \boldsymbol{\alpha}^+(t_\epsilon) + \epsilon \boldsymbol{z}^+(t_\epsilon) + o(\epsilon), \tag{C.8}$$

$$\boldsymbol{u}_\epsilon^+(t_\epsilon,\epsilon) = \boldsymbol{\mu}^+(t_\epsilon) + \epsilon \boldsymbol{v}^+(t_\epsilon) + o(\epsilon), \tag{C.9}$$

where $\boldsymbol{\alpha}(t)$ is a nominal reference trajectory that satisfies the dynamics of the system and $\boldsymbol{\mu}(t)$ an input that achieves this reference trajectory. Now we expand this in terms of ϵ, so with

$$\Delta = \left.\frac{\partial t_\epsilon}{\partial \epsilon}\right|_{\epsilon=0}, \tag{C.10}$$

we get

$$\boldsymbol{\alpha}^+(t_\epsilon) = \boldsymbol{\alpha}^+(\tau) + \epsilon\dot{\boldsymbol{\alpha}}^+(\tau)\Delta + o(\epsilon), \tag{C.11}$$
$$\boldsymbol{\mu}^+(t_\epsilon) = \boldsymbol{\mu}^+(\tau) + \epsilon\dot{\boldsymbol{\mu}}^+(\tau)\Delta + o(\epsilon), \tag{C.12}$$
$$\boldsymbol{z}^+(t_\epsilon) = \boldsymbol{z}^+(\tau) + \epsilon\dot{\boldsymbol{z}}^+(\tau)\Delta + o(\epsilon), \tag{C.13}$$
$$\boldsymbol{v}^+(t_\epsilon) = \boldsymbol{v}^+(\tau) + \epsilon\dot{\boldsymbol{v}}^+(\tau)\Delta + o(\epsilon), \tag{C.14}$$

which when substituted into (C.8) and (C.9) gives,

$$\boldsymbol{x}_\epsilon^+(t_\epsilon, \epsilon) = \boldsymbol{\alpha}^+(\tau) + \epsilon\dot{\boldsymbol{\alpha}}^+(\tau)\Delta + \epsilon\boldsymbol{z}^+(\tau) + o(\epsilon). \tag{C.15}$$
$$\boldsymbol{u}_\epsilon^+(t_\epsilon, \epsilon) = \boldsymbol{\mu}^+(\tau) + \epsilon\dot{\boldsymbol{\mu}}^+(\tau)\Delta + \epsilon\boldsymbol{v}^+(\tau) + o(\epsilon). \tag{C.16}$$

To find Δ, we evaluate the ante impact guard function

$$\gamma^-(\boldsymbol{x}_\epsilon^-(t_\epsilon), \boldsymbol{u}_\epsilon^-(t_\epsilon), t_\epsilon) = 0. \tag{C.17}$$

In previous work, the guard function γ was not dependent on $\boldsymbol{u}_\epsilon(t_\epsilon)$ because friction and release was not considered. We now expand $\gamma(\boldsymbol{x}_\epsilon(t_\epsilon), \boldsymbol{u}_\epsilon(t_\epsilon), t_\epsilon)$ wrt ϵ, giving

$$\gamma(\boldsymbol{x}_\epsilon(t_\epsilon), \boldsymbol{u}_\epsilon(t_\epsilon), t_\epsilon) = \gamma(\boldsymbol{\alpha}(\tau), \boldsymbol{\mu}(\tau), \tau) + \epsilon\left[\frac{\partial\gamma}{\partial\epsilon}(\boldsymbol{\alpha}(\tau), \boldsymbol{\mu}(\tau), \tau)\right]_{\epsilon=0} + o(\epsilon), \tag{C.18}$$
$$= \gamma(\boldsymbol{\alpha}(\tau), \boldsymbol{\mu}(\tau), \tau) + \epsilon\left[\frac{\partial\gamma}{\partial\boldsymbol{x}}\left(\frac{\partial\boldsymbol{x}}{\partial\epsilon} + \frac{\partial\boldsymbol{x}}{\partial t_\epsilon}\frac{dt_\epsilon}{d\epsilon}\right) + \frac{\partial\gamma}{\partial\boldsymbol{u}}\left(\frac{\partial\boldsymbol{u}}{\partial\epsilon} + \frac{\partial\boldsymbol{u}}{\partial t_\epsilon}\frac{dt_\epsilon}{d\epsilon}\right) + \frac{\partial\gamma}{\partial t_\epsilon}\frac{dt_\epsilon}{d\epsilon}\right]_{\epsilon=0} + o(\epsilon). \tag{C.19}$$

By definition $\gamma(\tau) = 0$, so we can rewrite (C.19) to

$$\gamma(\boldsymbol{x}_\epsilon(t_\epsilon), \boldsymbol{u}_\epsilon(t_\epsilon), t_\epsilon) = \epsilon\left[D_1\gamma \cdot (\overline{\boldsymbol{z}}(\tau) + \dot{\boldsymbol{\alpha}}(\tau)\Delta) + D_2\gamma \cdot (\overline{\boldsymbol{v}}(\tau) + \dot{\boldsymbol{\mu}}(\tau)\Delta) + D_3 \cdot \gamma\Delta\right] \tag{C.20}$$

Now we can evaluate (C.19) using (C.20), which gives

$$\epsilon\left[D_1\gamma^- \cdot \left(\boldsymbol{z}^-(\tau) + \dot{\boldsymbol{\alpha}}^-(\tau)\Delta\right) + D_2\gamma^- \cdot \left(\boldsymbol{v}^-(\tau) + \dot{\boldsymbol{\mu}}^-(\tau)\Delta\right) + D_3\gamma^- \cdot \Delta\right] = 0. \tag{C.21}$$

From (C.21) we can determine the expression for Δ,

$$\Delta = -\frac{D_1\gamma^- \cdot \boldsymbol{z}^-(\tau) + D_2\gamma^- \cdot \boldsymbol{v}^-(\tau)}{\dot{\gamma}^-}, \tag{C.22}$$

with

$$\gamma^- = \gamma^-(\boldsymbol{\alpha}^-(\tau), \boldsymbol{\mu}^-(\tau), \tau), \tag{C.23}$$
$$\dot{\gamma}^- = D_1\gamma^- \cdot \dot{\boldsymbol{\alpha}}^- + D_2\gamma^- \cdot \dot{\boldsymbol{\mu}}^- + D_3\gamma^-. \tag{C.24}$$

To find the expression for the right hand side of (C.7), we now expand $\boldsymbol{g}(\boldsymbol{x}_\epsilon^-(t_\epsilon, \epsilon), \boldsymbol{u}_\epsilon^-(t_\epsilon, \epsilon), t_\epsilon)$ with respect to ϵ as

$$\boldsymbol{g}(\boldsymbol{x}_\epsilon^-, \boldsymbol{u}_\epsilon^-, t_\epsilon) = \boldsymbol{g}(\boldsymbol{\alpha}^-(\tau), \tau) + \epsilon \left[\frac{\partial \boldsymbol{g}}{\partial \epsilon}\right] + o(\epsilon), \tag{C.25}$$

$$= \boldsymbol{\alpha}^+(\tau) + \epsilon \left[\frac{\partial \boldsymbol{g}}{\partial \boldsymbol{x}}\left(\frac{\partial \boldsymbol{x}}{\partial \epsilon} + \frac{\partial \boldsymbol{x}}{\partial t_\epsilon}\frac{dt_\epsilon}{d\epsilon}\right) + \frac{\partial \boldsymbol{g}}{\partial \boldsymbol{u}}\left(\frac{\partial \boldsymbol{u}}{\partial \epsilon} + \frac{\partial \boldsymbol{u}}{\partial t_\epsilon}\frac{dt_\epsilon}{d\epsilon}\right) + \frac{\partial \boldsymbol{g}}{\partial t_\epsilon}\frac{dt_\epsilon}{d\epsilon}\right]_{\epsilon=0} + o(\epsilon), \tag{C.26}$$

$$= \boldsymbol{\alpha}^+(\tau) + \epsilon \left[D_1\boldsymbol{g} \cdot \left(\boldsymbol{z}^- + \dot{\boldsymbol{\alpha}}^-\Delta\right) + D_2\boldsymbol{g} \cdot \left(\boldsymbol{v}^- + \dot{\boldsymbol{\mu}}(\tau)\Delta\right) + D_3\boldsymbol{g} \cdot \Delta\right] + o(\epsilon). \tag{C.27}$$

Note that $\boldsymbol{g}$ does not depend on the input $\boldsymbol{u}$. Jump maps are impulsive by definition, and since impulsive inputs do not exist it is impossible for the jump map to be dependent on $\boldsymbol{u}$. For small ϵ, we can rewrite (C.7), (C.22) and (C.27) to a general jump map with counter k as

$$\boldsymbol{x}_\epsilon^k(t_\epsilon, \epsilon) = \boldsymbol{g}^k(\boldsymbol{x}_\epsilon^{k-1}, \boldsymbol{u}_\epsilon^{k-1}, t_\epsilon), \tag{C.28}$$

$$\Delta^k = -\frac{D_1\gamma^k \cdot \boldsymbol{z}^{k-1}(\tau) + D_2\gamma^k \cdot \boldsymbol{v}^{k-1}(\tau)}{\dot{\gamma}^k}, \tag{C.29}$$

$$\boldsymbol{g}^k(\boldsymbol{x}_\epsilon^{k-1}, \boldsymbol{u}_\epsilon^{k-1}, t_\epsilon) = \boldsymbol{\alpha}^k(\tau) + \epsilon \left[D_1\boldsymbol{g}^k \cdot \left(\boldsymbol{z}^{k-1}(\tau) + \dot{\boldsymbol{\alpha}}^{k-1}\Delta^k\right) + D_2\boldsymbol{g}^k \cdot \left(\boldsymbol{v}^{k-1}(\tau) + \dot{\boldsymbol{\mu}}^{k-1}\Delta^k\right) + D_3\boldsymbol{g}^k \cdot \Delta^k\right]. \tag{C.30}$$

From (C.15) we get

$$\boldsymbol{z}^k(\tau) = \frac{1}{\epsilon}\left(\boldsymbol{x}_\epsilon^k(t_\epsilon) - \boldsymbol{\alpha}^k(\tau)\right) - \dot{\boldsymbol{\alpha}}^k(\tau)\Delta^k, \tag{C.31}$$

and by equating (C.28) and (C.30) we find an expression for $\overline{\boldsymbol{x}}_\epsilon^k(t_\epsilon, \epsilon)$ which we can substitute into (C.31) resulting in

$$\boldsymbol{z}^k(\tau) = D_1\boldsymbol{g}^k \cdot \left(\boldsymbol{z}^{k-1}(\tau) + \dot{\boldsymbol{\alpha}}^{k-1}\Delta^k\right) + D_2\boldsymbol{g}^k \cdot \left(\boldsymbol{v}^{k-1}(\tau) + \dot{\boldsymbol{\mu}}^{k-1}\Delta^k\right) + D_3\boldsymbol{g}^k \cdot \Delta^k - \dot{\boldsymbol{\alpha}}^k(\tau)\Delta^k. \tag{C.32}$$

Now, by substituting (C.29) into (C.32), we get

$$\boldsymbol{z}^k(\tau) = D_1\boldsymbol{g}^k \cdot \boldsymbol{z}^{k-1} + D_2\boldsymbol{g}^k \cdot \boldsymbol{v}^{k-1} - \left(D_1\boldsymbol{g}^k \cdot \boldsymbol{f}^{k-1} + D_2\boldsymbol{g}^k \cdot \dot{\boldsymbol{\mu}}^{k-1} + D_3\boldsymbol{g}^k \cdot 1 - \boldsymbol{f}^k\right)\frac{D_1\gamma^k \cdot \boldsymbol{z}^{k-1} + D_2\gamma^k \cdot \boldsymbol{v}^{k-1}}{\dot{\gamma}^k}, \tag{C.33}$$

$$\boldsymbol{z}^k(\tau) = \left(\frac{\boldsymbol{f}^k - \dot{\boldsymbol{g}}^k}{\dot{\gamma}^k}D_1\gamma^k + D_1\boldsymbol{g}^k\right) \cdot \boldsymbol{z}^{k-1} + \left(\frac{\boldsymbol{f}^k - \dot{\boldsymbol{g}}^k}{\dot{\gamma}^k}D_2\gamma^k + D_2\boldsymbol{g}^k\right) \cdot \boldsymbol{v}^{k-1}, \tag{C.34}$$

with

$$\dot{\boldsymbol{g}}^k = D_1\boldsymbol{g}^k \cdot \boldsymbol{f}^{k-1} + D_2\boldsymbol{g}^k \cdot \dot{\boldsymbol{\mu}}^{k-1} + D_3\boldsymbol{g}^k \cdot 1, \tag{C.35}$$

$$\boldsymbol{f}^k = {}^{s^k}\boldsymbol{f}(\boldsymbol{\alpha}^k(\tau), \boldsymbol{\mu}^k(\tau), \tau). \tag{C.36}$$

Now, using

$$\boldsymbol{G}_{\boldsymbol{z}}^k(\tau) = \frac{\boldsymbol{f}^k - \dot{\boldsymbol{g}}^k}{\dot{\gamma}^k}D_1\gamma^k \cdot 1 + D_1\boldsymbol{g}^k \cdot 1, \tag{C.37}$$

$$\boldsymbol{G}_{\boldsymbol{v}}^k(\tau) = \frac{\boldsymbol{f}^k - \dot{\boldsymbol{g}}^k}{\dot{\gamma}^k}D_2\gamma^k \cdot 1 + D_2\boldsymbol{g}^k \cdot 1, \tag{C.38}$$

we can write

$$\boldsymbol{z}^k(\tau) = \boldsymbol{G}_{\boldsymbol{z}}^k \boldsymbol{z}^{k-1} + \boldsymbol{G}_{\boldsymbol{v}}^k \boldsymbol{v}^{k-1}. \tag{C.39}$$

C.2 Linearization for multiple jumps

With $k+1 = k^+$ and $k-1 = k^-$, we now assume that we find the first order approximation of the perturbed post-impact state of two simultaneous jumps, by considering these jumps after each other as

$$\boldsymbol{z}^{k^+}(\tau) = \boldsymbol{G}_{\boldsymbol{z}}^{k^+} \boldsymbol{z}^k + \boldsymbol{G}_{\boldsymbol{v}}^{k^+} \boldsymbol{v}^k \tag{C.40}$$

$$\boldsymbol{z}^{k^+}(\tau) = \boldsymbol{G}_{\boldsymbol{z}}^{k^+} \left(\boldsymbol{G}_{\boldsymbol{z}}^k \boldsymbol{z}^{k^-} + \boldsymbol{G}_{\boldsymbol{v}}^k \boldsymbol{v}^{k^-} \right) + \boldsymbol{G}_{\boldsymbol{z}}^{k^+} \boldsymbol{v}^k, \tag{C.41}$$

$$= \boldsymbol{G}_{\boldsymbol{z}}^{k^+} \boldsymbol{G}_{\boldsymbol{z}}^k \boldsymbol{z}^{k^-} + \boldsymbol{G}_{\boldsymbol{z}}^{k^+} \boldsymbol{G}_{\boldsymbol{v}}^k \boldsymbol{v}^{k^-} + \boldsymbol{G}_{\boldsymbol{v}}^{k^+} \boldsymbol{v}^k. \tag{C.42}$$

We prove that this is true by deriving an expression for the post-impact state of two simultaneous jumps, and comparing it with (C.42). Now we evaluate the jump map of two jumps at the same time instant τ,

$${}^{s^{k^+} \leftarrow s^k \leftarrow s^{k^-}} \boldsymbol{x}_\epsilon(t_\epsilon^{k^+}) = \boldsymbol{g}^{k^+}(\boldsymbol{x}_\epsilon^k(t_\epsilon^{k^+}), \boldsymbol{u}_\epsilon^k(t_\epsilon^{k^+}), t_\epsilon^{k^+}), \tag{C.43}$$

with

$$\boldsymbol{x}_\epsilon^k(t_\epsilon^{k^+}) = \int_{t_\epsilon^k}^{t_\epsilon^{k^+}} \left[{}^{s^k}\boldsymbol{f}\left(\boldsymbol{x}_\epsilon^k(t), \boldsymbol{u}_\epsilon^k(t)\right)\right] dt + \boldsymbol{g}^k(\boldsymbol{x}_\epsilon^{k^-}(t_\epsilon^k), \boldsymbol{u}_\epsilon^{k^-}(t_\epsilon^k), t_\epsilon^k). \tag{C.44}$$

We rewrite the integral in (C.44) to

$$\int_{t_\epsilon^k}^{t_\epsilon^{k^+}} {}^{s^k}\boldsymbol{f}(t,\epsilon)dt = \boldsymbol{F}(t_\epsilon^{k^+}, \epsilon) - \boldsymbol{F}(t_\epsilon^k, \epsilon) = \boldsymbol{\Phi}(t_\epsilon^k, t_\epsilon^{k^+}, \epsilon), \tag{C.45}$$

where ${}^{s^k}\boldsymbol{f}\left(\boldsymbol{x}_\epsilon^k(t), \boldsymbol{u}_\epsilon^k(t)\right)$ can be written as ${}^{s^k}\boldsymbol{f}(t,\epsilon)$, because $\boldsymbol{x}_\epsilon$ and $\boldsymbol{u}$ depend solely on t and ϵ.
We now expand $\boldsymbol{\Phi}$ with respect to ϵ, which results in

$$\boldsymbol{\Phi}(t_\epsilon^k, t_\epsilon^{k^+}, \epsilon) = \boldsymbol{\Phi}(t_0^k, t_0^{k^+}, \epsilon) + \epsilon \left.\frac{\partial \boldsymbol{\Phi}}{\partial \epsilon}\right|_{\epsilon=0} + o(\epsilon), \tag{C.46}$$

$$= \boldsymbol{F}(\tau,0) - \boldsymbol{F}(\tau,0) + \left[{}^{s^k}\boldsymbol{f}(t_\epsilon^{k^+},\epsilon)\frac{dt_\epsilon^{k^+}}{d\epsilon} - {}^{s^k}\boldsymbol{f}(t_\epsilon^{k^+},\epsilon)\frac{dt_\epsilon^k}{d\epsilon} + \int_{t_\epsilon^k}^{t_\epsilon^{k^+}} \frac{\partial\, {}^{s^k}\boldsymbol{f}(t,\epsilon)}{\partial \epsilon} dt \right]_{\epsilon=0}, \tag{C.47}$$

$$= \boldsymbol{f}^k(\Delta^{k^+} - \Delta^k), \tag{C.48}$$

since $\int_{t_\epsilon^k}^{t_\epsilon^{k^+}} \frac{\partial\, {}^{s^k}\boldsymbol{f}(t,\epsilon)}{\partial \epsilon} dt_{\epsilon=0} = 0$. Note that ϵ is assumed sufficiently small, such that we can write t as a function of ϵ.

By expanding (C.43) with respect to ϵ, we find

$$ {}^{s^{k^+}\leftarrow s^k\leftarrow s^{k^-}}\boldsymbol{x}_\epsilon(t_\epsilon^{k^+}) = \boldsymbol{\alpha}^{k^+}(\tau) + \epsilon \left.\frac{\partial \boldsymbol{g}^{k^+}(\boldsymbol{x}_\epsilon^k(t_\epsilon^{k^+}), \boldsymbol{u}_\epsilon^k(t_\epsilon^{k^+}), t_\epsilon^{k^+})}{\partial \epsilon}\right|_{\epsilon=0} + o(\epsilon), \tag{C.49}$$

where

$$\begin{aligned}\left.\frac{\partial \boldsymbol{g}^{k^+}(\boldsymbol{x}_\epsilon^k(t_\epsilon^{k^+}), \boldsymbol{u}_\epsilon^k(t_\epsilon^{k^+}), t_\epsilon^{k^+})}{\partial \epsilon}\right|_{\epsilon=0} = \Bigg[&\frac{\partial \boldsymbol{g}^{k^+}}{\partial \boldsymbol{x}}\left(\frac{\partial \boldsymbol{\Phi}}{\partial \epsilon} + \frac{\partial \boldsymbol{g}^k}{\partial \boldsymbol{x}}\left(\frac{\partial \boldsymbol{x}^{k^-}}{\partial \epsilon} + \frac{\partial \boldsymbol{x}^{k^-}}{\partial t}\frac{dt_\epsilon^k}{d\epsilon}\right) + \right.\\ &\left.\frac{\partial \boldsymbol{g}^k}{\partial \boldsymbol{u}}\left(\frac{\partial \boldsymbol{u}^{k^-}}{\partial \epsilon} + \frac{\partial \boldsymbol{u}^{k^-}}{\partial t}\frac{dt_\epsilon^k}{d\epsilon}\right) + \frac{\partial \boldsymbol{g}^k}{\partial t}\frac{dt_\epsilon^k}{d\epsilon}\right) + \frac{\partial \boldsymbol{g}^{k^+}}{\partial t}\frac{dt_\epsilon^{k^+}}{d\epsilon}\Bigg]_{\epsilon=0},\end{aligned} \tag{C.50}$$

$$\begin{aligned}\left.\frac{\partial \boldsymbol{g}^{k^+}(\boldsymbol{x}_\epsilon^k(t_\epsilon^{k^+}), \boldsymbol{u}_\epsilon^k(t_\epsilon^{k^+}), t_\epsilon^{k^+})}{\partial \epsilon}\right|_{\epsilon=0} = {}& D_1\boldsymbol{g}^{k^+}\cdot\left(\boldsymbol{f}^k(\Delta^{k^+} - \Delta^k) + D_1\boldsymbol{g}^k\cdot\left(\boldsymbol{z}^{k^-} + \boldsymbol{f}^{k^-}\Delta^k\right)\right.\\ &\left. + D_2\boldsymbol{g}^k\cdot\left(\boldsymbol{v}^{k^-} + \dot{\boldsymbol{\mu}}^{k^-}\Delta^k\right) + D_3\boldsymbol{g}^k\cdot\Delta^k\right) + D_3\boldsymbol{g}^{k^+}\cdot\Delta^{k^+}.\end{aligned} \tag{C.51}$$

We now substitute (C.51) into (C.49), which we in turn substitute into (C.31) to get

$$\begin{aligned}\boldsymbol{z}^{k^+}(\tau) = {}& D_1\boldsymbol{g}^{k^+}\cdot\boldsymbol{f}^k\Delta^{k^+} - D_1\boldsymbol{g}^{k^+}\cdot\boldsymbol{f}^{k^+}\Delta^k + D_1\boldsymbol{g}^{k^+}\cdot\left(D_1\boldsymbol{g}^k\cdot\left(\boldsymbol{z}^{k^-} + \boldsymbol{f}^{k^-}\Delta^k\right)\right.\\ &\left. + D_2\boldsymbol{g}^k\cdot\left(\boldsymbol{v}^{k^-} + \dot{\boldsymbol{\mu}}^{k^-}\Delta^k\right) + D_3\boldsymbol{g}^k\cdot\Delta^k\right) + \left(D_3\boldsymbol{g}^{k^+}\cdot 1 - \boldsymbol{f}^{k^+}\right)\Delta^{k^+},\end{aligned} \tag{C.52}$$

under the assumption that ϵ is small. The four terms in (C.52) can be rewritten into

$$D_1\boldsymbol{g}^{k^+}\cdot\boldsymbol{f}^k\Delta^{k^+} = \frac{-D_1\boldsymbol{g}^{k^+}\cdot\boldsymbol{f}^{k^+}}{\dot{\gamma}^{k^+}}\left(D_1\gamma^{k^+}\cdot\left(\boldsymbol{G}_{\boldsymbol{z}}^k\boldsymbol{z}^{k^-} + \boldsymbol{G}_{\boldsymbol{v}}^k\boldsymbol{v}^{k^-}\right) + D_2\gamma^{k^+}\cdot\boldsymbol{v}^k\right), \tag{C.53}$$

$$D_1\boldsymbol{g}^{k^+}\cdot\left(-\boldsymbol{f}^k\Delta^k\right) = \frac{D_1\boldsymbol{g}^{k^+}\cdot\boldsymbol{f}^k}{\dot{\gamma}^k}\left(D_1\gamma^k\cdot\boldsymbol{z}^{k^-} + D_2\gamma^k\cdot\boldsymbol{v}^{k^-}\right), \tag{C.54}$$

$$\begin{aligned}&D_1\boldsymbol{g}^{k^+}\cdot\left(D_1\boldsymbol{g}^k\cdot\left(\boldsymbol{z}^{k^-} + \boldsymbol{f}^{k^-}\Delta^k\right) + D_2\boldsymbol{g}^k\cdot\left(\boldsymbol{v}^{k^-} + \dot{\boldsymbol{\mu}}^{k^-}\Delta^k\right) + D_3\boldsymbol{g}^k\cdot\Delta^k\right) =\\ &\quad D_1\boldsymbol{g}^{k^+}\cdot\left(\frac{-D_1\boldsymbol{g}^k\cdot\boldsymbol{f}^{k^-}}{\dot{\gamma}^k}D_1\gamma^k + \frac{-D_2\boldsymbol{g}^k\cdot\dot{\boldsymbol{\mu}}^{k^-}}{\dot{\gamma}^k}D_1\gamma^k + \frac{-D_3\boldsymbol{g}^k\cdot 1}{\dot{\gamma}^k}D_1\gamma^k + D_1\boldsymbol{g}^k\right)\cdot\boldsymbol{z}^{k^-}\\ &+ D_1\boldsymbol{g}^{k^+}\cdot\left(\frac{-D_1\boldsymbol{g}^k\cdot\boldsymbol{f}^{k^-}}{\dot{\gamma}^k}D_2\gamma^k + \frac{-D_2\boldsymbol{g}^k\cdot\dot{\boldsymbol{\mu}}^{k^-}}{\dot{\gamma}^k}D_2\gamma^k + \frac{-D_3\boldsymbol{g}^k\cdot 1}{\dot{\gamma}^k}D_2\gamma^k + D_2\boldsymbol{g}^k\right)\cdot\boldsymbol{v}^{k^-},\end{aligned} \tag{C.55}$$

$$\left(D_3\boldsymbol{g}^{k^+}\cdot 1 - \boldsymbol{f}^{k^+}\right)\Delta^{k^+} = \frac{-D_3\boldsymbol{g}^{k^+}\cdot 1 + \boldsymbol{f}^{k^+}}{\dot{\gamma}^{k^+}}\left(D_1\gamma^{k^+}\cdot\left(\boldsymbol{G}_{\boldsymbol{z}}^k\boldsymbol{z}^{k^-} + \boldsymbol{G}_{\boldsymbol{v}}^k\boldsymbol{v}^{k^-}\right) + D_2\gamma^{k^+}\cdot\boldsymbol{v}^k\right). \tag{C.56}$$

When we substitute the equations above into (C.52), after reordering the expression we get

$$\begin{aligned}\boldsymbol{z}^{k^+}(\tau) = &\left(\frac{\boldsymbol{f}^{k^+} - D_1\boldsymbol{g}^{k^+}\cdot\boldsymbol{f}^k - D_2\boldsymbol{g}^{k^+}\cdot\dot{\boldsymbol{\mu}}^k - D_3\boldsymbol{g}^{k^+}\cdot 1}{\dot{\gamma}^{k^+}} D_1\gamma^{k^+}\cdot\boldsymbol{G}_{\boldsymbol{z}}^k\right.\\
&\left.+D_1\boldsymbol{g}^{k^+}\cdot\frac{\boldsymbol{f}^k - D_1\boldsymbol{g}^k\cdot\boldsymbol{f}^{k^-} - D_2\boldsymbol{g}^k\cdot\dot{\boldsymbol{\mu}}^{k^-} - D_3\boldsymbol{g}^k\cdot 1}{\dot{\gamma}^k} D_1\gamma^{k^+} + D_1\boldsymbol{g}^{k^+}D_1\boldsymbol{g}^k\cdot 1\right)\boldsymbol{z}^{k^-}\\
&+\left(\frac{\boldsymbol{f}^{k^+} - D_1\boldsymbol{g}^{k^+}\cdot\boldsymbol{f}^k - D_2\boldsymbol{g}^{k^+}\cdot\dot{\boldsymbol{\mu}}^k - D_3\boldsymbol{g}^{k^+}\cdot 1}{\dot{\gamma}^{k^+}} D_1\gamma^{k^+}\cdot\boldsymbol{G}_{\boldsymbol{v}}^k\right.\\
&\left.+D_1\boldsymbol{g}^{k^+}\cdot\frac{\boldsymbol{f}^k - D_1\boldsymbol{g}^k\cdot\boldsymbol{f}^{k^-} - D_2\boldsymbol{g}^k\cdot\dot{\boldsymbol{\mu}}^{k^-} - D_3\boldsymbol{g}^k\cdot 1}{\dot{\gamma}^k} D_2\gamma^{k^+} + D_1\boldsymbol{g}^{k^+}D_2\boldsymbol{g}^k\cdot 1\right)\boldsymbol{v}^{k^-}\\
&+\left(\frac{\boldsymbol{f}^{k^+} - D_1\boldsymbol{g}^{k^+}\cdot\boldsymbol{f}^k - D_2\boldsymbol{g}^{k^+}\cdot\dot{\boldsymbol{\mu}}^k - D_3\boldsymbol{g}^{k^+}\cdot 1}{\dot{\gamma}^{k^+}} D_2\gamma^{k^+}\right)\boldsymbol{v}^k, \quad \text{(C.57)}\end{aligned}$$

from which we can isolate $\boldsymbol{G}_{\boldsymbol{z}}^k$, and $\boldsymbol{G}_{\boldsymbol{v}}^k$ resulting in

$$\begin{aligned}\boldsymbol{z}^{k^+}(\tau) = &\left(\frac{\boldsymbol{f}^{k^+} - D_1\boldsymbol{g}^{k^+}\cdot\boldsymbol{f}^k - D_2\boldsymbol{g}^{k^+}\cdot\dot{\boldsymbol{\mu}}^k - D_3\boldsymbol{g}^{k^+}\cdot 1}{\dot{\gamma}^{k^+}} D_1\gamma^{k^+} + D_1\boldsymbol{g}^{k^+}\cdot 1\right)\boldsymbol{G}_{\boldsymbol{z}}^k\boldsymbol{z}^{k^-}\\
&+\left(\frac{\boldsymbol{f}^{k^+} - D_1\boldsymbol{g}^{k^+}\cdot\boldsymbol{f}^k - D_2\boldsymbol{g}^{k^+}\cdot\dot{\boldsymbol{\mu}}^k - D_3\boldsymbol{g}^{k^+}\cdot 1}{\dot{\gamma}^{k^+}} D_1\gamma^{k^+} + D_1\boldsymbol{g}^{k^+}\cdot 1\right)\boldsymbol{G}_{\boldsymbol{v}}^k\boldsymbol{v}^{k^-}\\
&+\left(\frac{\boldsymbol{f}^{k^+} - D_1\boldsymbol{g}^{k^+}\cdot\boldsymbol{f}^k - D_2\boldsymbol{g}^{k^+}\cdot\dot{\boldsymbol{\mu}}^k - D_3\boldsymbol{g}^{k^+}\cdot 1}{\dot{\gamma}^{k^+}} D_2\gamma^{k^+}\right)\boldsymbol{v}^k, \quad \text{(C.58)}\end{aligned}$$

which is equal to

$$\boldsymbol{z}^{k^+}(\tau) = \boldsymbol{G}_{\boldsymbol{z}}^{k^+}\boldsymbol{G}_{\boldsymbol{z}}^k\boldsymbol{z}^{k^-} + \boldsymbol{G}_{\boldsymbol{z}}^{k^+}\boldsymbol{G}_{\boldsymbol{v}}^k\boldsymbol{v}^{k^-} + \boldsymbol{G}_{\boldsymbol{v}}^{k^+}\boldsymbol{v}^k. \quad \text{(C.59)}$$

Here we see that (C.59) is equal to (C.42). This proves that for any k, the first-order approximation of the post-impact state of two simultaneous jumps at τ can be found by evaluating the two jumps separately. Since k is a variable in this proof, using an induction-like proof, this holds for any amount of jumps as well. This is illustrated in Figure C.1.

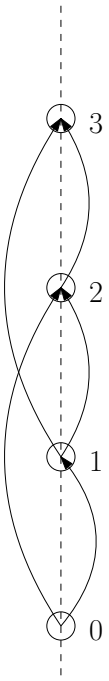

Figure C.1

When we take $k = 1$, we show that the jumps from 0 to 2 can be described by evaluating the jump from 0 to 1 and the jump 1 to 2 in succession. This also holds for $k = 2$. The jump from 0 to 3 can be described by evaluating the jump from 0 to 2 and the jump from 2 to 3 in succession. This way we proved that we can use (C.59) to find an expression for the first-order approximation of the post-impact state for l simultaneous jumps, with $l \in \mathbb{Z}$. Also, we show that multiple constant jump gains will result in a total jump which can also be described by a constant jump gain.

For l simultaneous jumps, we can find the first-order approximation of the post-impact state using

$$ {}^{l\leftarrow 0}\boldsymbol{z}(\tau) = {}^{l\leftarrow 0}\boldsymbol{L}(\boldsymbol{z}^0(\tau), \boldsymbol{v}(\tau), \tau) = {}^{l\leftarrow 0}\boldsymbol{G}\boldsymbol{z}^0(\tau) + \sum_{i=0}^{l-1} \left({}^{l\leftarrow i+1}\boldsymbol{G}\ {}^{i+1\leftarrow i}\boldsymbol{J}\boldsymbol{v}^i(\tau) \right), \tag{C.60} $$

where the superscript

$$ b \leftarrow a = b \leftarrow (b-1) \leftarrow \cdots \leftarrow (a+1) \leftarrow a, \tag{C.61} $$

and

$$ {}^{b\leftarrow a}\boldsymbol{G}_{\boldsymbol{z}} = {}^{b\leftarrow (b-1)}\boldsymbol{G}_{\boldsymbol{z}} \cdots {}^{(a+2)\leftarrow (a+1)}\boldsymbol{G}_{\boldsymbol{z}}^{(a+1)\leftarrow a}\boldsymbol{G}_{\boldsymbol{z}}, \tag{C.62} $$

$$ {}^{b\leftarrow a}\boldsymbol{G}_{\boldsymbol{v}} = {}^{b\leftarrow (b-1)}\boldsymbol{G}_{\boldsymbol{v}} \cdots {}^{(a+2)\leftarrow (a+1)}\boldsymbol{G}_{\boldsymbol{v}}^{(a+1)\leftarrow a}\boldsymbol{G}_{\boldsymbol{v}}. \tag{C.63} $$

C.3 Stability analysis of LTTHS

DEFINITION 1 AND 5 OF [55]

Appendix D

Positive Homogenization for Input-Dependent Guards

D.1 Conewise constant jump gain

This section is written under the assumption that in one macro event, only two modes are possible per contact point. The general form of a jump map for simultaneous impacts with is

$$ {}^{s^l \leftarrow s^0}\boldsymbol{z}(\tau) = {}^{s^l \leftarrow s^0}\boldsymbol{H}(\boldsymbol{z}^0(\tau), \boldsymbol{v}(\tau), \tau) = \begin{cases} \boldsymbol{G}^1(\boldsymbol{z}^0, \boldsymbol{v}^0, \tau), & \text{if condition 1 is true,} \\ \boldsymbol{G}^2(\boldsymbol{z}^0, \boldsymbol{v}^0, \tau), & \text{if condition 1 is true,} \\ \vdots & \vdots \\ \boldsymbol{G}^{p^{c_i}}(\boldsymbol{z}^0, \boldsymbol{v}^0, \tau), & \text{if condition } p^{c_i} \text{ is true,} \end{cases} \tag{D.1} $$

where $\boldsymbol{G}$ is in the form of (C.60). We will now derive the jump maps and associated conditions in (D.1) to make the expression explicit.

During a macro event for a certain perturbation, only a single order of micro events is feasible. This order can be found by determining the perturbed jump time of all possible micro events, and selecting the micro event with the earliest impact time as the next event. Mathematically, this is written as

$$ s^{k+1} = \underset{s^{k+1}}{\operatorname{argmin}} \left({}^{s^{k+1} \leftarrow S^k}t_\epsilon \right). \tag{D.2} $$

The impact time of the next micro event ${}^{s^{k+1} \leftarrow S^k}t_\epsilon$ can be approximated using the first order approximation

$$ {}^{s^{k+1} \leftarrow S^k}t_\epsilon = \tau + \epsilon \Delta^{k+1}. \tag{D.3} $$

Now, since τ and ϵ are equal for each impact time, we can rewrite (D.2) to

$$ s^{k+1} = \underset{s^{k+1}}{\operatorname{argmin}} \left(\Delta^{k+1} \right), \tag{D.4} $$

which can be written as

$$ s^{k+1} = s^k + \underset{\eta^* \in \chi}{\operatorname{argmin}} \left(- \frac{D_1 \gamma^{\eta^*} \left({}^{s^k}\alpha, {}^{s^k}\mu, \tau \right) \; {}^{S^k}\overline{\boldsymbol{z}} + D_2 \gamma^{\eta^*} \left({}^{s^k}\alpha, {}^{s^k}\mu, \tau \right) \; {}^{S^k}\overline{\boldsymbol{v}}}{\dot{\gamma}^{\eta^*}} \right), \tag{D.5} $$

with χ the set of guard identifiers that are still open. Then

$$\eta^{k+1} = \underset{\eta^* \in \chi}{\operatorname{argmin}} \left(- \frac{D_1 \gamma^{\eta^*} \left({}^{s^k}\alpha, {}^{s^k}\mu, \tau \right) \ {}^{S^k}\overline{\boldsymbol{z}} + D_2 \gamma^{\eta^*} \left({}^{s^k}\alpha, {}^{s^k}\mu, \tau \right) \ {}^{S^k}\overline{\boldsymbol{v}}}{\dot{\gamma}^{\eta^*}} \right), \tag{D.6}$$

with $s^{k+1} = s^k + \eta^{k+1}$ and η^{k+1} a guard function identifier. Finally, with

$$ {}^{S^k}\boldsymbol{a} = - \frac{D_1 \gamma^{\eta} \left({}^{S^k}\alpha, {}^{s^k}\mu, \tau \right)}{\dot{\gamma}^{\eta}}, \quad {}^{S^k}\boldsymbol{b} = - \frac{D_2 \gamma^{\eta} \left({}^{S^k}\alpha, {}^{s^k}\mu, \tau \right)}{\dot{\gamma}^{\eta}}, \tag{D.7}$$

(D.6) can be rewritten as

$$\eta^{k+1} = \underset{\eta^* \in \chi}{\operatorname{argmin}} \left({}^{S^k}\boldsymbol{a}^T \ {}^{S^k}\overline{\boldsymbol{z}} + \ {}^{s^k}\boldsymbol{b}^T \ {}^{S^k}\overline{\boldsymbol{v}} \right). \tag{D.8}$$

Now, by checking (D.6) for every micro event, we know which jump gains we should take to substitute into (C.60). For example a system with $c_i = 2$ and $p = 3$, with a macro event starting in $s_0 = 00$ and ending in $s_l = 22$, this gives

$$ {}^{S^{2\leftarrow 0}}\boldsymbol{H}(\ {}^{s^0}\boldsymbol{z}(\tau), \ {}^{S^2}\boldsymbol{v}(\tau), \tau) = \begin{cases} {}^{(12)S^{2\leftarrow 0}}\boldsymbol{G_z} \ {}^{s^0}\boldsymbol{z} + {}^{(12)S^{2\leftarrow 0}}\boldsymbol{G_v} \ {}^{s^0}\boldsymbol{v}, & \text{if (I)}, \\ {}^{12}S^{2\leftarrow 1}\boldsymbol{G_z} \ {}^{1}S^{1\leftarrow 0}\boldsymbol{G_z} \ {}^{s^0}\boldsymbol{z} + {}^{12}S^{2\leftarrow 1}\boldsymbol{G_z} \ {}^{1}S^{1\leftarrow 0}\boldsymbol{G_v} \ {}^{s^0}\boldsymbol{v} + {}^{12}S^{2\leftarrow 1}\boldsymbol{G_v} \ {}^{1}S^{1}\boldsymbol{v}, & \text{if (II)}, \\ {}^{21}S^{2\leftarrow 1}\boldsymbol{G_z} \ {}^{2}S^{1\leftarrow 0}\boldsymbol{G_z} \ {}^{s^0}\boldsymbol{z} + {}^{21}S^{2\leftarrow 1}\boldsymbol{G_z} \ {}^{2}S^{1\leftarrow 0}\boldsymbol{G_v} \ {}^{s^0}\boldsymbol{v} + {}^{21}S^{2\leftarrow 1}\boldsymbol{G_v} \ {}^{2}S^{1}\boldsymbol{v}, & \text{if (III)}, \end{cases} \tag{D.9}$$

with

$$\text{(I)}: \ {}^{2}S^{1}\boldsymbol{a}^T \ {}^{2}S^{1}\boldsymbol{z} + \ {}^{2}S^{1}\boldsymbol{b}^T \ {}^{2}S^{1}\boldsymbol{v} = \ {}^{1}S^{1}\boldsymbol{a}^T \ {}^{1}S^{1}\boldsymbol{z} + \ {}^{1}S^{1}\boldsymbol{b}^T \ {}^{1}S^{1}\boldsymbol{v}, \tag{D.10}$$

$$\text{(II)}: \ {}^{2}S^{1}\boldsymbol{a}^T \ {}^{2}S^{1}\boldsymbol{z} + \ {}^{2}S^{1}\boldsymbol{b}^T \ {}^{2}S^{1}\boldsymbol{v} > \ {}^{1}S^{1}\boldsymbol{a}^T \ {}^{1}S^{1}\boldsymbol{z} + \ {}^{1}S^{1}\boldsymbol{b}^T \ {}^{1}S^{1}\boldsymbol{v}, \tag{D.11}$$

$$\text{(III)}: \ {}^{2}S^{1}\boldsymbol{a}^T \ {}^{2}S^{1}\boldsymbol{z} + \ {}^{2}S^{1}\boldsymbol{b}^T \ {}^{2}S^{1}\boldsymbol{v} < \ {}^{1}S^{1}\boldsymbol{a}^T \ {}^{1}S^{1}\boldsymbol{z} + \ {}^{1}S^{1}\boldsymbol{b}^T \ {}^{1}S^{1}\boldsymbol{v}. \tag{D.12}$$

These conditions are illustrated in Figure D.1. Since the conditions are linear in $\boldsymbol{z}$ and $\boldsymbol{v}$, they appear as lines in the state space of $\boldsymbol{z}$ and $\boldsymbol{v}$. When we introduce more conditions, we will find several cones that relate a certain jump gain to $\boldsymbol{z}, \boldsymbol{v}$ pair. When we look at the vector $r(\boldsymbol{z}, \boldsymbol{v})$ in Figure D.1, we notice that when r is multiplied with a constant α we will always stay in the same cone, i.e. use the same jump gain. Hence the name, conewise constant jump gain.

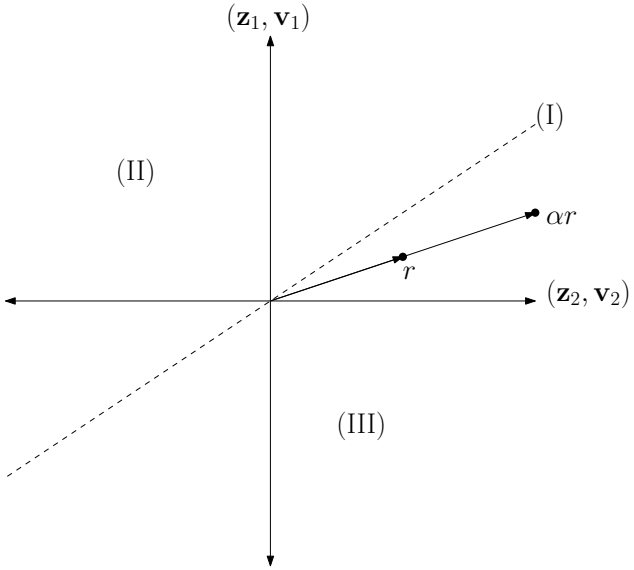

Figure D.1

D.2 Positive homogeneity

The first order approximation of the perturbed trajectory $\boldsymbol{x}_\epsilon$ can be found using $\boldsymbol{\alpha} + \epsilon \boldsymbol{z}$, with

$$\begin{aligned} {}^{s^{k-1}}\dot{\boldsymbol{z}} &= {}^{s^{k-1}}\boldsymbol{A}(t)\ {}^{s^{k-1}}\boldsymbol{z} + {}^{s^{k-1}}\boldsymbol{B}(t)\ {}^{s^{k-1}}\boldsymbol{v}, \\ {}^{s^{k}}\boldsymbol{z} &= {}^{s^{k} \leftarrow s_{k-1}}\ \boldsymbol{H}\left({}^{s^{k-1}}\boldsymbol{z}, t\right), \\ {}^{s^{k}}\dot{\boldsymbol{z}} &= {}^{s^{k}}\boldsymbol{A}(t)\ {}^{s^{k}}\boldsymbol{z} + {}^{s^{k}}\boldsymbol{B}(t)\ {}^{s^{k-1}}\boldsymbol{v}, \end{aligned} \tag{D.13}$$

where

$${}^{s^{k}}\boldsymbol{A}(t) = D_1\ {}^{s^{k}}\boldsymbol{f}\left({}^{s^{k}}\boldsymbol{\alpha}(t),\ {}^{s^{k}}\boldsymbol{\mu}(t)\right), \tag{D.14}$$

$${}^{s^{k}}\boldsymbol{B}(t) = D_2\ {}^{s^{k}}\boldsymbol{f}\left({}^{s^{k}}\boldsymbol{\alpha}(t),\ {}^{s^{k}}\boldsymbol{\mu}(t)\right). \tag{D.15}$$

When we look at (D.13), the continuous dynamics of the system are linear. Because of the conewise constant jump gain however, this linearity property is lost. We can see this by looking at the general solution of (D.13). A system $f(x, u)$ with state x and input u is linear if $f(x_1, v_1) + f(x_2, v_2) = f(x_1 + x_2, v_1 + v_2)$. Two solutions of (D.13) before jump are

$${}^{s^{k-1}}\boldsymbol{z}_1(\tau) = {}^{s^{k-1}}\boldsymbol{\phi}(t, t_0)\ {}^{s^{k-1}}\boldsymbol{z}_1(t_0) + \int_{t_0}^{\tau} \left[\ {}^{s^{k-1}}\boldsymbol{\phi}(t, s)\ {}^{s^{k-1}}\boldsymbol{B}(s)\boldsymbol{v}_1(s)\right] ds, \tag{D.16}$$

$${}^{s^{k-1}}\boldsymbol{z}_2(\tau) = {}^{s^{k-1}}\boldsymbol{\phi}(t, t_0)\ {}^{s^{k-1}}\boldsymbol{z}_2(t_0) + \int_{t_0}^{\tau} \left[\ {}^{s^{k-1}}\boldsymbol{\phi}(t, s)\ {}^{s^{k-1}}\boldsymbol{B}(s)\boldsymbol{v}_2(s)\right] ds, \tag{D.17}$$

with t_0 the initial time and τ the jump time. When we add these solutions together we find

$$\begin{aligned} {}^{s^{k-1}}\boldsymbol{z}_1(\tau) + {}^{s^{k-1}}\boldsymbol{z}_2(\tau) = {}^{s^{k-1}}\boldsymbol{\phi}(t, t_0) &\left({}^{s^{k-1}}\boldsymbol{z}_1(t_0) + {}^{s^{k-1}}\boldsymbol{z}_2(t_0)\right) \\ &+ \int_{t_0}^{\tau} \left[\ {}^{s^{k-1}}\boldsymbol{\phi}(t, s)\ {}^{s^{k-1}}\boldsymbol{B}(s)\left(\boldsymbol{v}_1(s) + \boldsymbol{v}_2(s)\right)\right] ds, \end{aligned} \tag{D.18}$$

which is equal to the solution of ${}^{s^{k-1}}\boldsymbol{z}_3(t_0) = {}^{s^{k-1}}\boldsymbol{z}_1(t_0) + {}^{s^{k-1}}\boldsymbol{z}_2(t_0)$ with $\boldsymbol{v}_3(t) = \boldsymbol{v}_1(t) + \boldsymbol{v}_2(t)$. When ${}^{s^{k-1}}\boldsymbol{z}_1$ jumps with $\boldsymbol{G}^1(\boldsymbol{z}, \tau)$ and ${}^{s^{k-1}}\boldsymbol{z}_1(\tau)$ jumps with $\boldsymbol{G}^2(\boldsymbol{z}, \tau)$ we find the solutions post jump to be

$$ {}^{s^k}\boldsymbol{z}_1(\tau) = {}^{s^k}\boldsymbol{\phi}(t, t_0)\ \boldsymbol{G}^1({}^{s^{k-1}}\boldsymbol{z}_1(t_0), \tau) + \int_{t_0}^{\tau} \left[{}^{s^k}\boldsymbol{\phi}(t, s)\ {}^{s^k}\boldsymbol{B}(s)\boldsymbol{v}_1(s) \right] ds, \tag{D.19} $$

$$ {}^{s^k}\boldsymbol{z}_2(\tau) = {}^{s^k}\boldsymbol{\phi}(t, t_0)\ \boldsymbol{G}^2({}^{s^{k-1}}\boldsymbol{z}_2(t_0), \tau) + \int_{t_0}^{\tau} \left[{}^{s^k}\boldsymbol{\phi}(t, s)\ {}^{s^k}\boldsymbol{B}(s)\boldsymbol{v}_2(s) \right] ds, \tag{D.20} $$

which when added together results in

$$ \begin{aligned} {}^{s^k}\boldsymbol{z}_1(\tau) + {}^{s^k}\boldsymbol{z}_2(\tau) = {}^{s^k}\boldsymbol{\phi}(t, t_0) \Big(\boldsymbol{G}^1_{\boldsymbol{z}}\ {}^{s^{k-1}}\boldsymbol{z}_1 + \boldsymbol{G}^1_{\boldsymbol{v}}\ {}^{s^{k-1}}\boldsymbol{v}_1 + \boldsymbol{G}^2_{\boldsymbol{z}}\ {}^{s^{k-1}}\boldsymbol{z}_2 + \boldsymbol{G}^2_{\boldsymbol{v}}\ {}^{s^{k-1}}\boldsymbol{v}_2 \Big) \\ + \int_{t_0}^{\tau} \left[{}^{s^k}\boldsymbol{\phi}(t, s)\ {}^{s^k}\boldsymbol{B}(s) \left(\boldsymbol{v}_1(s) + \boldsymbol{v}_2(s) \right) \right] ds. \end{aligned} \tag{D.21} $$

Here we see that the solution of ${}^{s^{k-1}}\boldsymbol{z}_3(t_0) = {}^{s^{k-1}}\boldsymbol{z}_1(t_0) + {}^{s^{k-1}}\boldsymbol{z}_2(t_0)$ with $\boldsymbol{v}_3(t) = \boldsymbol{v}_1(t) + \boldsymbol{v}_2(t)$, which jumps with $\boldsymbol{G}_3(\boldsymbol{z}, \tau)$, is only the equal to (D.21) if $\boldsymbol{G}_1(\boldsymbol{z}, \tau) = \boldsymbol{G}_2(\boldsymbol{z}, \tau) = \boldsymbol{G}_3(\boldsymbol{z}, \tau)$. In other words, the system only maintains its linearity after jump if the jump maps are equal for each ante jump state. Because this is generally not true, we show that the system is positive homogeneous for any jump gains. A system $f(x, u)$ with state x and input u is called positive homogeneous, when $\alpha f(x, u) = f(\alpha x, \alpha u)$. If we multiply (D.19) with a constant α, we find

$$ {}^{s^k}\boldsymbol{z}_1(\tau) = \alpha\ {}^{s^k}\boldsymbol{\phi}(t, t_0)\ \left(\boldsymbol{G}^1_{\boldsymbol{z}}\ {}^{s^{k-1}}\boldsymbol{z}_1 + \boldsymbol{G}^1_{\boldsymbol{v}}\ {}^{s^{k-1}}\boldsymbol{v}_1 \right) + \alpha \int_{t_0}^{\tau} \left[{}^{s^k}\boldsymbol{\phi}(t, s)\ {}^{s^{k-1}}\boldsymbol{B}(s)\boldsymbol{v}_1(s) \right] ds. \tag{D.22} $$

If we now look at the solution for $\boldsymbol{z}_4(t_0) = \alpha \boldsymbol{z}_1(t_0)$ with $\boldsymbol{v}_4(t) = \alpha \boldsymbol{v}_1(t)$ jumping with $\boldsymbol{G}^4(\tau)$, and using the fact that $\boldsymbol{G}^4(\tau) = \boldsymbol{G}^1(\tau)$ since the gains are conewise constant as illustrated in Figure D.1, we find the same solution as (D.22). This shows that (D.13) is positive homogeneous for any conewise constant jump gain ${}^{s^k \leftarrow s^{k-1}}\boldsymbol{H}\left({}^{s^{k-1}}\boldsymbol{z}, t\right)$. Hence the name, positive homogenization.

D.3 Stability analysis of PTTHS

Appendix E

Considered Trajectories

E.1 Associativity

E.2 Transversality

E.3 Superfluous Contacts

E.4 Nominal Guard-Activations

For impacts, the theory is valid for impacts away from a simultaneous impacts and for simultaneous impacts, but not for impacts very close to simultaneous impacts. In this case the nominal impact is not a simultaneous impact, but a perturbation can cause the order of impacts to change. I believe the jump gain is not conewise constant anymore in this case.

The same is true for impacts close to the border of stick and slip.

E.5 Non-impacting contact points can not switch modes

E.6 All closed contact points are in the same mode

If I do not assume this, then every combination of Γ_{i_C} has to be iterated until a feasible solution is found. If we do assume this, we can just check if all Γ_{i_C} go to stick. If not, then all Γ_{i_C} go to slip.

In this work only trajectories where all closed contacts are in the same mode are considered. This means that when (A.2) is smaller than zero, i.e. the reaction forces are infeasible for a stick post-impact mode, all contact points have a feasible slip post-impact mode. For trajectories where different contact points can be in slip and in stick at the same time, this conclusion can not be drawn. One should then iterate over all possible post-impact modes until a post-impact mode is found which has feasible reaction forces.

Appendix F

Simulation Design

F.1 Plank box dynamics

In Figure F.1 the plank-box model is illustrated. The block is fully actuated and the plank is attached to the solid environment with a spring and damper. The line contact is for now modeled using two contact-points C_L and C_R.

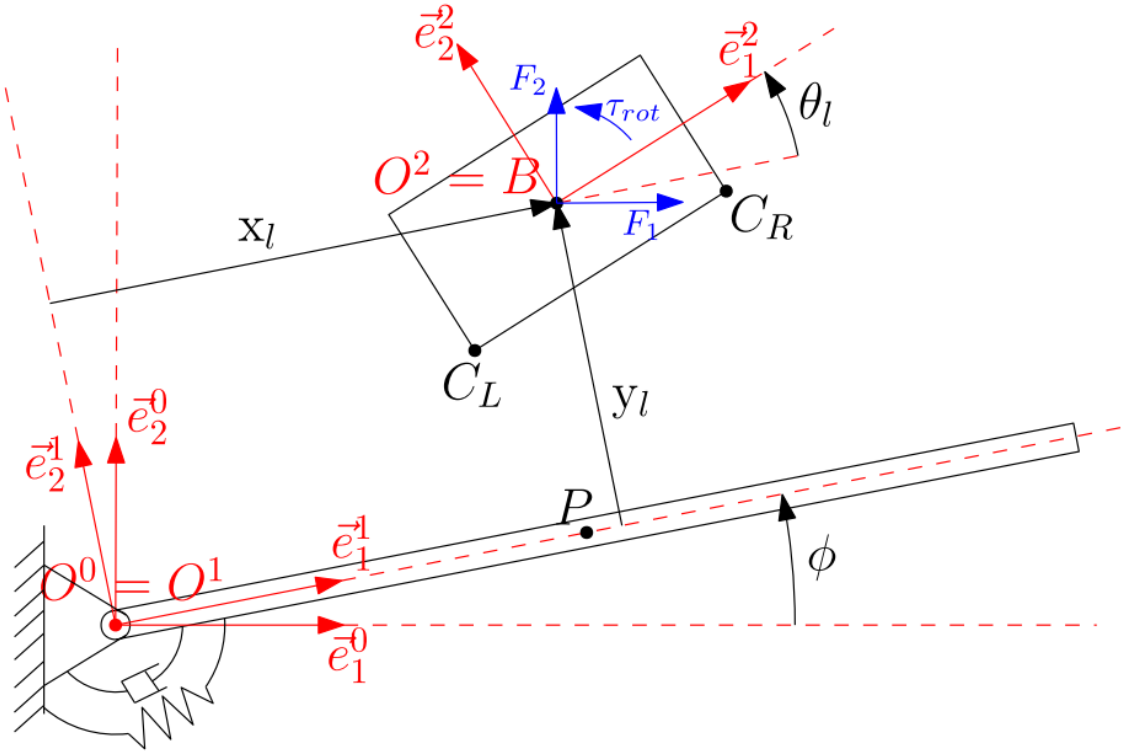

Figure F.1: *Block-plank model*

Global unconstrained dynamics

The global generalized coordinates are defined as

$$q_g = \begin{bmatrix} x_g & y_g & \theta_g & \varphi \end{bmatrix}, \tag{F.1}$$

$$v_g = \begin{bmatrix} \dot{x}_g & \dot{y}_g & \dot{\theta}_g & \dot{\varphi} \end{bmatrix}. \tag{F.2}$$

The equations of motion for the global unconstrained dynamics are then described by

$$\boldsymbol{M}_g(\boldsymbol{q}_g)\dot{\boldsymbol{v}}_g - \boldsymbol{H}_g(\boldsymbol{q}_g, \boldsymbol{v}_g) = \boldsymbol{S}_g(\boldsymbol{q}_g)\boldsymbol{u}, \tag{F.3}$$

with

$$\boldsymbol{M}_g(\boldsymbol{q}_g) = \begin{bmatrix} m_B & 0 & 0 & 0 \\ 0 & m_B & 0 & 0 \\ 0 & 0 & J_B & 0 \\ 0 & 0 & 0 & \frac{m_P {L_p}^2}{4} + J_P \end{bmatrix} \tag{F.4}$$

$$\boldsymbol{H}_g(\boldsymbol{q}_g, \boldsymbol{v}_g) = \begin{bmatrix} 0 \\ -g m_B \\ 0 \\ k_P\varphi - b_P\dot{\varphi} - \frac{L_p g m_P \cos(\varphi)}{2} \end{bmatrix} \tag{F.5}$$

$$\boldsymbol{S}_g(\boldsymbol{q}_g) = \begin{bmatrix} 1 & 0 & 0 \\ 0 & 1 & 0 \\ 0 & 0 & 1 \\ 0 & 0 & 0 \end{bmatrix}. \tag{F.6}$$

Local unconstrained dynamics

The global generalized coordinates $\boldsymbol{q}_g$ can be rewritten to a set of local coordinates $\boldsymbol{q}_l$. In the plank box case they are related via

$$\boldsymbol{q}_g(\boldsymbol{q}_l) = \begin{bmatrix} \cos(\varphi)x_l - \sin(\varphi)y_l \\ \sin(\varphi)x_l + \cos(\varphi)y_l \\ \theta_l + \varphi \\ \varphi \end{bmatrix}. \tag{F.7}$$

The local unconstrained equations of motion are then defined as

$$\boldsymbol{M}_l(\boldsymbol{q}_l)\dot{\boldsymbol{v}}_l - \boldsymbol{H}_l(\boldsymbol{q}_l, \boldsymbol{v}_l) = \boldsymbol{S}_l(\boldsymbol{q}_l)\boldsymbol{u}, \tag{F.8}$$

with

$$\boldsymbol{M}_l(\boldsymbol{q}_l) = \begin{bmatrix} m_B & 0 & 0 & -m_B y_l \\ 0 & m_B & 0 & m_B x_l \\ 0 & 0 & J_B & J_B \\ -m_B y_l & m_B x_l & J_B & \frac{m_P {L_p}^2}{4} + m_B {x_l}^2 + m_B {y_l}^2 + J_B + J_P \end{bmatrix} \tag{F.9}$$

$$\boldsymbol{H}_l(\boldsymbol{q}_l, \boldsymbol{v}_l) = \begin{bmatrix} m_B \left(x_l \dot{\varphi}^2 + 2\dot{y}_l \dot{\varphi} - g \sin(\varphi) \right) \\ -m_B \left(-y_l \dot{\varphi}^2 + 2\dot{x}_l \dot{\varphi} + g \cos(\varphi) \right) \\ 0 \\ k_P \varphi - b_P \dot{\varphi} - 2 m_B \dot{\varphi} x_l \dot{x}_l - 2 m_B \dot{\varphi} y_l \dot{y}_l - \frac{L_p g m_P \cos(\varphi)}{2} - g m_B x_l \cos(\varphi) + g m_B y_l \sin(\varphi) \end{bmatrix} \tag{F.10}$$

$$\boldsymbol{S}_l(\boldsymbol{q}_l) = \begin{bmatrix} \cos(\varphi) & \sin(\varphi) & 0 \\ -\sin(\varphi) & \cos(\varphi) & 0 \\ 0 & 0 & 1 \\ -y_l \cos(\varphi) - x_l \sin(\varphi) & x_l \cos(\varphi) - y_l \sin(\varphi) & 1 \end{bmatrix}. \tag{F.11}$$

Local constrained dynamics

First we have to determine the position vectors of the points C_L and C_R using Figure F.2. First we define the position vector of C_R,

$$r_{C_R} = r_B + r_{BC_R} \text{ with,} \tag{F.12}$$

$$r_B = \begin{bmatrix} x_l & y_l & 0 \end{bmatrix} \vec{\boldsymbol{e}}^1, \tag{F.13}$$

$$r_{BC_R} = \begin{bmatrix} BH & HC_R & 0 \end{bmatrix} \vec{\boldsymbol{e}}^1, \tag{F.14}$$

using the axis systems defined in the report of Hao. From Figure F.2 and that $\triangle BFG \cong \triangle C_R HG$ we can say

$$HC_R = \cos(\theta_l) C_R G, \tag{F.15}$$

$$C_R G = FG - FC_R, \tag{F.16}$$

$$FG = \tan(\theta_l) BF, \tag{F.17}$$

and with $FC_R = \frac{l_B}{2}$ and $BF = \frac{L_B}{2}$ we find

$$HC_R = \sin(\theta_l) \frac{L_B}{2} - \cos(\theta_l) \frac{l_B}{2}. \tag{F.18}$$

For BH we say

$$BH = BG - HG, \tag{F.19}$$

$$BG = \frac{1}{\sin(\theta_l)} FG, \tag{F.20}$$

$$HG = \sin(\theta_l) C_R G, \tag{F.21}$$

which gives us

$$BH = \cos(\theta_l) \frac{L_B}{2} - \sin(\theta_l) \frac{l_B}{2}. \tag{F.22}$$

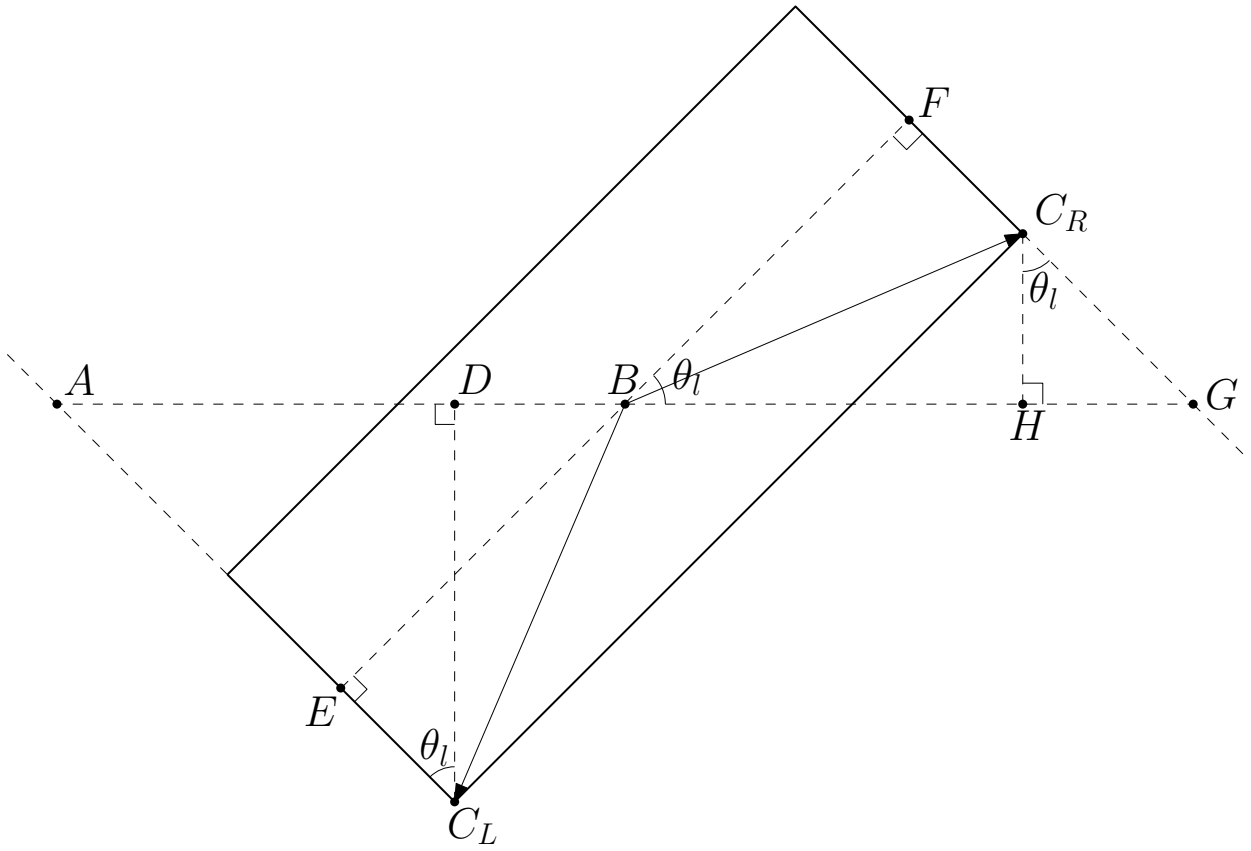

Figure F.2: *Geometry of the box, used to determine the position vectors of contactpoints C_L and C_R.*

With HC_R and BH known, the position vector of C_R is

$$r_{C_R} = \begin{bmatrix} x_l + \cos(\theta_l)\frac{L_B}{2} - \sin(\theta_l)\frac{l_B}{2} \\ y_l + \sin(\theta_l)\frac{L_B}{2} - \cos(\theta_l)\frac{l_B}{2} \\ 0 \end{bmatrix}^T \vec{\boldsymbol{e}}^1. \tag{F.23}$$

Using a similar approach for C_L we find

$$r_{C_L} = \begin{bmatrix} x_l + \cos(\theta_l)\frac{L_B}{2} + \sin(\theta_l)\frac{l_B}{2} \\ y_l - \sin(\theta_l)\frac{L_B}{2} - \cos(\theta_l)\frac{l_B}{2} \\ 0 \end{bmatrix}^T \vec{\boldsymbol{e}}^1. \tag{F.24}$$

The guard functions g_{N1} and g_{N2} are defined as

$$g_{N1} = \vec{\boldsymbol{r}}^1_{C_L}\vec{\boldsymbol{e}}^1_2 - l_p = y_l - \frac{l_P}{2} - \sin(\theta_l)\frac{L_B}{2} - \cos(\theta_l)\frac{l_B}{2} = 0, \tag{F.25}$$

$$g_{N2} = \vec{\boldsymbol{r}}^1_{C_R}\vec{\boldsymbol{e}}^1_2 - l_p = y_l - \frac{l_P}{2} + \sin(\theta_l)\frac{L_B}{2} - \cos(\theta_l)\frac{l_B}{2} = 0, \tag{F.26}$$

Since we are in a 2D-environment, the tangential reaction forces have the same dimensions as the normal reaction-forces. Therefore Equations (**??**), (**??**) and (**??**) can now be considered as, respectively,

$$\boldsymbol{g}_T = \left[g_{Ti_1}; g_{Ti_2}; ...; g_{Ti_c}\right] \in \mathbb{R}^c \tag{F.27}$$
$$\boldsymbol{\Lambda}_T = \left[\Lambda_{Ti_1}; \Lambda_{Ti_2}; ...; \Lambda_{Ti_c}\right] \in \mathbb{R}^c \tag{F.28}$$
$$\boldsymbol{W}_T = \left[\boldsymbol{w}_{Ti_1}; \boldsymbol{w}_{Ti_2}; ...; \boldsymbol{w}_{Ti_c}\right]. \in \mathbb{R}^{n\times c} \tag{F.29}$$

The velocity vectors $\dot{r}_{C_L}$ and $\dot{r}_{C_R}$ are found by taking the time-derivative of r_{C_L} and r_{C_R}, and can be written as

$$\dot{r}_{C_L} = \begin{bmatrix} \dot{x}_l - \dot{\theta}_l \sin(\theta_l)\frac{L_B}{2} + \dot{\theta}_l \cos(\theta_l)\frac{l_B}{2} \\ \dot{y}_l - \dot{\theta}_l \cos(\theta_l)\frac{L_B}{2} + \dot{\theta}_l \sin(\theta_l)\frac{l_B}{2} \\ 0 \end{bmatrix} =: \begin{bmatrix} \dot{g}_{T1} \\ \dot{g}_{N1} \\ 0 \end{bmatrix}, \tag{F.30}$$

$$\dot{r}_{C_R} = \begin{bmatrix} \dot{x}_l - \dot{\theta}_l \sin(\theta_l)\frac{L_B}{2} - \dot{\theta}_l \cos(\theta_l)\frac{l_B}{2} \\ \dot{y}_l + \dot{\theta}_l \cos(\theta_l)\frac{L_B}{2} + \dot{\theta}_l \sin(\theta_l)\frac{l_B}{2} \\ 0 \end{bmatrix} =: \begin{bmatrix} \dot{g}_{T2} \\ \dot{g}_{N2} \\ 0 \end{bmatrix}, \tag{F.31}$$

with $\dot{g}_{Ni}$ and $\dot{g}_{Ti}$ the normal and tangential relative velocities. From (**??**) and (**??**) we can write

$$\dot{\boldsymbol{g}}_N = \boldsymbol{W}_N^T \boldsymbol{v} = \begin{bmatrix} \dot{y}_l - \dot{\theta}_l \cos(\theta_l)\frac{L_B}{2} + \dot{\theta}_l \sin(\theta_l)\frac{l_B}{2} \\ \dot{y}_l + \dot{\theta}_l \cos(\theta_l)\frac{L_B}{2} + \dot{\theta}_l \sin(\theta_l)\frac{l_B}{2} \end{bmatrix}, \tag{F.32}$$

$$\dot{\boldsymbol{g}}_T = \boldsymbol{W}_T^T \boldsymbol{v} = \begin{bmatrix} \dot{x}_l - \dot{\theta}_l \sin(\theta_l)\frac{L_B}{2} + \dot{\theta}_l \cos(\theta_l)\frac{l_B}{2} \\ \dot{x}_l - \dot{\theta}_l \sin(\theta_l)\frac{L_B}{2} - \dot{\theta}_l \cos(\theta_l)\frac{l_B}{2} \end{bmatrix}, \tag{F.33}$$

from which we can deduce

$$\boldsymbol{W}_N^T = \begin{bmatrix} 0 & 1 & -\cos(\theta_l)\frac{L_B}{2} + \sin(\theta_l)\frac{l_B}{2} & 0 \\ 0 & 1 & \cos(\theta_l)\frac{L_B}{2} + \sin(\theta_l)\frac{l_B}{2} & 0 \end{bmatrix}, \tag{F.34}$$

$$\boldsymbol{W}_T^T = \begin{bmatrix} 0 & 1 & -\sin(\theta_l)\frac{L_B}{2} + \cos(\theta_l)\frac{l_B}{2} & 0 \\ 0 & 1 & -\sin(\theta_l)\frac{L_B}{2} - \cos(\theta_l)\frac{l_B}{2} & 0 \end{bmatrix}. \tag{F.35}$$

Now we have all the information to write down the local constrained dynamics

$$\boldsymbol{M}_l(\boldsymbol{q}_l)\dot{\boldsymbol{v}}_l - \boldsymbol{H}_l(\boldsymbol{q}_l, \boldsymbol{v}_l) = \boldsymbol{S}_l(\boldsymbol{q}_l)\boldsymbol{u} + \boldsymbol{W}(\boldsymbol{q}_l)\boldsymbol{\Lambda}, \tag{F.36}$$

with

$$\boldsymbol{W}(\boldsymbol{q}_l) := \begin{bmatrix} \boldsymbol{W}_N & \boldsymbol{W}_T \end{bmatrix} \text{ and } \boldsymbol{\Lambda} := \begin{bmatrix} \boldsymbol{\Lambda}_N \\ \boldsymbol{\Lambda}_T \end{bmatrix}. \tag{F.37}$$

F.2 Reference Trajectory Design